Flanders
State of the Art

Wave climate and sediment dynamics in the tidal flats and marshes of Galgeschoor

Synthesis report

Alexander Van Braeckel, Jean-Philippe Belliard, Dieter Meire, Frank Van de Meuter, Alexandra Silinski, Stijn Temmerman, Sieglien De Roo, Gerasimos Kolokythas, Yaïr Levy, Tjeerd Bouma en Erika Van den Bergh

INBO.be

Authors:
Alexander Van Braeckel, Jean-Philippe Belliard, Dieter Meire, Frank Van de Meuter, Alexandra Silinski, Stijn Temmerman, Sieglien De Roo, Gerasimos Kolokythas, Yaïr Levy, Tjeerd Bouma en Erika Van den Bergh
Research Institute for Nature and Forest (INBO)

Reviewers:
Stefaan Ides

The Research Institute for Nature and Forest (INBO) is an independent research institute of the Flemish government. Through applied scientific research, open data and knowledge, integration and disclosure, it underpins and evaluates biodiversity policy and management.

Location:
INBO Brussel
Havenlaan 88 bus 73, 1000 Brussel
www.inbo.be

e-mail:
alexander.vanbraeckel@inbo.be

Way of quoting:
Van Braeckel A.,Belliard J., Meire D., Van de Meuter F., Silinski A., De Roo S., Kolokythas G., Levy Y., Temmerman S., Bouma T. en Van den Bergh E. (2019). Wave climate and sediment dynamics in the tidal flats and marshes of Galgeschoor. Reports of the Research Institute for Nature and Forest 2019 (48). Research Institute for Nature and Forest , Brussels.
DOI: doi.org/10.21436/inbor.17169167

D/2009/3241/300
Reports of the Research Institute for Nature and Forest 2019 (48)
ISSN: 1782-9054

Responsible publisher:
Maurice Hoffmann

Cover photograph:
Alexander Van Braeckel

This research was carried out in collaboration with:
Flanders Hydraulics, University of Antwerp - group ECOBE, NIOZ -Yrseke (NL)
on behalf of Port of Antwerp

WAVE CLIMATE AND SEDIMENT DYNAMICS IN THE TIDAL FLATS AND MARSHES OF GALGESCHOOR

Synthesis report

Alexander Van Braeckel, Jean-Philippe Belliard, Dieter Meire, Frank Van de Meuter, Alexandra Silinski, Stijn Temmerman, Sieglien De Roo, Gerasimos Kolokythas, Yaïr Levy, Tjeerd Bouma en Erika Van den Bergh

doi.org/10.21436/inbor.17169167

Flanders State of the Art
RESEARCH INSTITUTE NATURE AND FOREST
Flanders Hydraulics Research
Universiteit Antwerpen
ECOSYSTEM MANAGEMENT RESEARCH GROUP
NIOZ

Preface

In 2006 the Deurganck dock, a tidal dock just opposite the Galgeschoor, became operational. The Natuurpunt 'Schorrenwerkgroep' started to monitor the marsh edge dynamics just opposite the dock opening, where container vessels have to take a wide bent before they enter the dock. The purpose was to assess possible effects of increased wave climate on the nature reserve, an aspect not fully considered in the EIA for the dock.

In view of the EIA for a potential second tidal dock near Doel, the Saeftinghe dock, the working group MONA LISA defined three research topics to fill in the knowledge gaps needed for this EIA. One of the topics was the influence of wave impact on tidal mudflat and marsh morphology of the Galgeschoor and the relative influence of wind and ship induced waves. This was studied by INBO (Research Institute for Nature and Forest), and FHR (Flanders Hydraulics Research) commissioned by the Port of Antwerp.

The conclusion of this study was that increased hydrodynamics in front of the tidal marsh edge facing Deurganck dock since 1990 coincided with subtidal and intertidal morphological changes, yet no direct link or causality with waves or ship movements could be found.

On the mudflats correlations were found between wave height and sedimentation/ erosion, between maximum wind speed and wave height, ship passage and wave height, fetch and sedimentation/ erosion. However the limited dataset and the applied measuring method did not allow identifying the relative importance of wind and ship waves on morphologic changes. Moreover the study did not compare tidal currents and waves as morphodynamic drivers.

In the present study, also commissioned by the Port of Antwerp, the goal is to assess the (relative) importance of hydrodynamic stressors tidal current, wind and ship waves and the related morphological response of the Galgeschoor lower and higher tidal mudflats and marsh edge.

doi.org/10.21436/inbor.17169167

Summary

In spring 2016 the MSC shipping line activities were moved to Deurganck dock and in June 2016 the Kieldrecht Lock, connecting the latter dock to the Waaslandhaven, became operational. In the near future container handling capacity in the Port of Antwerp may be increased by the construction of a new tidal dock on the left bank of the river Scheldt.

The possible impact of increased shipping traffic on the tidal mudflats and marshes of the Galgeschoor, a protected area facing Deurganck dock is investigated. The relative importance of hydrodynamic stressors (tidal currents, wind and ship waves) is studied and the wave climate before and after the MSC relocation and opening of the Kieldrecht Lock is compared. The results can provide input for an environmental impact assessment of a new tidal dock.

MORPHODYNAMICS

The morphodynamic long term and short term evolution on the Galgeschoor is reconstructed with the integration of data from MONEOS ecotope mapping, NGO Natuurpunt and INBO marsh edge monitoring, MONA LISA cross shore profile data and specific monitoring on the same transects for this project.

Due to high morphodynamics at the Galgeschoor, soft bottom low **tidal mudflat ecotopes** evolved into middle tidal mudflats and into low tidal hard substrate zones in respectively 2012-2013 and 2015-2016. Tidal marsh ecotope areas, including glaux-vegetation, near the marsh edge seemed relatively stable.

Tidal marsh edge retreat clearly differed between the northern and southern transect with respectively long term retreat rates of 2.5 and 14.6 cm/year since 2010, respectively. Consequently the proportion of high solid old marsh area decreased. However, pioneer marsh vegetation seems to be establishing itself. Whether this will consolidate and develop into a tidal marsh or may only be an ephemeral event is not clear at this point.

Tidal flat-bed level changes were in general much more pronounced at the southern plots (order of magnitude 5 – 10 cm) than at the northern plots (<5 cm). This is likely due to differences in sediment type and sediment cohesion. Net bed level changes are difficult to infer from the data because of strong daily and seasonal variation. The southern transect was generally more dynamic showing larger seasonal and day-to-day variations. Also low tidal plots were much more dynamic than high tidal plots. The daily bed level fluctuations on the low tidal flat plots displayed a spring-neap tidal cycle signature (i.e. 14.77 days).

HYDRODYNAMICS

Maximum tidal current velocity on the low tidal flat varied between 0.3 m/s and 1.25 m/s. Maximum tidal current velocity at ebb was relatively constant over a neap-spring tide cycle. Maximum flood current however, was significantly related to tidal amplitude. Highest current velocities were invariably recorded during the flood phase near spring tide, hence the flood phase may be predominant in tidally-induced (eroding) morphodynamics. Less is known of current velocities at the high tidal flats, but the available data suggest current velocities are generally lower.

An averaged significant **wind wave** height of 0.06 to 0.07m was found. Above 10 m/s, wind speed positively affected wind wave height. At higher wind speed, significant wave height per tidal cycle increased to 0.2m (approx. 0.38m maximum wave height at the highest wind speeds

recorded during the study (between 15-20m/s). At higher wind speed, wind waves very slightly increase from the low towards the high tidal flats. Fetch may become increasingly important and is longest at the high plots for the most commonly observed wind directions (dominant SW-wind). Wind wave height appeared marginally higher at the southern transect compared to the northern transect, as such no clear effect of the Deurganck dock fetch length could be observed.

Ship passing intensity increased with 15% between October 2015 and 2016. Tugboats and cargo ships, sailing upstream, pass slower along the southern than along the northern transect but for tankers and downstream moving vessels we found no difference. **Ship wave height** (both primary and secondary waves) tended to be related to ship sailing speed and vessel size, yet additional analyses may be needed to corroborate these trends and to see how they may interact with vessel type. Ship waves reached large wave heights (to 0.7m) more regularly than wind waves, yet for short durations. Primary ship wave height tends to increase near low tide. This may be attributed to the proportionally larger water displacement at low tide or shoaling. Ship secondary waves attenuated from low to high tidal flat, whereas wind waves propagated towards the high flat at high wind speed. The observed increase of ship passages has lead to an overall increase in ship waves. The concerted effect of ship waves, wind waves and tidal currents makes it difficult, however, to isolate the effect of ship waves, and thus the MSC move and the opening of the Kieldrecht lock, on old marsh retreat. The effect of these hydrodynamic stressors on the marsh cliff may also depend on the shape of the tidal mudflat, which has changed recently.

PHYSICAL FORCING FACTORS

In November 2016, current-induced **bed shear stress** was more important than wave-induced bed shear stress at the low tidal flats, whereas this was opposite at the high tidal flats. It should be noted however that current-induced bed shear stress was not directly measured but calculated from sediment and current properties. At the low tidal flats, we observed a spring-neap tidal cycle pattern in the relative importance of current versus wave-induced bed shear stress.

At the northern **low tidal flat,** current induced bed shear stress only exceeded the local critical Shields stress (a threshold above which resuspension starts) at spring tide; at the southern transect, critical Shields stress was also exceeded at average tidal conditions. On the low tidal flat, impact of waves is secondary to tidal currents in morphodynamics, yet they are an important additional factor shaping local morphology, especially on the southern transect. Differences between the northern and the southern transect are partially attributed to differences in sediment cohesion.

On the **high tidal flat** both waves and currents are less strong, inducing less pronounced bed level changes. Waves are relatively more important in controlling morphodynamics, especially under high tidal conditions. This is more pronounced at the southern compared to the northern transect. In addition to sediment cohesion, the difference in height range of the riprap zone may have an influence.

CONCLUSIONS AND RECOMMENDATIONS

The results of the present study are more conclusive, compared to Michels et al (2012) and Verelst et al (2011), with respect to the relative importance of hydrodynamic stressors on the morphological response of the Galgeschoor lower and higher tidal mudflats and marsh edge facing Deurganck dock and the location of the possible future Saeftinghe dock.

 doi.org/10.21436/inbor.17169167

We did not observe more extreme ship waves after the move of MSC and the opening of the Kieldrecht lock but the number of ship wave events increased and ship waves regularly caused large wave heights. It is unclear as yet however how this increased ship wave stress may have contributed to the observed marsh cliff erosion, against a background of tidal currents and wind waves. Further analysis of the ship wave data and special focus on the cliff area is recommended.

In view of the long term evolution Michels et al (2012) concluded that an average marsh edge retreat of 25 cm/year can be considered as a background value for a normal tidal marsh cycle at the Galgeschoor, allowing for establishment of pioneer marsh. This might be what is happening at the Galgeschoor, but the establishment of the pioneer marsh may be ephemeral and can only be rightly assessed on the longer term. It is recommended to monitor this positive evolution of pioneer marsh growth more closely in relation to the physical driving forces.

Nederlandse samenvatting

In 2016 verhuisden de activiteiten van MSC in de Antwerpse haven naar het Deurganckdok, én de Kieldrechtsluis die dit dok met de Waaslandhaven verbindt werd operationeel.

De bouw van een potentieel tweede getijdedok in de buurt van Doel is één van de bouwstenen van het Complex Project Extra Containercapaciteit Antwerpse haven (CP-ECA).

In deze studie wordt de mogelijke impact van toegenomen scheepvaart op de slikken en schorren van het natuurgebied Galgeschoor, tegenover het Deurganckdok, bestudeerd.

De relatieve impact van hydrodynamische stressoren (getij, wind en golven) wordt onderzocht. Tevens wordt het golfklimaat voor en na de verhuis van MSC en de opening van de Kieldrechtsluis vergeleken. De resultaten kunnen mogelijks input leveren voor een project MER van CP-ECA.

MORFODYNAMIEK

De morfologische evolutie van het Galgeschoor op korte en lange termijn wordt gereconstrueerd door integratie van MONEOS ecotopenkaarten, schorrandmetingen van INBO en Natuurpunt, MONA LISA en MONEOS-dwarse hoogteprofielen en specifieke metingen voor dit project langs diezelfde raaien.

De intense morfodynamiek op het Galgeschoor wordt duidelijk uit de omzetting van laag slik tot middelhoog slik in de periode 2012-2013 en tot lage harde substraat zones in 2015-2016. De totale schoroppervlakte nabij de schorrand (inclusief pionierende melkkruidvegetatie) veranderde nagenoeg niet.

De schorranderosie verschilt tussen de noordelijke en zuidelijke raai met respectievelijk gemiddelde erosiesnelheden van 2.5 en 14.6 cm/jaar sinds 2010. Het aandeel oud schorplateauvermindert dus maar anderzijds ontwikkelt zich ook pionierschor in de potentiële pionierzone. De vraag is hoe duurzaam deze ontwikkeling is.

Bodemhoogte-ontwikkelingen op het slik waren over het algemeen meer uitgesproken aan de zuidelijke raai (grootteorde 5-10 cm) vergeleken met de noordelijke raai (<5 cm). Dit houdt mogelijk verband met verschillen in sedimentcohesie (want verschillen in de samenstelling van het sediment) tussen beide locaties. Netto bodemhoogte wijzigingen zijn moeilijk te duiden uit de gegevens omdat er sterk interfererende dagelijkse en seizoensgebonden schommelingen zijn. Algemeen is het zuidelijk transect meer dynamisch en vertoont het meer uitgesproken korte termijn schommelingen. Ook zijn de lage slikken algemeen meer dynamisch in vergelijking met de hoge slikken. De kortetermijnschommelingen op het laag slik vertonen een duidelijke springtij-doodtij variatie (i.e. 14.77 dagen).

HYDRODYNAMIEK

Maximale stroomsnelheid op het laag slik varieert tussen 0.3 m/s en 1.25 m/s. De maximale ebsnelheid is redelijk constant over springtij-doodtij maar de maximale vloedsnelheid is significant gecorreleerd met de getijamplitude en dus de springtij-doodtij cyclus: de grootste stroomsnelheden worden telkens tijdens springvloed gemeten. Vloed is dus logischerwijze de belangrijkste getijfase voor wat betreft getij-geïnduceerde morfodynamiek. Er zijn minder data over stroomsnelheden op hoog slik, maar de weinige die er zijn suggereren alvast dat die over het algemeen lager zijn.

doi.org/10.21436/inbor.17169167

De gemiddelde significante **wind golf**hoogte per getijcyclus was 0.06 tot 0.07 m. Vanaf windsnelheden boven 10 m/s is de golfhoogte gecorreleerd met windsnelheid. Bij de hoogst gemeten windsnelheden kon de significante golfhoogte per getij oplopen tot 0.2 m (ongeveer 0.38m maximum golfhoogte bij de hoogst gemeten windsnelheid van de campagne: 15-20 m/s). Windgolven versterken van laag naar hoog slik als de windsnelheid voldoende hoog is. De strijklengte wordt mogelijks belangrijker bij hoge windsnelheid én is het grootst op de hoogst liggende locaties voor de meest dominante windrichting (ZW-wind). Windgolven waren iets hoger langs de zuidelijke raai dan langs de noordelijke, ook hierin kan de strijklengte een rol spelen.

Het aantal scheepsbewegingen nam met ca. 15% toe tussen oktober 2015 en 2016. Stroomopvarende sleepboten en containerschepen varen met iets kleinere snelheid voorbij de zuidelijke raai dan voorbij de noordelijke. Voor tankers en voor afvarende schepen werd geen verschil gevonden. De studie van **scheepsgolven** suggereerde een positieve trend tussen vaarsnelheid, scheepgrootte en grote van de scheepsgolven (zowel voor primaire als secundaire golven). De gegenereerde golf was bovendien groter bij laag water, waarschijnlijk doordat er proportioneel meer water verplaatst wordt of eventueel door *shoaling*. Scheepsgolven vertoonden regelmatig erg grote maximale golfhoogtes (tot 70 cm), maar vooral secundaire golven vertoonden een graduele demping van laag naar hoog slik. Er zijn nog bijkomende analyses nodig om een aantal van bovenstaande trends beter te onderbouwen of statistisch te bevestigen. Het aantal scheepsgolven nam toe door de ingebruikname van de Kieldrechtsluis en de verhuis van MSC, maar het is voorlopig niet mogelijk om een uitspraak te doen over de bijdrage hiervan aan schorerosie, in vergelijking met windgolven of getijstromingen.

DRIJVENDE KRACHT VOOR MORFODYNAMIEK

Data van de meetcampagne uit november 2016 werd omgerekend naar schuifspanning. Daaruit kon afgeleid worden dat op het laag slik getijstroming meer schuifspanning veroorzaakt dan golven en dat daar een spring-doodtij patroon in waar te nemen is. Op het hoog slik genereren golven de grootste schuifspanning.

Om getij en golven als drijvende krachten voor morfodynamiek (component: erosie) te evalueren werd de schuifspanning die ze veroorzaken vergeleken met de lokale kritische schuifspanning. Aan de noordelijke raai werd de lokale kritische schuifspanning op het laag slik enkel bij springtij overschreden door getijstroming, aan de zuidelijke raai ook bij gemiddeld getij. Golfimpact op het laag slik is ondergeschikt aan getij-impact maar toch kunnen (scheeps)golven met piekmomenten een belangrijke bijkomende drijvende kracht voor de lokale morfologie betekenen, vooral aan de zuidelijke raai. Verschillen in morfodynamiek tussen laag slik op de zuid- en noordraai kunnen gedeeltelijk aan sedimentcohesie toegeschreven worden.

Golven en getij op het hoog slik zijn minder sterk en veroorzaken dan ook minder bodemhoogte veranderingen. (Wind)Golven zijn relatief belangrijker, vooral bij hoge getijden. Dit patroon is meer uitgesproken aan de zuidraai dan aan de noordraai. Bovenop het verschil in sedimentcohesie spelen hier ook het verschil in hoogterange van de breuksteengordel en strijklengte bij hoogtij voor de overheersende windrichting een rol.

BESLUIT EN AANBEVELINGEN

In vergelijking tot Michels et al (2012) en Verelst et al. (2011) weten we meer over de relatieve bijdrage van hydrodynamische krachten getij, wind- en scheepsgolven tot de morfologische

respons van hoog en laag slik en de schorrand van het Galgeschoor tegenover het Deurganckdok en de mogelijk toekomstige locatie van een Saefthingedok.

Het aantal scheepsgolven ter hoogte van het Galgeschoor nam recent toe door de ingebruikname van de Kieldrechtsluis en de verhuis van MsC, maar het is voorlopig niet mogelijk om een uitspraak te doen het relatieve belang hiervan aan schorerosie, in vergelijking met windgolven of getijstromingen.

Michels et al. (2012) beschouwden een gemiddelde schorranderosie van 25 cm/jaar voor het oud schorplateau van het Galgeschoor als een achtergrondwaarde, die deel uitmaakt van een normale schorcyclus waarbij pionierschor zich kan vestigen. De vestiging van het pionierschor op het Galgeschoor duidt mogelijk echter vrij recent. Om te beoordelen of deze positieve evolutie werkelijk onderdeel uitmaakt van een natuurlijke schorcyclus is het aan te bevelen om deze nauwgezet te monitoren in relatie tot de heersende hydrodynamische krachten

doi.org/10.21436/inbor.17169167

Table of contents

//

doi.org/10.21436/inbor.17169167

List of figures

 doi.org/10.21436/inbor.17169167

//

 doi.org/10.21436/inbor.17169167

//

List of tables

 doi.org/10.21436/inbor.17169167

1 INTRODUCTION

Shipping traffic movements in the port of Antwerp changed in 2016 due to the transfer of the MSC shipping company activities to the Deurganck dock (April- May 2016) and the commissioning of the Kieldrechtlock which connects the latter dock to the Waaslandhaven (June 2016). Overall, the number of seagoing vessels decreased in the port of Antwerp in recent times, yet at the same time more freight is shipped due to increasing vessel size. A possible future scenario for the realisation of extra container handling capacity is the construction of a new tidal dock at the left bank of the river Scheldt. This economic development may induce environmental impacts. In particular, the protected nature reserve of Galgeschoor which lies within the port of Antwerp area may experience changes in hydrodynamic exposure as a result of the expected increase in ship-induced wave climate intensity. For this reason, a study was initiated by the Antwerp Port Authority with the aim to assess the morphological response of the tidal flats and marsh edge of Galgeschoor, with respect to effects of tidal currents, ship and wind waves on sedimentation-erosion dynamics.

The goal of this study is to assess the (relative) importance of hydrodynamic stressors and the related morphological response of the Galgeschoor lower and higher tidal mudflats and marsh edge. To this end the evolution of the habitats is studied in different time scales. Tidal currents and waves are measured, wind and ship waves are isolated and compared before and after the move of MSC and the opening of the new Kieldrecht lock.

The project, carried out by INBO (Research Institute for Nature and Forest), UA (University of Antwerp), FHR (Flanders Hydraulics Research) and NIOZ (Royal Netherlands Institute for Sea Research) comprises a long-term measurement campaign that took place from November 2015 to May 2017 intersected with two intensive one-month measurement campaigns in November 2015 and November 2016 respectively (i.e. before and after the opening of the Kieldrecht Lock). The long-term measurement campaign investigated the morphological evolution of the tidal flats of the Galgeschoor and attempted to elucidate potential internal and/or external controls. Results and findings based on the analysis of the long-term measurement campaign are reported in Silinski et al. (2016) and Beillard et al. (2017). The intensive campaigns focused on a range of measurements including current velocities, water levels and wave climate. It also aimed at differentiating ship and wind wave characteristics and their relative importance. The findings and conclusions for these intensive campaigns are reported in Kolokythas et al. (2016) and Levy et al. (2017) respectively. A synthesis of all results and findings as well as reflection in time and space are documented in this report.

In detail, the report is organised as follows:

Chapter 1 is the introduction, chapter 2 describes the Galgeschoor, including its history and the measuring set up, chapter 3 focuses on the morphodynamic measurements for this study as well as earlier data from the previous Galgeschoor projects, chapter 4 contains the analysis of wind and ship wave measurements and tidal current measurements. In chapter 5 the relation is made between the morpho- and hydrodynamic measurements in the study. Chapter 6 and 7 contain the discussion and conclusions.

Figure 1.1 Aerial photograph of the Galgeschoor in the inner bend of the Scheldt (© Vildaphoto-Yves Adams)

doi.org/10.21436/inbor.17169167

2 DESCRIPTION AND HISTORY OF THE STUDY SITE AND THE RESEARCH STATIONS

2.1 DESCRIPTION AND HISTORY OF THE STUDY SITE

The Galgeschoor nature reserve is located on the right bank of the lower Sea Scheldt, within the brackish zone of the Scheldt Estuary, between the village of Lillo and the Europaterminal (Figure 2-1). On the left bank of the Scheldt, directly opposite from the Galgeschoor, lies the Deurganck dock (S-GSc) as well as a plan scenario location for a potential new tidal dock (Saeftinghe dock – N -GSb).

The Galgeschoor is a wetland area (46 ha) of tidal flats and marshes protected by national and international legislative and policy frameworks (Nature reserve, Natura 2000, Habitats and Birds directives, Ramsar convention). The boundary between the marshes and flats is at most places formed by a cliff with a height of up to 50cm. *Phragmites australis* is the dominant plant species present on the marsh. The tidal flat extends seaward from the marsh edge where a riprap ridge first covers an elevation gradient of up to 4 m locally (Figure 2-4) to stabilize a steep slope, followed by a gentle slope toward the low water line.

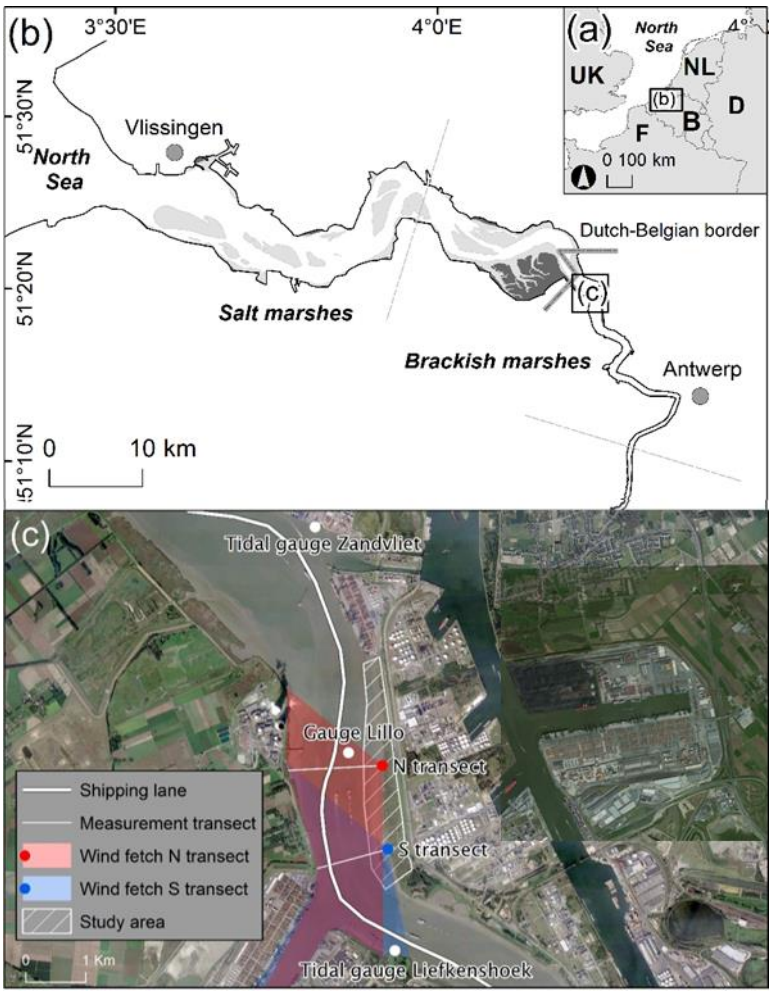

Figure 2.1 Overview of the location of the Scheldt Estuary (a) within Europe, (b) over the stretch from Antwerp to the North Sea and (c) of the study area. Locations of the Galgeschoor (hatched area), the two monitoring transects (white lines) of the Deurganck dock (S-GSc) and a plan scenario location for a new tidal dock (Saeftinghe dok –N-GSb), the gauge stations

Figure 2.2 Boundary between the marsh and tidal flats at Galgeschoor with the presence of the riprap ridge

Historical changes on planimetry including riprap (1940 – 2010)

An important characteristic of the Galgeschoor is the manmade riprap zone, established at the tidal marsh edge in the nineties to restrain the increased marsh edge retreat, induced by dike reinforcements (i.e. coastal squeeze).

A

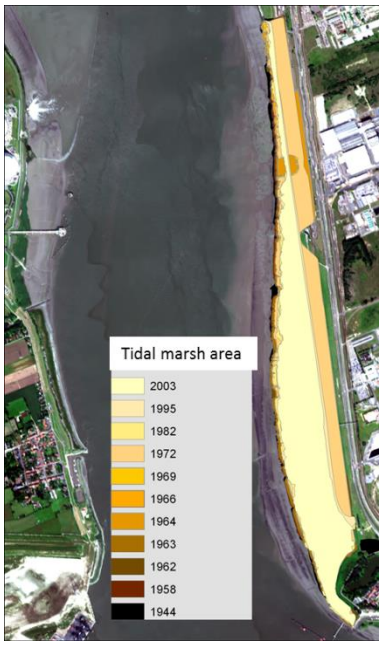

B

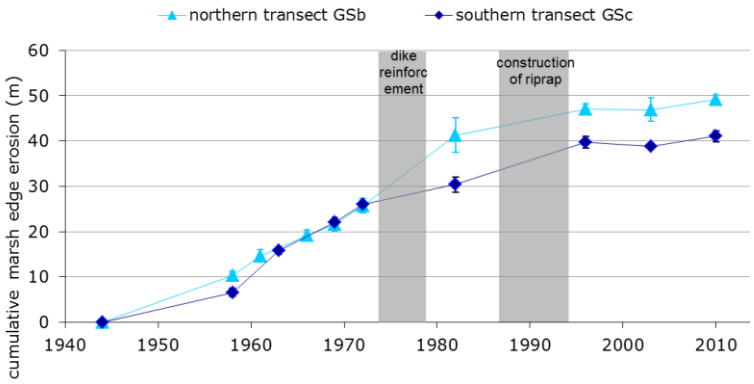

Figure 2.3(A) Map showing declining tidal marsh area of Galgeschoor over time (B) Long-term cumulative marsh edge erosion (m) with indication of direct impact measures.

This riprap zone is located along the complete Galgeschoor river bank but exhibits height and elevation differences along the study area. Figure 2.4 shows the altitudinal range covered by riprap, displayed as the lower (blue line) and upper (green line) end of the riprap zone. The maximum height as well as the elevation range of the riprap can influence wave attenuation

doi.org/10.21436/inbor.17169167

on the higher tidal mudflat and marsh edge. The vertical dashed lines indicate the southern and northern transects of current study. The lower riprap range at the Southern transect may lead to a higher erosion vulnerability. In 2005 the tidal Deurganck dock was opened on the opposite site of the river.

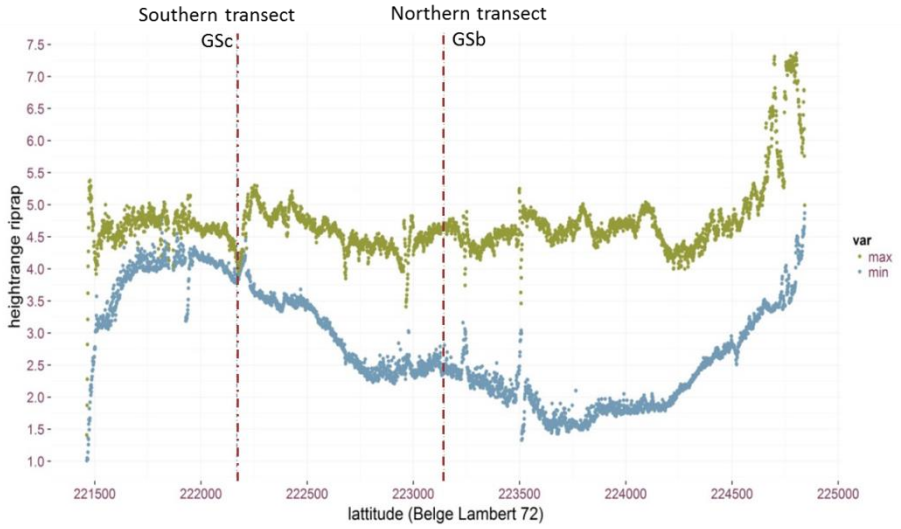

Figure 2.4 Absolute height range of the rip rap zone (mTAW) at Galgeschoor from south (left) to north (right)

Morphological changes around the study area (2010 – 2016)

The subtidal area adjacent to the Galgeschoor is morphologically heavily managed due to the nearby presence of the sandbar of Frederick at the merging of a restricted flood channel and the main ebb channel (Figure 2-5 A). Guaranteed safe port access for larger ships requires continuous dredging in the maritime access routes in the lower Sea Scheldt. The yearly maintenance dredging volumes for the nearby sandbar fluctuate around 300.000 m³. Between July 2009 and July 2010 an additional 2.5 mm³ of sand was dredged to deepen and widen the navigation channel locally (Figure 2-5 A).

After this deepening and widening the river reacts in search of a new morphological equilibrium. A consistency map of erosion/sedimentation between 2011-2016 (Figure 2-5 B) shows a continuous sedimentation on the tidal mudflats (>0m T.A.W.) and shallow water zones on the left bank of the river and in front of the southern end of the Galgeschoor on the right bank. In front of the remainder of the Galgeschoor to the north, the river bed has mainly eroded.

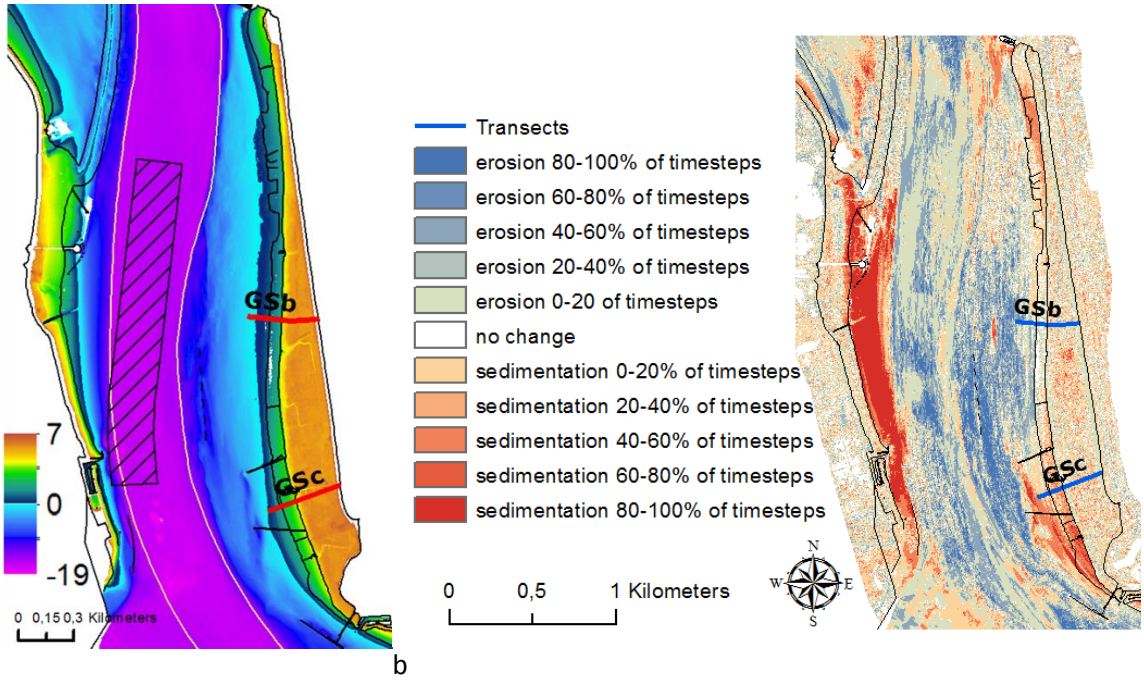

a b

Figure 2.5 (a) Digital Elevation Model (DEM) of Galgeschoor area in 2016 based on a multibeam and lidar data (elevation unit meter T.A.W.), dashed polygon is dredging area of Frederick, white line is fairway, 0m TAW is the low water mark (b) Consistent erosion/sedimentation map based on the yearly DEM difference classification map between 2011 and 2016 (% of 5 maps see Figure 2-6)

doi.org/10.21436/inbor.17169167

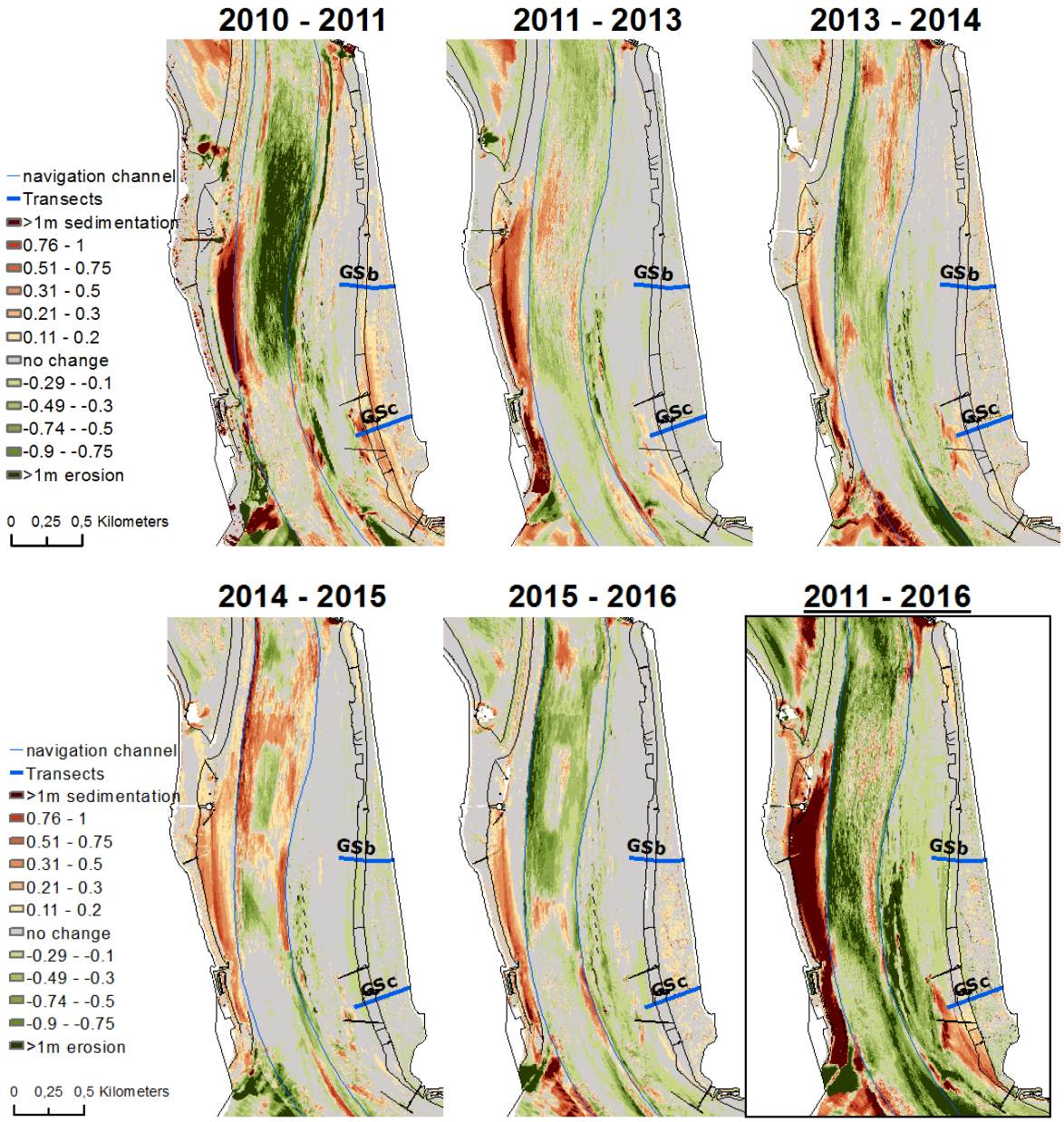

Figure 2.6 Yearly Digital Elevation Model (DEM) difference classification map of Galgeschoor area between 2011 and 2016 (except of 2012) supplemented with the DEM difference classification map of the total period 2016-2011 (all DEM data provided by Maritime Access Division), high erosion/deepening in 2009-2010 is an effect of the 3th deepening of the navigation channel, high sedimentation is a response (f.e. on the left river bank and inner bend at GSc).

The net sedimentation at the tidal mudflats and shallow water areas was strongest in 2010-2011 (Figure 2-6). In 2013-2014 the inner bend near Galgeschoor endured high sediment depositions within the navigation channel but that stopped thereafter. After 2014 a period of relative stability occurred and some locations even eroded.

Intertidal cross-shore profiles (2008 – 2017)

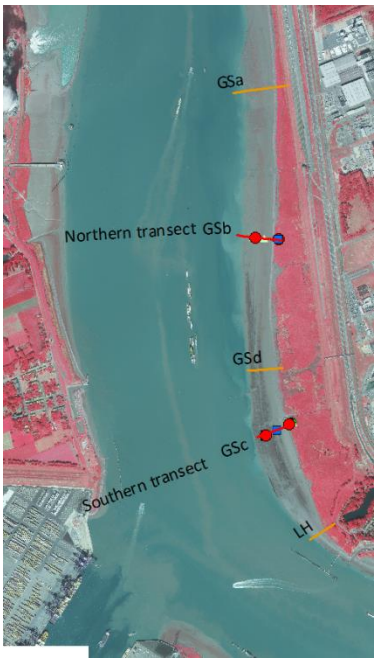

The Galgeschoor shows a downstream-upstream gradient towards a wider tidal marsh and decreasing riprap range and tidal flat slopes that decreases in upstream direction towards the inner river bend. A typical tidal flat at present extends riverward from the marsh edge where a riprap ridge first covers an elevation gradient of up to 2 m locally to stabilize a steep slope, followed by a gentle slope towards the lower mudflat zones (Figure 2-7 A-E).

The cross shore profile GSa mainly exist of a stable hard substrate bank of peat in the low tidal flat range. At the northern transect profile GSb the hard peat layer is covered by a thin mud layer that showed an eroding trend between 2010 and 2015. The profile GSd, where the measurements started before the deepening in 2009, shows half a meter sedimentation between 2008 and 2012. At the southern transect (Gsc) the elevation profile of the complete low and middle tidal flat profile has increased significantly since 2010, which continued longer on the low tidal flat. The old cross shore profile LH also showed sedimentation since 2008 with the highest increase rate between 2008-2011 and 2011-2013.

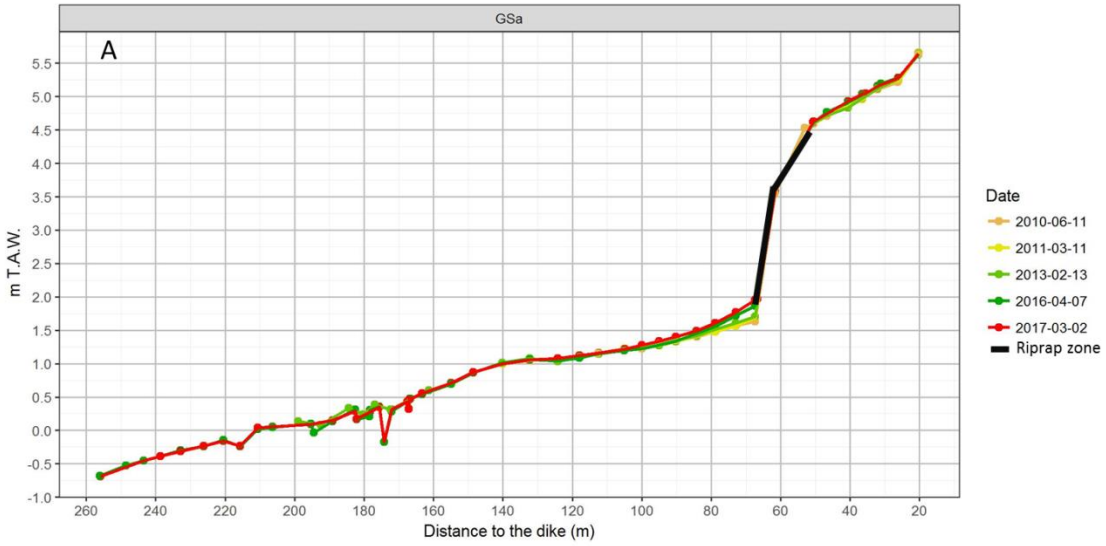

doi.org/10.21436/inbor.17169167

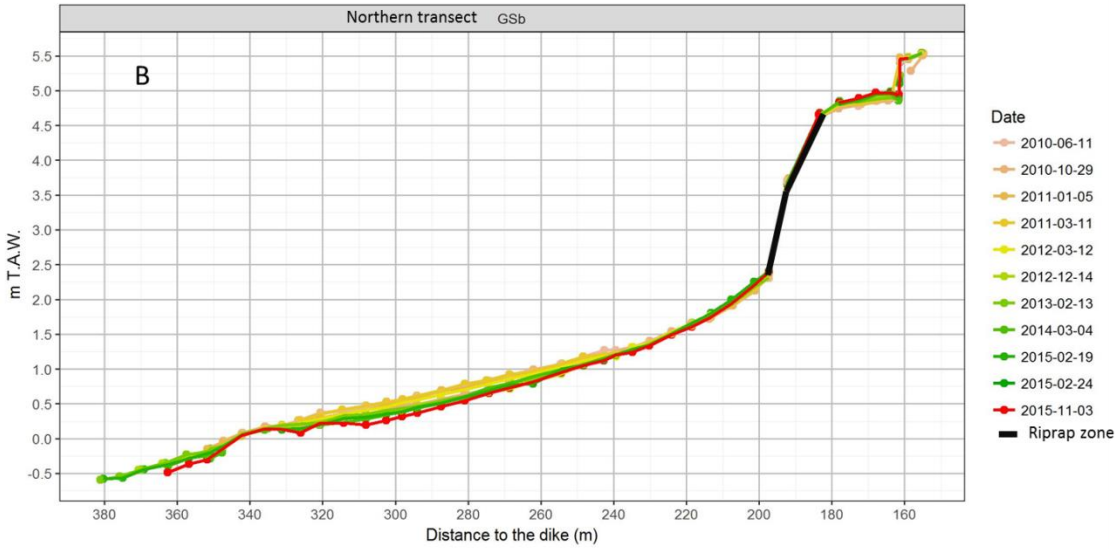
Northern transect GSb
B
m T.A.W.
Distance to the dike (m)
Date
2010-06-11
2010-10-29
2011-01-05
2011-03-11
2012-03-12
2012-12-14
2013-02-13
2014-03-04
2015-02-19
2015-02-24
2015-11-03
Riprap zone

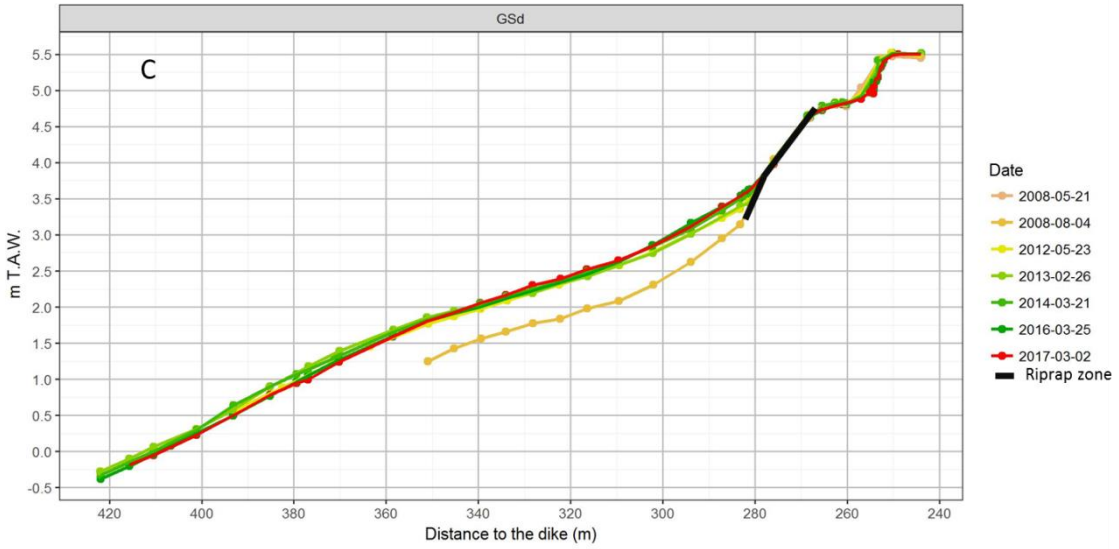
GSd
C
m T.A.W.
Distance to the dike (m)
Date
2008-05-21
2008-08-04
2012-05-23
2013-02-26
2014-03-21
2016-03-25
2017-03-02
Riprap zone

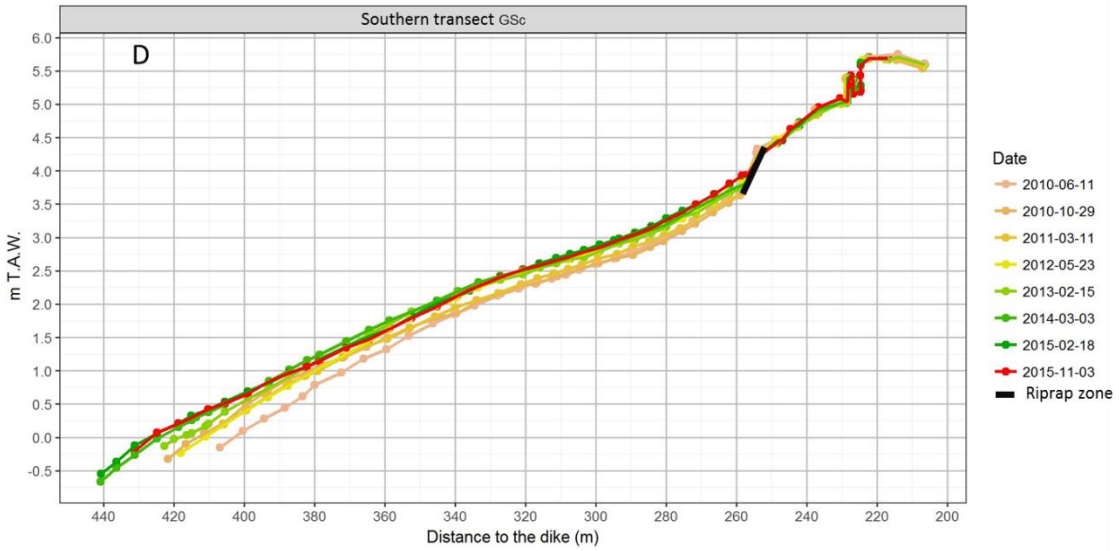
Southern transect GSc
D
m T.A.W.
Distance to the dike (m)
Date
2010-06-11
2010-10-29
2011-03-11
2012-05-23
2013-02-15
2014-03-03
2015-02-18
2015-11-03
Riprap zone

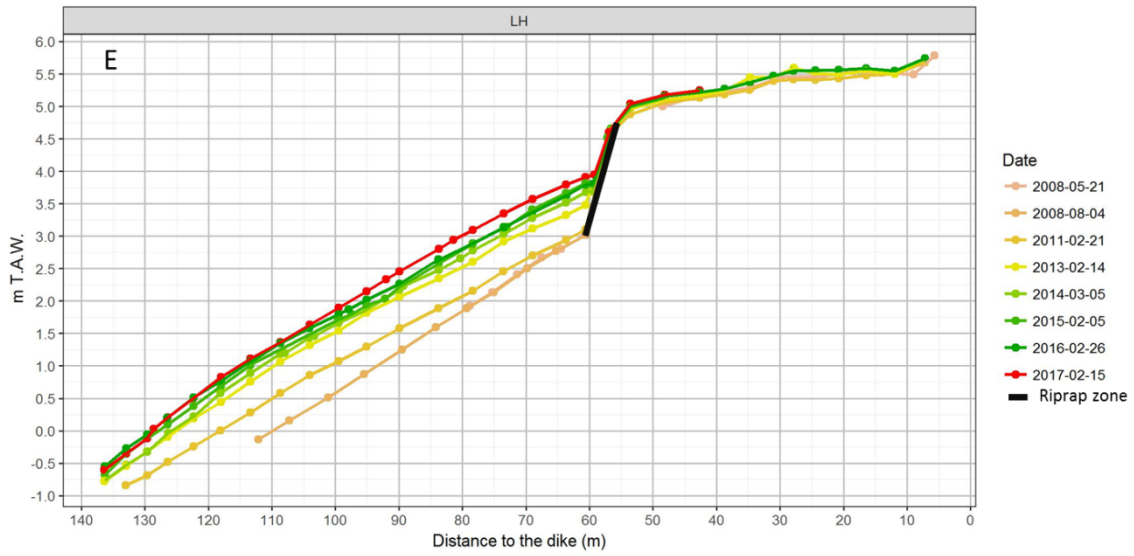

Figure 2.7 Topographical changes at the intertidal cross shore profiles of the Galgeschoor (A-E, GSa-d & LH). Since 6/2010 for GSa, GSb, GSc and since 5/2008 (before the channel deepening) for GSd and LH)

Tidal marsh edge measurements (2006 – 2017)

Since 2006 NGO working group 'Natuurpunt Schorrenwerkgroep' measures the marsh edge retreat near the southern transect (GSc) of Galgeschoor using vertical pins. These pins are located within 4 so-called erosion tongues, and showed that these erosion tongues further eroded nearly 45 cm inwards within 10 years (Figure 2.8); a retreat rate of 3.9 cm per year.

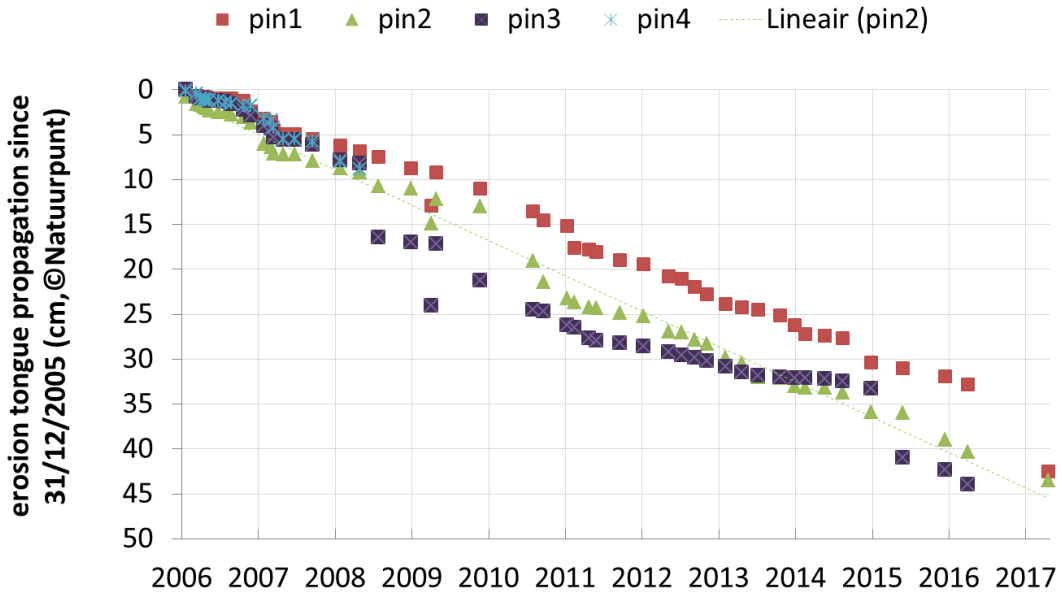

Figure 2.8 Tidal marsh edge retreat at erosion tongues near the Southern cross shore profile location (GSc) in the period 5/2006 -9/2017 (data Natuurpunt Schorrenwerkgroep, www.scheldeschorren.be/wp/studie-en-monitoring)

doi.org/10.21436/inbor.17169167

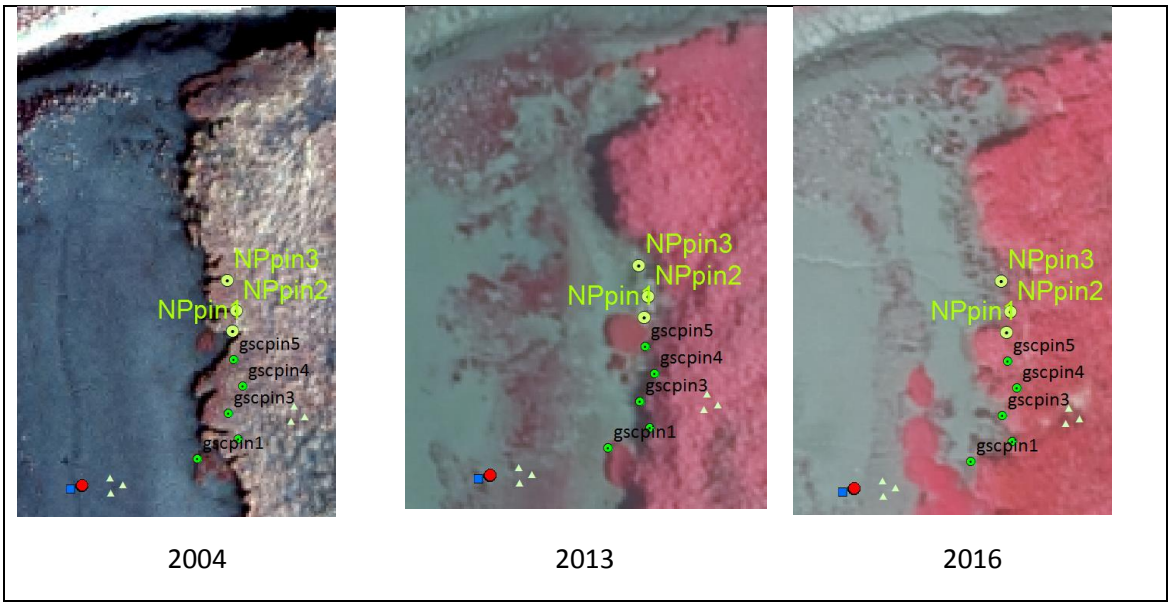

Figure 2.9 Tidal marsh edge retreat measurement locations of the vertical pins of Natuurpunt and the horizontal erosion pins of this campaign at the Southern cross shore profile location (GSc) in the period 2004, 2013 and 2016.

Since August 2016 Natuurpunt member- Hug Van Beek measures the elevation of the tidal marsh edge more in detail near the central cross shore profile GSd using local reference points. Results show that tidal marsh edge retreat is accompanied by erosion of the tidal marsh surface over 3m width. These short term vertical differences in the zone of 2 to 5m from the reference point reflect the instable layer near the marsh edge with periodic sedimentation/ erosion.

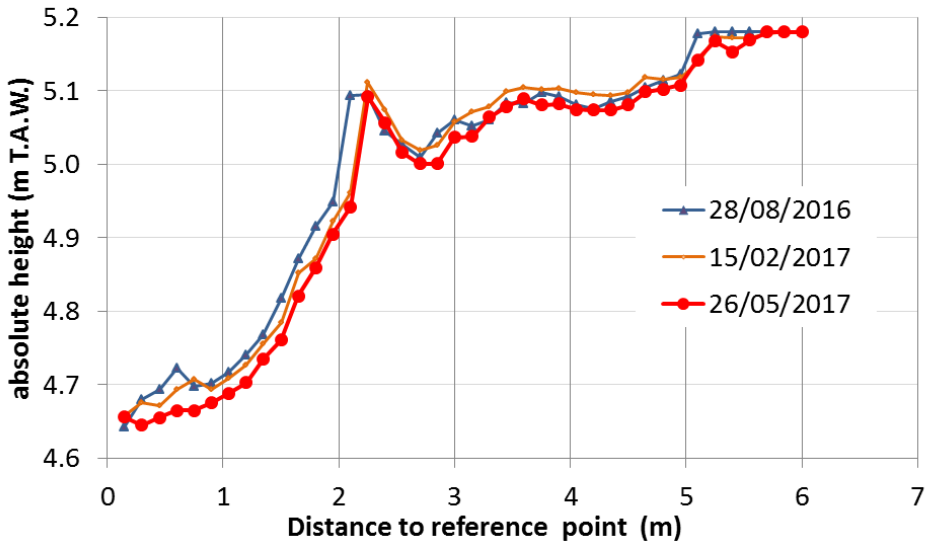

Figure 2.10 Detailed measurements of the tidal marsh edge near the Galgeschoor central cross shore profile location (GSd, data Hug Van Beek-Natuurpunt); local reference points is measured with a RTK-GPS

//

2.2 RESEARCH STATIONS FOR THIS STUDY (2015 – 2017): TRANSECTS GSB (N) AND GSC (S)

Of the above shown cross shore profiles, two were selected for this study: a northern transect GSb (Figure 2-3 top), in the fetch of the potential location for a new tidal dock (Saeftinghe dock –SDK or GSb) (see also Figure 2-1) and a southern transect called DGK or GSc (Figure 2-3 bottom), in the fetch of the Deurganck dock (see also Figure 2-1). These two transects are similar to those already mentioned in Verelst et al. (2011 & 2012), Michels et al. (2012), Silinski & Temmerman (2016), Kolokythas et al. (2016), Belliard & Temmerman (2017) and Levy (2017). The location of these transects was chosen in order to (i) analyse the effect of the evolution of ship traffic near the Deurganck dock after the opening of the Kieldrecht lock on wave climate intensity and (ii) collect information as a reference situation near the location of the planned Saeftinghe dock. Additionally, these two locations allow gaining insights into differences between ship wave and wind wave characteristics. These transects cover an elevation gradient of about 5 m, extending from approximately 0.5 m TAW on the low tidal flat to about 5.5 m TAW on top of the cliffed marsh edge, although slight elevation changes may occur between years (see Table 2-1).

Table 2.1 Overview of the coordinates and elevations of the different plots for the two measurement transects recorded by a Real Time Kinematic Global Positioning System (RTK-GPS). Coordinates are given in WGS 1984. Note that elevations of the plots located in the tidal flats were recorded at the start of each of the two intensive campaigns, i.e. in November 2015 and November 2016.

Transect	Location	Plot ID	Latitude (°N)	Longitude (°E)	Elevation (m TAW)	
					Nov. 2015	Nov. 2016
North (GSb)	Marsh	GSb1	51.318087944	4.282887075	5.50	-
	High flat	GSb2	51.318101220	4.282651453	5.00	5.00
	Middle flat	GSb3	51.318149699	4.281687978	1.20	-
	Low flat	GSb4	51.318193706	4.280844119	0.57	0.56
South (GSc)	Marsh	GSc1	51.309393794	4.283916865	5.69	-
	High flat	GSc2	51.309330421	4.283657855	4.69	4.66
	Middle flat	GSc3	51.309058105	4.282691246	2.69	2.57
	Low flat	GSc4	-	-	1.11	1.11

doi.org/10.21436/inbor.17169167

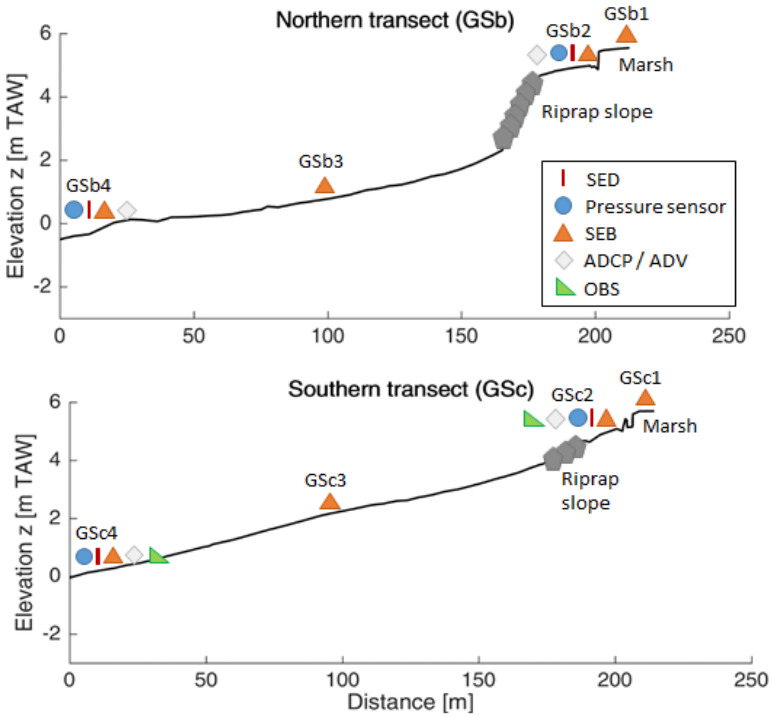

Figure 2.11 Topographic profiles of (top) the northern (GSb) transect and (bottom) the southern (GSc) transect. These profiles were processed using elevation data recorded with the help of a RTK GPS on November 3rd 2015 (at the start of the 2015 intensive measurement campaign). The displayed experimental set-up corresponds to that during the 2016 intensive campaign (see Kolokythas et al. (2016), Belliard & Temmerman (2017) and Levy (2017)).

Measurements performed at the transects

The measurements performed at the research stations including the current study have been performed from 2010 untill 2017. Two types of data have been collected: data on morphodynamics over the whole research period with more frequent measurements in 2010-2011 (Michels et al. 2012, Verelst et al. 2012) and 2015-2017 in the current study. Very detailed data of a large number of variables (see further) were collected during two intensive measuring campaigns in October 2015 and October 2016.

The variables/parameters measured or collected for this study are listed in Table 2-2.

Table 2.2 Summary table of the measured variables/parameters during the measurement campaign. NIOZ: Netherlands Institute of Sea Research; INBO: Research Institute for Nature and Forest; UA: University of Antwerp; FHR: Flanders Hydraulics Research; HA: Antwerp Port Authority; SRK = Schelde Radar Keten.

Measurement	Respons-ible	Location	Duration	Frequency	Measurement principle	Comments
Horizontal changes of the marsh edge	INBO	GSb transect GSc transect	5/2010 – 9/2017	1 month *(1 year)*	Erosion pins	Deployed at low, middle, high tidal flat and marsh plots
Elevation changes	INBO	GSb transect GSc transect	5/2010 – 9/2017	1 month *(1 year)*	SEB	Deployed at low, middle, high tidal flat and marsh plots
Elevation changes	INBO	GSb transect GSc transect	5/2010 – 9/2017	1 month *(1 year)*	RTK GPS measuremen ts	Cross-shore profiles
Elevation changes	NIOZ	GSb transect GSc transect	11/2015 – 05/2017	1 day	SED sensors (Phototransis tors)	Deployed at low and high tidal flat plots
Sediment characteristi cs	INBO	GSb transect GSc transect	11/2015 – 01/2017	1 month	Sediment samples	Performed at all tidal flat and marsh plots
Waves	UA	GSc transect	11/2015 – 05/2017	16 Hz	Pressure transducers (PDCR 1830)	Deployed at GSc4 and GSc2
Waves	FHR	GSb transect GSc transect	11/2015 ; 11/2016	20 Hz	Pressure transducers (OSSI-010-003B/C)	Deployed at GSb4, GSc4 and GSc3
Water velocities	UA INBO	GSb transect GSc transect	11/2016	1 month	Point velocity measuremen ts (ADV)	Performed at both high tidal flat plots
Water velocities	FHR	GSb transect GSc transect	11/2016	1 month	Profile velocity measuremen ts (ADCP)	Performed at both low tidal flat plots
Turbidity	UA INBO	GSc transect	11/2016	1 month	LISST OBS	Deployed at GSc4 and GSc2
Wind	HA	Zandvliet	11/2015 – 01/2017	1 min		10 m above ground level
Water level	FHR	Zandvliet Liefkenshoek	11/2015 – 05/2017	1 min	Radar (OTT-RLS)	MONEOS
Ship traffic	SRK	Region of Galgeschoor	11/2015 – 01/2017	Ship dependent		GSb and GSc transects define entry lines for ship passages
Turbidity	FHR	Lillo	11/2015 – 01/2017	10 min	Aanderaa Seaguard	MONEOS

doi.org/10.21436/inbor.17169167

3 MORPHODYNAMICS

3.1 LONG-TERM MORPHODYNAMICS

3.1.1 Ecotope evolution

Some patterns in ecotope surface area changes can be identified based on the ecotope maps which are since 2009 yearly made for the lower Sea-Scheldt by INBO within the MONEOS monitoring program (Figure 3.1). Since 2009 an initial increase of low tidal flat area occurred. Due to sedimentation some low tidal flat zones evolved in the period 2012-2014 to middle tidal flat (see chapter 3.1). Since 2014 this evolution has reversed. More recently soft bottom low tidal mudflat is eroded exposing bigger areas of natural hard substrate areas of an old peat layer.

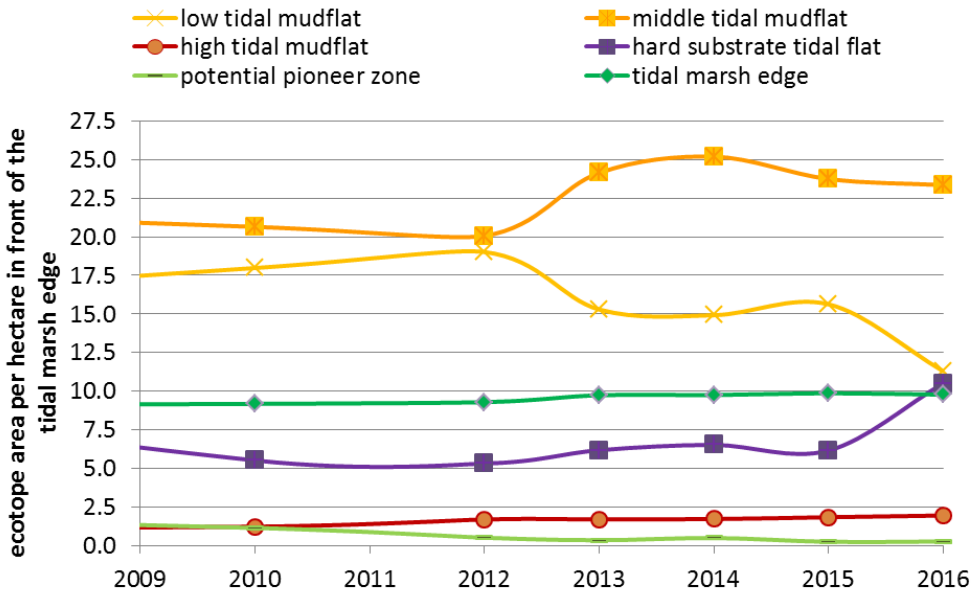

Figure 3.1 Ecotope evolution in the marsh edge zone of Galgeschoor and Tidal marsh edge erosion at erosion tongues at the Southern cross shore profile location (GSc) in the period 5/2010 -9/2017)

Despite the relative stability of the tidal marsh ecotopes in the marsh edge neighbourhood (based on MONEOS Ecotopemaps Van Ryckegem et al. 2017; Table 3.1), the proportion of higher old marsh area decreases as a results of tidal marsh edge retreat (Figure 2.8). At the same time pioneer marsh vegetation area increases partly by a conversion of high mudflat with *Vaucheria* algae mats to *Glaux maritima* vegetation, partly by reed outgrow (unpublished data on vegetation 2003-2013; Vandevoorde in Van Ryckegem et al. 2016). The expansion of *Glaux maritima* especially in the northern part of the Galgeschoor is illustrated in Figure 3.2 Evolution of the tidal marsh in summer at the northern cross shore profile location (GSb) in the period 9/2003 -7/2016)Figure 3.2 and Figure 3.3). The expansion of reed also occurred at the northern GSb marsh edge location due to a local decrease of grazing impact by cattle and/or horses.

Table 3.1 Net area change of tidal flat and marsh ecotopes near the marsh edge of Galgeschoor since 2010

Ecotope		To reference 2010 (ha)				
		2012	**2013**	**2014**	**2015**	**2016**
tidal flat	natural hard substrate tidal flat	-0.2	+0.7	+1.0	+0.6	+5.0
	low tidal mudflat	+1.0	-2.7	-3.1	-2.4	-6.7
	middle tidal mudflat	-0.6	+3.5	+4.6	+3.1	+2.7
	high tidal mudflat	+0.5	+0.5	+0.5	+0.6	+0.7
	potential pioneer zone	-0.6	-0.8	-0.7	-0.9	-0.9
Marsh	tidal marsh edge	+0.1	+0.6	+0.6	+0.7	+0.6

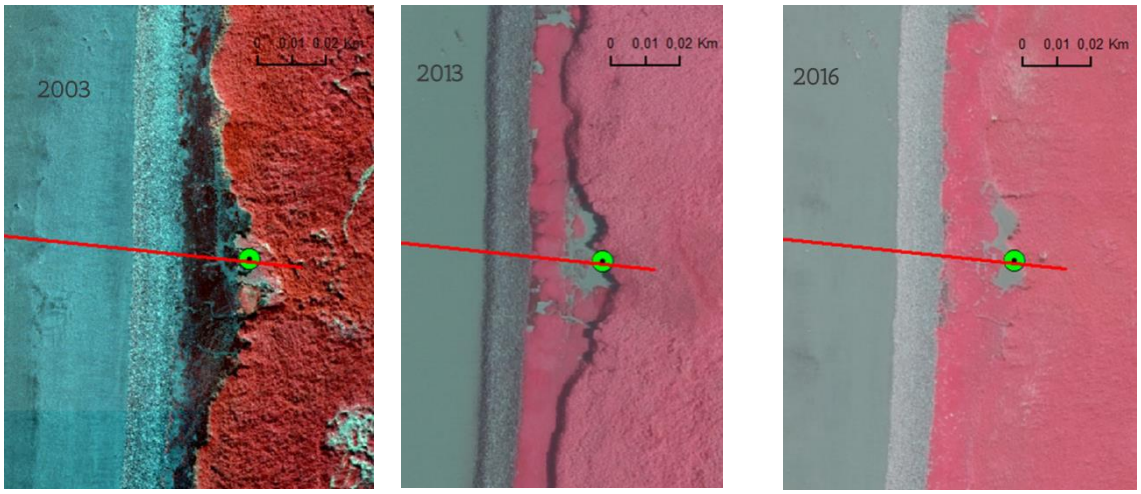

Figure 3.2 Evolution of the tidal marsh in summer at the northern cross shore profile location (GSb) in the period 9/2003 -7/2016)

doi.org/10.21436/inbor.17169167

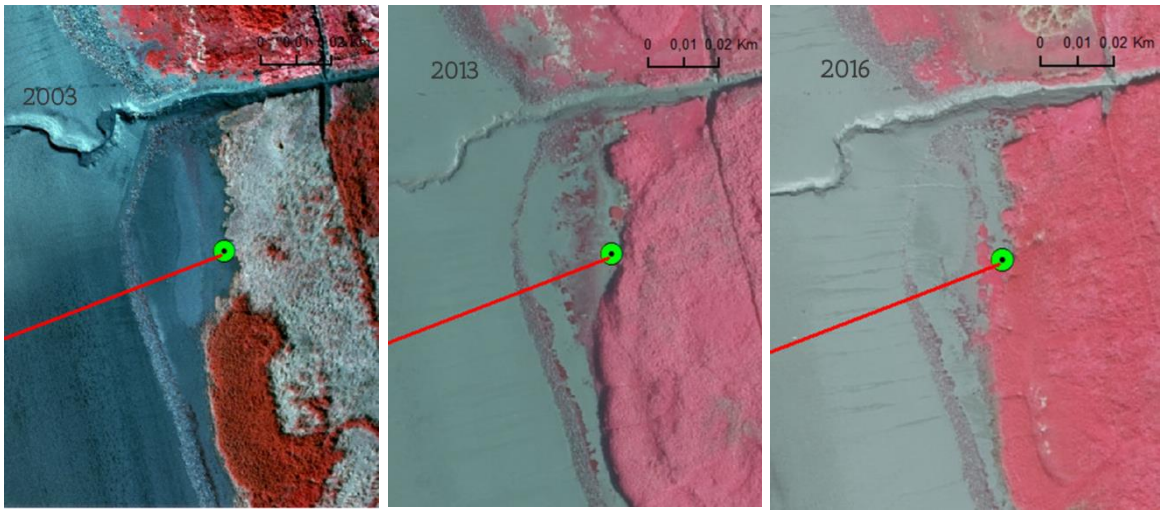

Figure 3.3 False-colour images at summer conditions showing evolution of the tidal marsh at the Southern cross shore profile location (GSc) in the period 9/2003 -7/2016

Especially at the northern plot, since 2011 an increasing abundance (Figure 3.4) of Vaucheria and the higher plant pioneer vegetation *Glaux maritima* in front of the marsh cliff can be found.

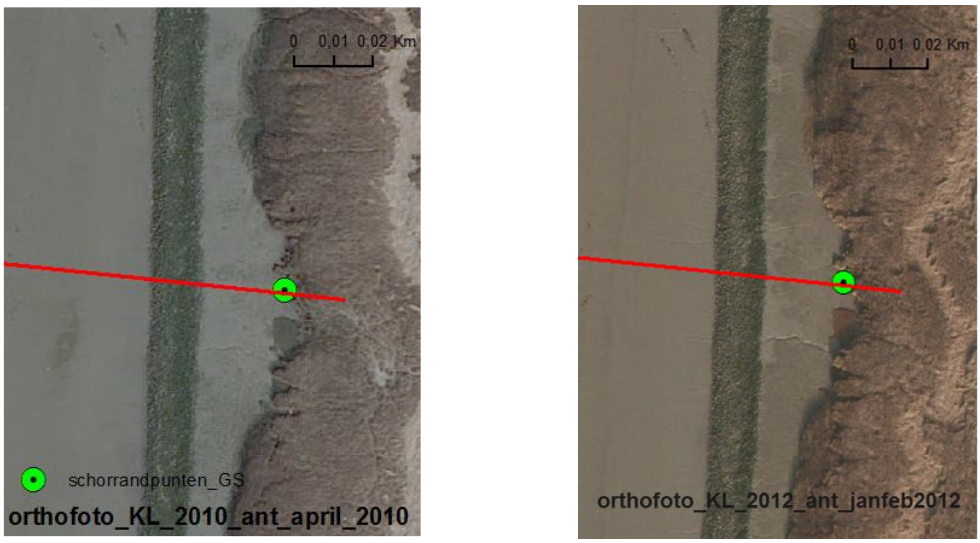

Figure 3.4 True colour areal image at winter conditions of high tidal flat and pioneer zone with increasing cover of *Vaucheria* and *Glaux maritima* (darker zones between the rip rap and marsh cliff)

3.1.2 Horizontal morphological changes

In 2010 INBO started to monitor the tidal marsh edge retreat with horizontal pins at 5 random locations for both the southern and northern transect (Michels et al. 2012). A difference in retreat rate between the transects (Figure 3.5) was found. A low retreat rate of 2.5cm/ year occurred at the northern transect while at the southern transect the marsh edge retreats with 14.6cm/year. Marsh edge retreat is a discontinuous process: the period of strongest erosion occurred in the first 2 years (2010 – 2012) with a retreat rate of 31.7cm/year. In the last 2 years with the commissioning of Kieldrechtlock the retreat rate has slow down to less than a cm per year.

//

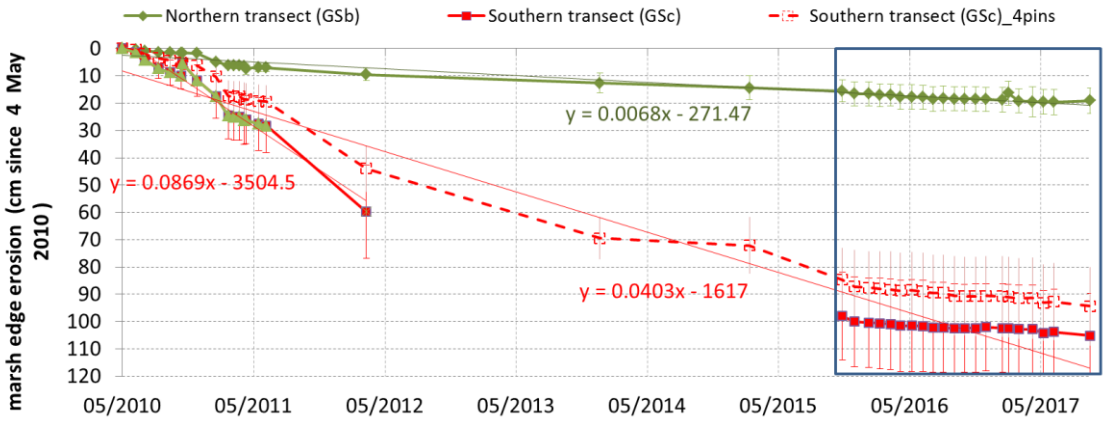

Figure 3.5 Tidal marsh edge retreat (horizontal erosion, cm + SE) at the Northern and Southern cross shore profile location in the period 5/2010 -9/2017, rectangle focuses on the study period

doi.org/10.21436/inbor.17169167

3.1.3 Vertical morphological changes

Also vertical changes differ between the southern and northern transect. In general tidal marshes raise similar to the rise of the mean high water level. In a period of mean high water raise of nearly 3cm, the mean elevation of the marsh at the northern GSb1 increased parallel with 2.25cm. This in contrast with the tidal marsh plot at the southern GSc1 which increased with 4.7cm between June 2010 and July 2017. Based on these SEB (sedimentation erosion bars) measurement locations in the old *tidal marsh plateau*, mean raising rate at the southern transect (GSc1, 2.26cm/year) is since 2010 two times higher than the northern transect (GSb1, 1.2cm/year). A higher sedimentation rate can result in a higher marsh plateau and marsh cliff which is more vulnerable for erosion in the southern versus the northern location. .

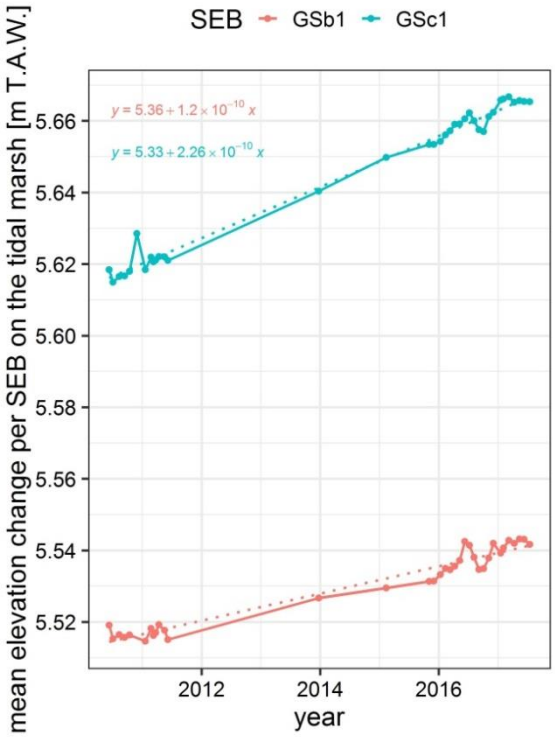

Figure 3.6 Mean elevation changes at the SEB in absolute values (m T.A.W.) in the **tidal marsh** of the northern transect (GSb1, red) and the southern transect (GSc1) in the period 5/2010 -3/2017. The SEB locations are presented in Figure 2-11.

Based on RTK-GPS measurements the different *tidal flat zones* at the two transects show clear differences in sedimentation/erosion patterns (Figure 3-7). To compare temporal changes of mean elevation for fixed zones are used at the start of the measurements t_0 with class boundaries for GSc of 405,365,256/250,230 meters to the dike and for GSb at 325,260,197.5/178, 162 meters to the dike.

The mudflat zones beneath the riprap zone shows at the northern transect (GSb, Figure 3.7) mainly an eroding trend, while the southern transect shows a trend of sedimentation which amplifies downwards along the profile from middle to the low water zone. Conversely the high tidal flats above the riprap zone increases of the northern transect increases while the high tidal flat of the southern transect fluctuates around zero. In 2016 the only change in trend is the middle tidal flat that starts to increase again after a period of slight decrease.

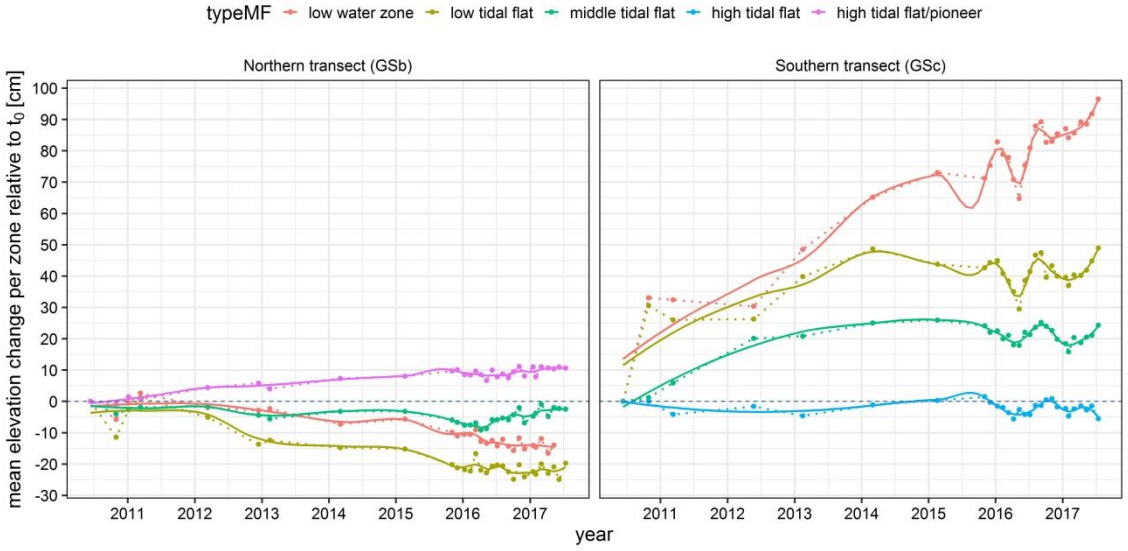

Figure 3.7. Elevation changes along the northern and southern cross shore profile (GSb &c) on the **tidal mud flat** in the period 5/2010 -3/2017

Taking the tidal flat zone area into account along a one meter wide cross shore profile, the total sediment volume balance of each tidal flat zone can be calculated relative to May 2010. In the northern profile the highest sediment volume are lost at the low tidal flat while the high zone traps small volumes of sediment (

Figure 3.8). On the other hand the southern profile traps sediment in the mudflat beneath the riprap zone while above sediment volumes stay stable. Initially the low water zone trapped the highest volumes of sediment but after one year the middle tidal flat is the biggest sediment trap

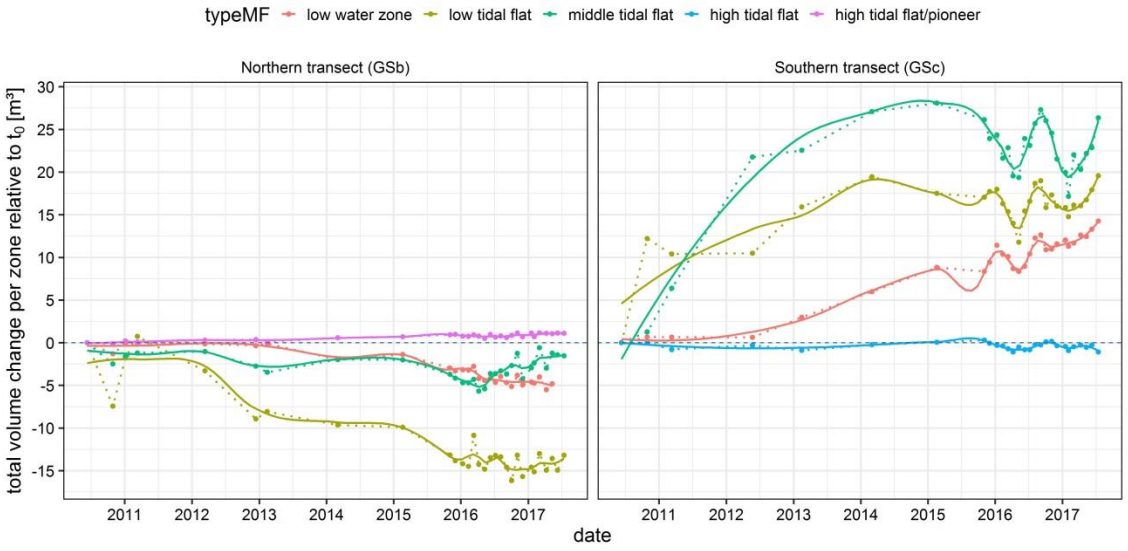

Figure 3.8. Total volume changes along the northern and southern cross shore profile (GSb &GSc) on the **tidal mud flat** in the period 5/2010 -3/2017

doi.org/10.21436/inbor.17169167

3.2 SHORT-TERM DETAILED MORPHODYNAMICS

3.2.1 Horizontal changes: tidal marsh edge retreat

In the last two years, from the end of October 2015 until September 2017, marsh edge retreat is limited with means of 4cm and 8cm at the northern and southern transect, respectively. Except for pin 5 at the southern transect GSc, which eroded 20cm, erosion was of a largely similar magnitude in the northern and southern transect, (Figure 3.9). This pin 5 is the erosion pin most to the north and nearest to the measuring points of Natuurpunt (Figure 2.8).

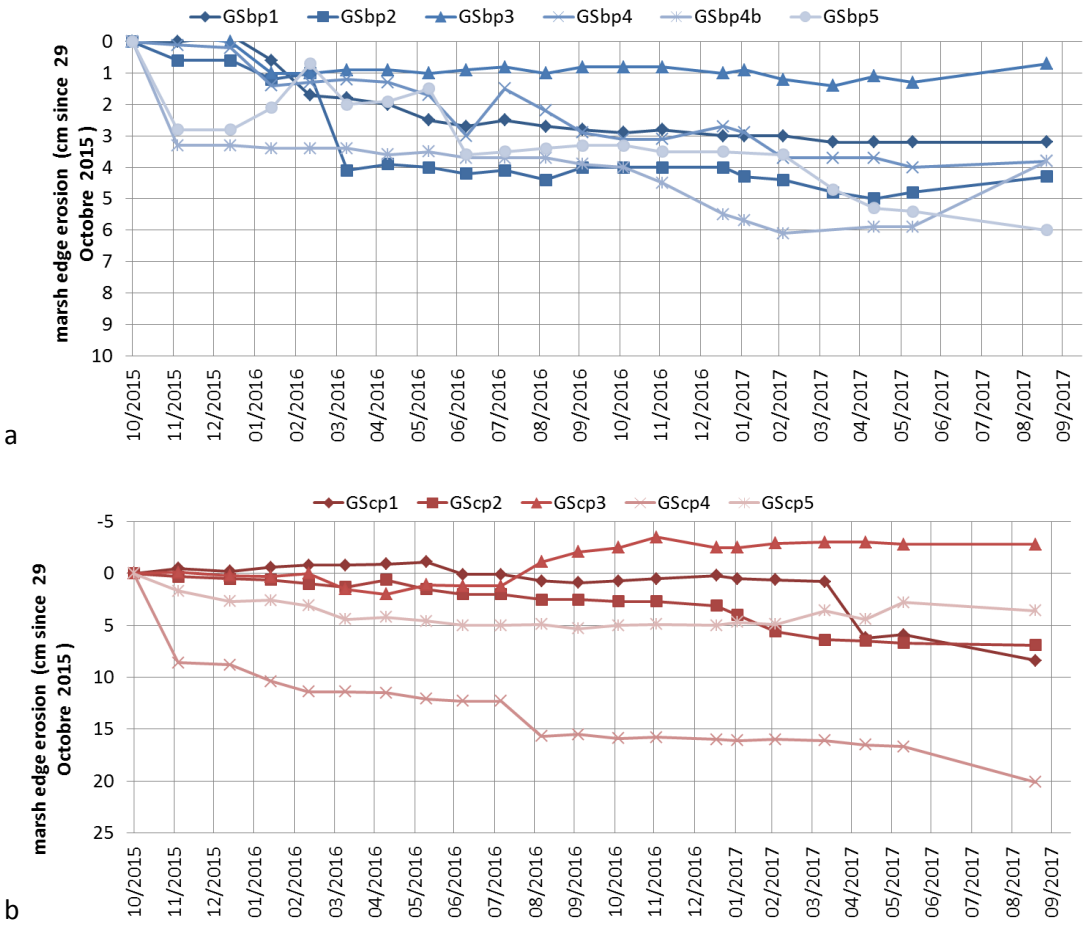

Figure 3.9. Tidal marsh edge retreat at A) the Northern and B) Southern cross shore profile location in the period 10/2015 -9/2017)

Figure 3.10. A) Picture of the marsh edge at the Southern transect B) the horizontal pin in the marsh edge which has retreated 20cm in the period 10/2015 -9/2017)

The retreat of the marsh edge is not constant in time but shows the highest rates in winter (December – January), with often stormy periods (e.g. 2010-2011), or in May-June, at the beginning of the dry summer period and the start of the seasonal shrinkage of the soil.

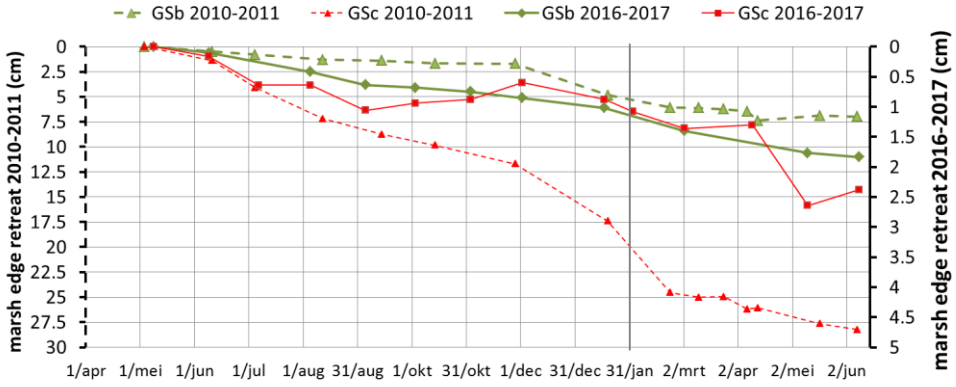

Figure 3-11 Seasonality of marsh edge retreat in the Galgeschoor at the Northern transect GSb and the Southern transect GSc, mention dotted line for period 2010- 2011 (left axis), solid line for period 2016-2017 (right axis)

3.2.2 Vertical morphological changes

Vertical morphological tidal flat changes along the cross shore profiles

The RTK GPS measurements along the cross shore profiles are used to calculate mean bed level (Figure 3.11) and volume changes (Figure 3.12) for 4 elevation classes across the tidal window: low water zone, low tidal flat, middle tidal flat and the high tidal flat (including pioneer zone).

On the short term the different *tidal flat zones* at the two transects show clear differences in sedimentation/erosion patterns (Figure 3.11). The northern transect (GSb) shows a small eroding trend in the low mudflat zones, while the higher zones starts to increase halfway 2016 with a net increase in the summer of 2017. At the southern profile there is more variation in 2016 which evolve in a net increase in the lower mudflat zones, a stable middle tidal flat and a small lowering of the high tidal flat in July 2017 compared to November 2015.

doi.org/10.21436/inbor.17169167

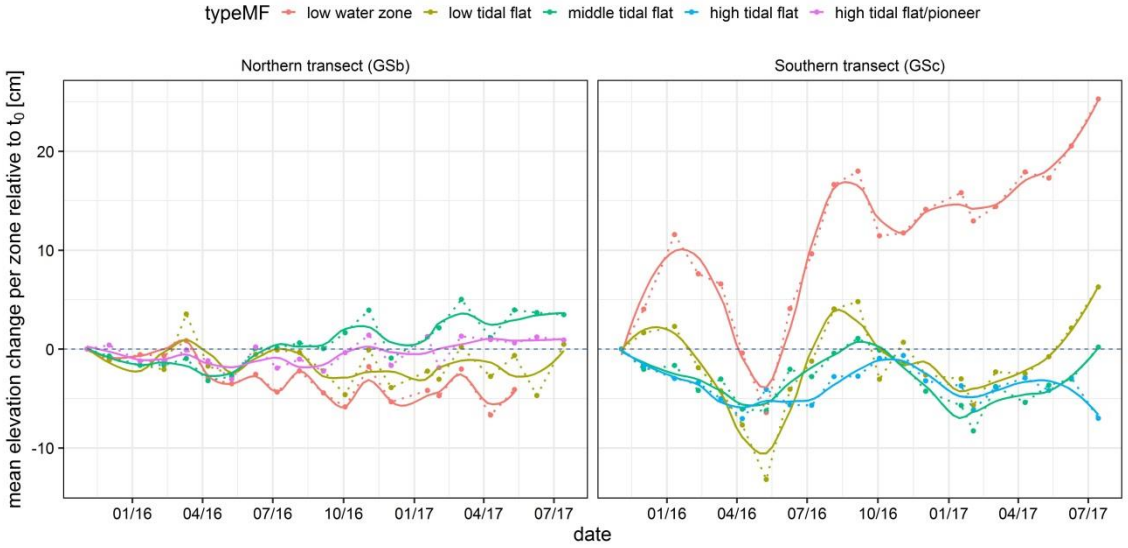

Figure 3.11. Temporal evolution of bed level changes relative to t_0 at the Northern (GSb) and Southern cross shore profile (GSc) in the study period 11/2015 -7/ 2017

Taking the tidal flat zone area into account along a one meter wide cross shore profile, the total sediment volume balance of each tidal flat zone can be calculated relative to the start of this campaign (November 2015, Figure 3.12).To estimate the sediment volumes per fixed zone [1]RTK-measurements are interpolated for every 0.5m to handle the variable distance between field measure points .

At the northern transect sediment volumes are steady in the high tidal flat pioneer zones. In the lower zones sediment volumes shows strong monthly patterns of resuspension and deposition and net more losses of sediment in the low water zone. The middle tidal mudflat has started to trap sediment since June 2016.

At the southern transect there is more variation in 2016 which evolve in a net trapping of sedimentation in the lower mudflat zones. The middle tidal flat shows the highest seasonal variation with a period of sedimentation losses from autumn till spring and a period of sedimentation trapping from spring till autumn. The high tidal flat shows also a seasonal variation but less pronounced.

[1] *zone classe boundaries are for GSc 405,365,256/250,230 meters to the dike and for GSb at 325,260,197.5/178, 162 meters to the dike*

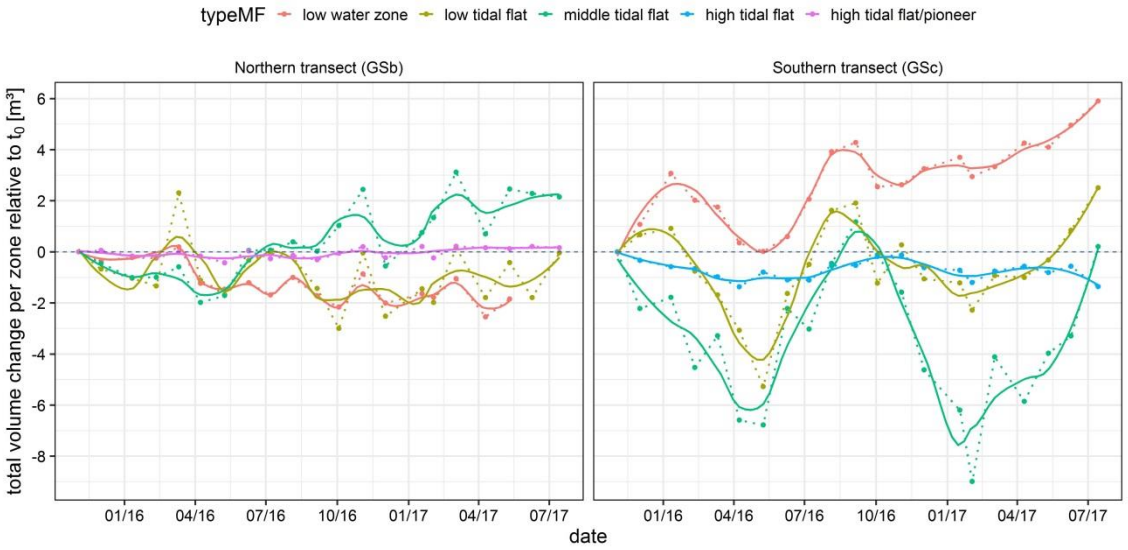

Figure 3.12. Temporal evolution of sediment volume changes relative to t_0 at the Northern (GSb) and Southern cross shore profile (GSc) in the study period 11/2015 -7/ 2017

Vertical morphological changes at the low and high tidal flat stations

The SED measurements performed at the low (GSb4 and GSc4) and high (GSb2 and GSc2) tidal flat plots during the long-term campaign, i.e. from November 2015 to May 2017, indicate clearly different temporal bed level changes (Figure 3.13). Generally, low tidal flat plots show more pronounced seasonal bed level changes compared to their respective high tidal flat counterparts.

These seasonal patterns are also apparent in the SEB-derived monthly bed-level changes at GSc2 and GSc4, and to a lesser extent GSb2, in 2015-2017 (Figure 3.13). This seasonal pattern may be a truly recurrent phenomenon, which is shown by the SEB-derived monthly bed level changes measured from June 2010 to June 2011 at the high tidal flat plots (GSb2 and GSc2) where a similar temporal pattern is revealed. This is illustrated in a photo sequence in Figure 3.14.

All sites also exhibit short-term (daily) fluctuations, that are larger at the low compared to the high tidal flat plots. Both seasonal and day-to-day bed level changes scale larger than any longer-term trend present in the data during 2015-2017. The northern low plot, however, may be prone to a decreasing trend of bed level during the two studied years. These results indicate the need for long term but also frequent data on erosion and sedimentation. Infrequent snapshot measurements are liable to large inter-seasonal or even inter-daily variation which makes them relatively insensitive and slow for detecting changes, especially at the dynamic lower section of the tidal flats.

doi.org/10.21436/inbor.17169167

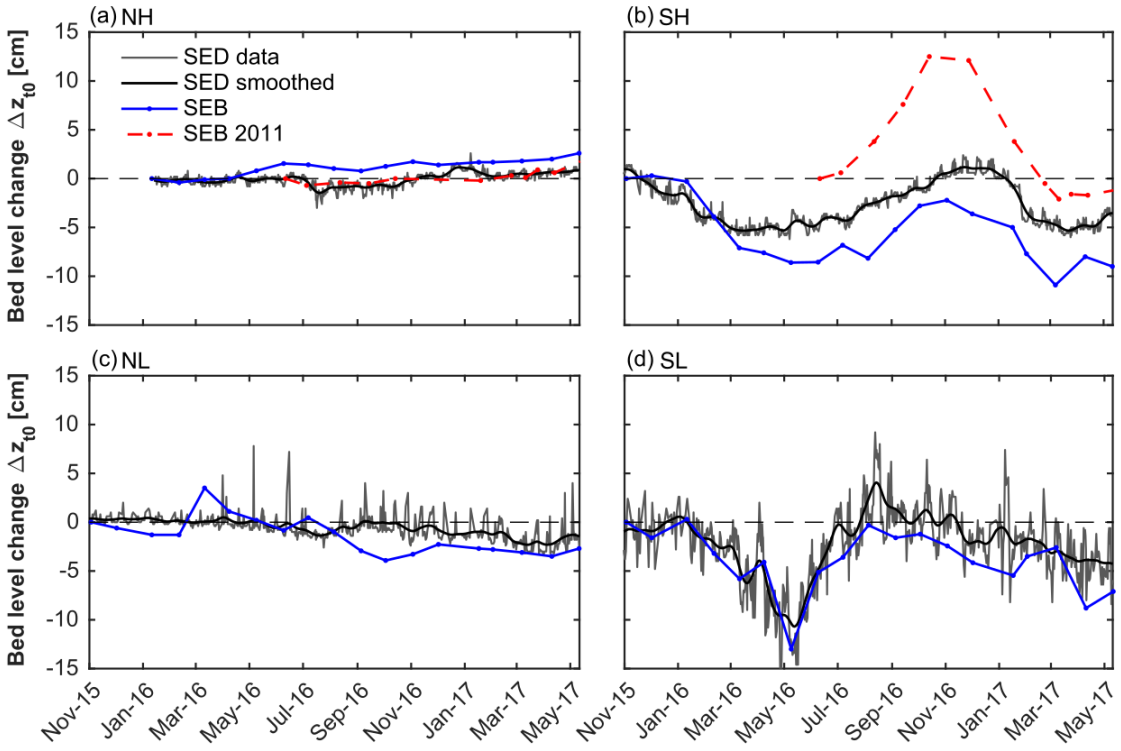

Figure 3.13. Temporal evolution of SED-derived (grey lines) and monthly SEB-derived (blue dotted lines) bed level changes relative to t_0 (Δz_{t0}) recorded at the (a) northern high (NH- GSb2), (b) southern high (SH GSc2), (c) northern low (NL- GSb4) and (d) southern low (SL-GSb4) tidal flat measurement stations during the long-term campaign (i.e. from October 29 2015 to May 11 2017). The absence of bed level data at NH at the beginning of the field campaign was due to a technical failure of the corresponding SED sensor. Every SED-derived bed level change time series was smoothed out using a weighted moving average with a Gaussian window of 1 month (black lines). Time evolution of monthly SEB-derived bed level changes monitored at NH – GSb2 and SH – GSc2 as part of a previous field campaign from June 2010 to June 2011 (red dotted lines) are displayed for comparison. For all data series, negative values represent net erosion and positive values represent net deposition. Note that the corresponding SEB plot and SED sensor were deployed at the same exact location at site SL, while at the other sites, the respective SEB plot and SED sensor were placed a few meters apart.

Figure 3.14. Photo sequence of SEB plot on the high tidal flat of (a) the northern transect and (b) the southern transect between December 2016 and January 2017 on moments of a changing bed level trend

Location dependent cohesion characteristics of the upper sediment layer

In the tidal marsh plot the median grain size throughout the long-term campaign is lower than 63µm (Figure 3.15) which classifies it as fine silt, a rather cohesive sediment-type[2]. The median grain size of the upper 2cm sediment layer is higher, thus including more sand, at the southern marsh plot (GSc1) than at the northern marsh plot (GSb1). Sediment composition at the high tidal flat (GSb2 and GSc2) is very similar to that of the marsh at the northern plot while at the southern plot it is more variable, sometimes finer and at other times coarser.

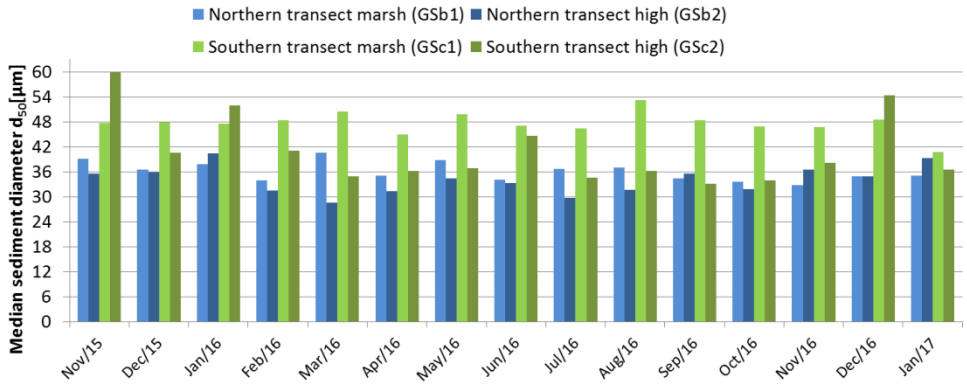

Figure 3.15. Temporal evolution of the median grain size diameter d50 of the upper 2cm in sediment samples collected monthly *at the tidal marsh* (GSb1 and GSc1) and *high* (NH-GSb2 and SH-GSc2) *tidal flat* plots of the two measurement transects. Samples collect sediment from the upper 2cm.

In the tidal flat plots (Figure 3.16), the mud fraction (i.e. d < 63µm) at the GSb2, GSb4 and GSc2 accounts for more than 50 % of the total sediment composition throughout the long-term campaign, implicating that cohesion between sediment grains in these locations is rather important. Sediment composition at GSc4 on the other hand is characterized by a dominant sand (non-cohesive) fraction throughout the whole campaign. This is also reflected in the grain size distribution with the median sediment diameter at GSc4 being always above the threshold diameter d_{50} = 63 µm (Figure 3.16).

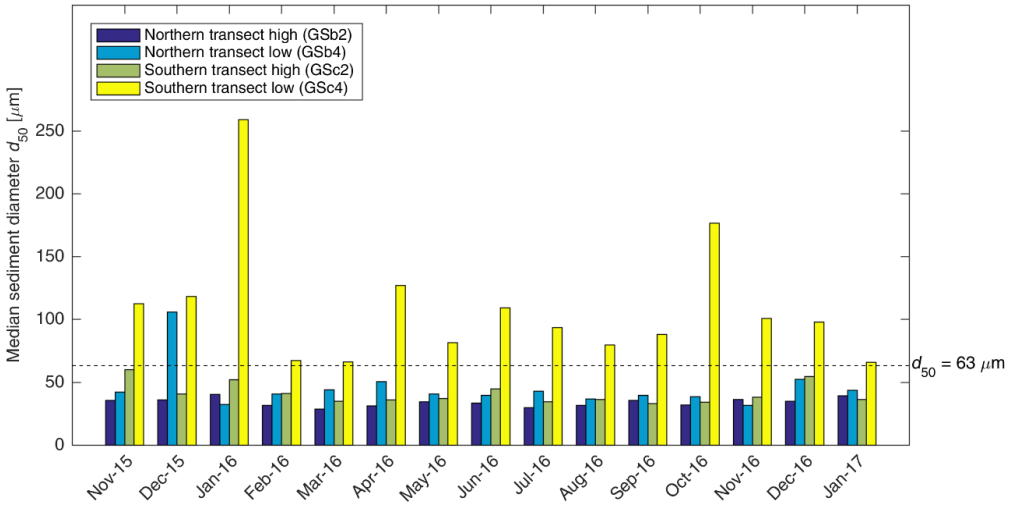

Figure 3.16. Temporal evolution of the median sediment diameter d_{50} of sediment samples collected monthly at the northern high (NH-GSb2), northern low (NL-GSb4), southern high (SH-GSc2) and southern low (SL-GSc4) tidal flat measurement

[2] *The cohesiveness is above all determined by the percentage of clay in mud (with 5-10% of clay being the threshold above which the sediment starts to behave cohesively).*

doi.org/10.21436/inbor.17169167

stations. Sediment samples were collected up to a depth of 2 cm from the surface. Sediment grain size was determined using LDPSA. The dash line $d_{50} = 63$ µm defines the limit between cohesive and non-cohesive sediments based on the grain size distribution.

Periodicity in detrended morphological data at the tidal flat stations

Spectral analysis applied to the detrended (deseasonalized) bed level changes (i.e. by consecutive differencing) allow to further investigate recurrent patterns (periodicity) in the short-term (daily) fluctuations in bed level changes (Figure 3.17).

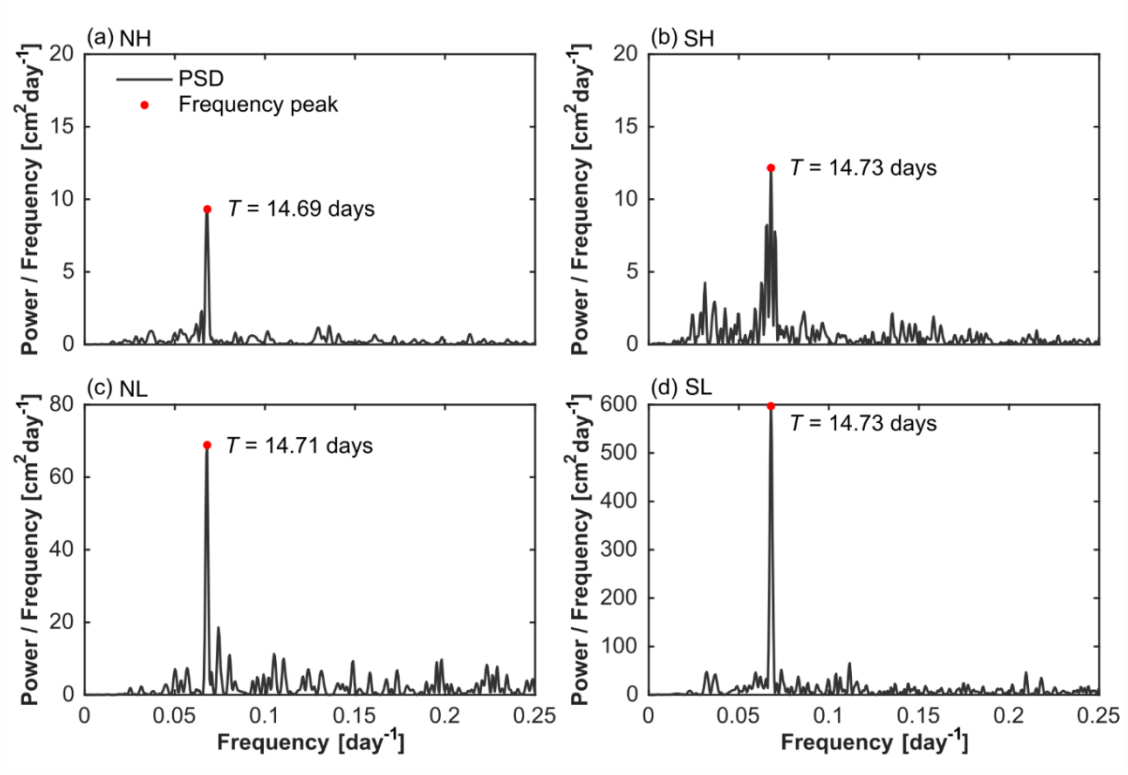

Figure 3.17 Lomb-Scargle power spectral density (PSD) of the detrended bed level changes recorded at the (a) northern high (NH, GSb2), (b) southern high (SH, GSc2), (c) northern low (NL, GSb4) and (d) southern low (SL, GSc4) tidal flat measurement stations during the long-term campaign (i.e. from October 29 2015 to May 11 2017). Main frequency peaks occurred precisely at (a) $f = 0.068$ days^{-1} ($T = 14.74$ days) for NH, (b) $f = 0.068$ days^{-1} ($T = 14.73$ days) for SH, (c) $f = 0.067$ days^{-1} ($T = 14.76$ days) for NL and (d) $f = 0.068$ days^{-1} ($T = 14.73$ days) for SL.

A highly significant frequency peak, corresponding to a fortnightly period (i.e. T~ 14.7 days), occurred at the low stations SL-GSc4 and NL-GSb4 (the latter to a lesser extent). This observed fortnightly periodicity suggests the presence of a spring–neap tidal signature in the daily fluctuations of bed level changes at the low tidal flat. Comparatively, the same primary frequency peak in the daily bed level changes was much less pronounced at the high tidal flat stations SH-GSc2 and NH –GSb2.

To examine the temporal evolution of the strength of the observed fortnightly periodicity present at the low tidal flat, Figure 3.18 shows the continuous wavelet power spectrum performed on the corresponding detrended and interpolated bed level changes. The power of

this fortnightly periodicity at SL - GSc4 varies in time with the occurrence of peaks in March – June 2016, August – September 2016 and January – February 2017, as illustrated by the respective clusters of high wavelet power. This fortnightly periodicity also depicts a time variability at NL-GSb4, yet with a much lower power globally and with peak periods not necessarily coinciding with those observed at SL- GSc4.

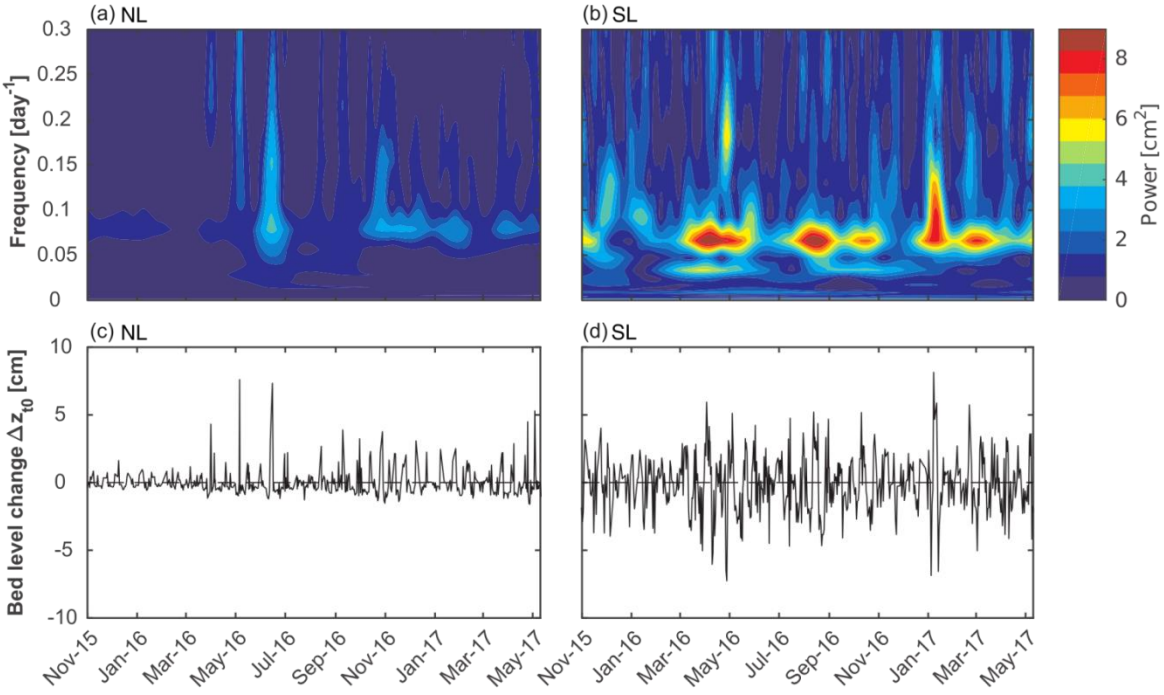

Figure 3.18 Wavelet power spectrum of the detrended bed level changes recorded at the (a) northern low (NL) and (b) southern low (SL) tidal flat measurement stations during the long-term campaign (i.e. from October 29 2015 to May 11 2017), and supplemented with corresponding time series of detrended bed level changes at the low tidal flat plots (c) NL-GSb4 and (d) SL-GSc4.

doi.org/10.21436/inbor.17169167

3.3 CONCLUSIONS ON MORPHODYNAMICS

The morphodynamics chapter starts with the general ecotope evolution, includes horizontal changes at the tidal marsh edge and focuses on vertical changes at the tidal flats on different time scales.

Due to high morphodynamics at the Galgeschoor the area of soft bottom low tidal mudflat **ecotopes** evolved to middle tidal mudflats in the period 2012-2013 and in low tidal hard substrate zones in the period 2015-2016. Tidal marsh ecotope areas near the marsh edge neighbourhood seem relatively stable.

Tidal marsh edge retreat clearly differs between the northern and southern transect with respectively long term retreat rates of 2.5 and 14.6 cm/ year since 2010 with the biggest losses before 2013. Consequently the proportion of high solid old marsh plateau area decreases. However in the same period pioneer marsh vegetation seems to establish along the marsh whether or not temporarily. In the last 2 years the retreat slowed down except for the most north erosion pin at the Southern transect near the Natuurpunt marsh retreat measurement points.

At the long term the northern transect the bed level of the high tidal flat tended to increase and traps small volumes of sediment while the tidal mudflat zones beneath the riprap decreased and lost sediment volume. The southern transect has shown an opposite trend with bed levels of lower mudflats increasing, trap large sediment volumes while the high tidal flat fluctuates around zero. The sediment trapping at the southern transect in the tend to slow down since 2014 and the net increase stopped since 2016 at the middle and high mudflat. At the northern transect only the middle tidal mudflat level trend changed since 2016 and started to increase.

In general, **bed level changes** at the southern plots were much more pronounced (order of magnitude 5 – 10cm) than those at the northern plots (<5cm), difference in sediment properties can be a reason. Both seasonal and day-to-day variation were clearly larger at the southern plots of Galgeschoor. This means that the southern transect was more dynamic. Further, low tidal plots were much more dynamic than high tidal plots. The seasonal variation at southern transect knows a period of sedimentation between spring and autumn while between autumn and spring mostly erosion takes place. The daily fluctuations in bed level in the low and less pronounced in the high tidal flat plots reveals a spring-neap tidal cycle signature (i.e. 14.77 days).

doi.org/10.21436/inbor.17169167

4 HYDRODYNAMICS

4.1 TIDAL CURRENTS ON THE LOW TIDAL MUDFLAT

Velocity profile measurements are performed using Acoustic Doppler Profile (ADCP). These ADCP's were installed on the low tidal flat during the two intensive measuring campaigns. An overview of the data is shown in the analysis reports (Kolokythas et al. 2017, Levy et al. 2018). Here, we focus on the maximal velocities measured during the ebb and flood phase, as we are mainly interested in the potential influence of the tidal current on the morphological changes (Figure 4.1, Figure 4.2).

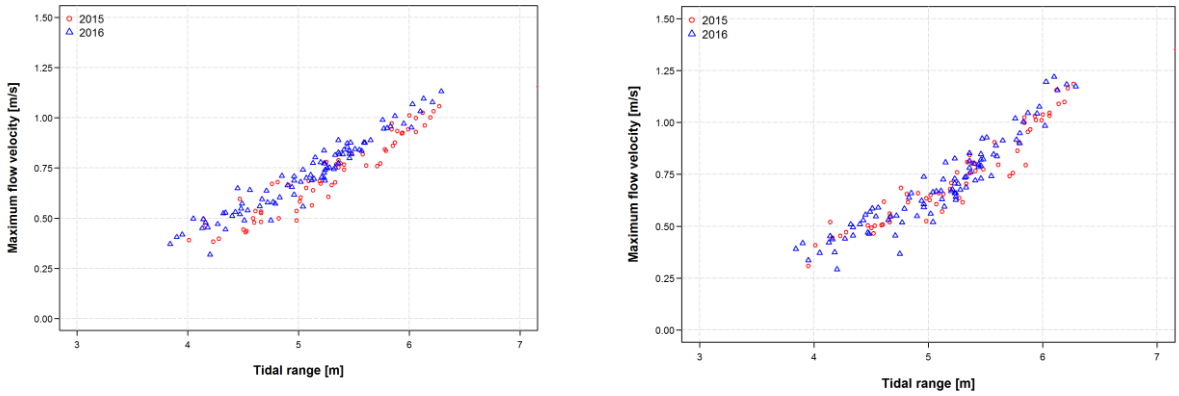

Figure 4.1: Relation between tidal range [m] and maximum flow velocities [m/s] at the low plot of the northern transect (left) and southern transect (right) in the flood phase. Values from 2015 are indicated in red, values from 2016 are indicated in blue

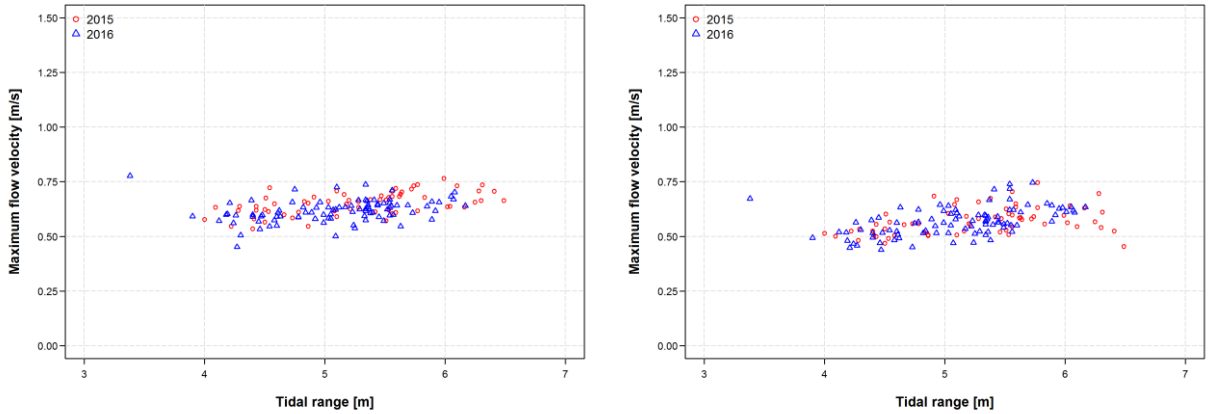

Figure 4.2: Relation between tidal range [m] and maximum flow velocities [m/s] at the low plot of the northern transect (left) and southern transect (right) in the ebb phase. Values from 2015 are indicated in red, values from 2016 are indicated in blue.

For the ebb phase, the maximum values range between 0.5 and 0.75 m/s, quasi independent of the tidal range. For the flood phase however, the relation between the tidal range and the maximum flow velocities is strong (Table 4.1). Over the measured range of tidal ranges, between approximately 4 and 6.5 m, the maximum velocities almost triple from ca. 0.40 m/s up to 1.25 m/s. As the bed shear stress scales with the squared value of the velocity, the potential for erosion because of the tidal currents increases clearly in the spring tides on the

(low) tidal flats of the Galgeschoor. In general, no clear (statistical) distinction can be made between the measured values for 2015 and 2016.

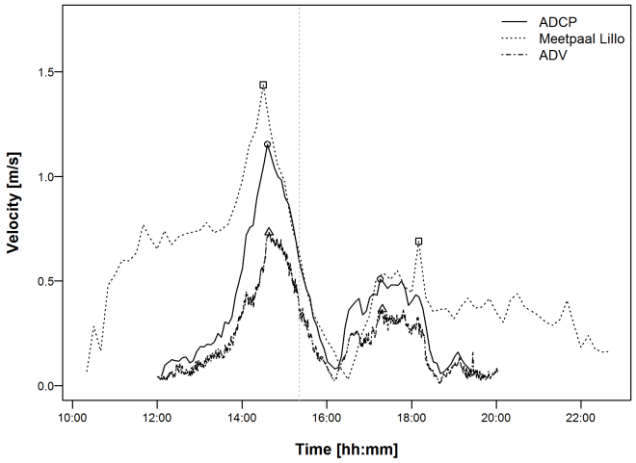

Figure 4.3 Velocity measurements with ADCP (solid line) and ADV (dashed line) on the lower tidal flat and measurements at Meetpaal Lillo (dotted line). The vertical line indicates the moment of high water at Liefkenshoek. The shown ADV measurements are averaged values over 1 minute.

Table 4.1 Overview of the slopes and the coefficient of determination of the linear relationships (y = ax+b) between the tidal range and maximum depth-averaged velocities in 2015 and 2016 for both transects.

	Northern transect		**Southern transect**	
	Flood	*Ebb*	*Flood*	*Ebb*
2015	0.329 (R^2 = 0.81)	0.034 (R^2 = 0.11)	0.276 (R^2 = 0.86)	0.072 (R^2 = 0.06)
2016	0.303 (R^2 = 0.93)	0.025 (R^2 = 0.06)	0.342 (R^2 = 0.81)	0.058 (R^2 = 0.24)

In addition to the ADCP measurements conducted at the low tidal flat, velocity measurements are also performed at the high tidal flat for this intensive campaign using Acoustic Doppler Velocimeters (ADV). Table 4.2 displays the mean, minimum and maximum ebb and flood peak velocities recorded throughout the current measurement campaign.

doi.org/10.21436/inbor.17169167

		Northern transect GSb4	Southern transect GSc4	
		ADCP	ADV	ADCP
Ebb	*Mean*	0.62 (*0.65*)	0.22	0.57 (*0.56*)
	Min	0.45 (*0.53*)	0.17	0.43 (*0.45*)
	Max	0.77 (*0.76*)	0.30	0.75 (*0.74*)
Flood	*Mean*	0.72 (*0.71*)	0.22	0.69 (*0.75*)
	Min	0.32 (*0.37*)	0.13	0.12 (*0.32*)
	Max	1.13 (*1.15*)	0.28	1.22 (*1.34*)

Table 4.2 Overview of the minimum, mean and maximum ebb and flood peak velocities of the ADV near the ground and ADCP with depth-average flow velocities (m/s) at the Northern and Southern transect at the intensive campaign of 2015 (italic) and 2016.

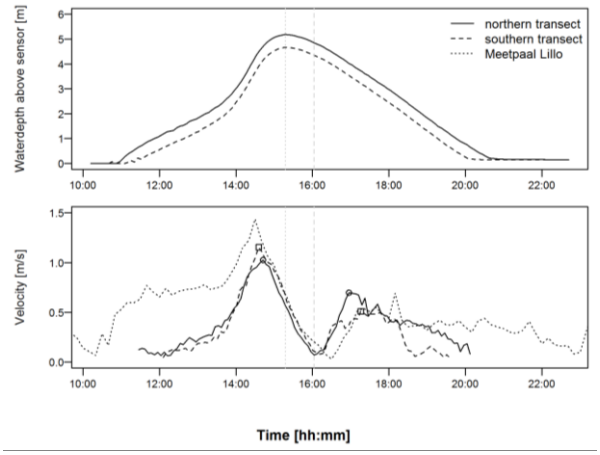

Figure 4.4: Water level above the ADCP measurements (top). Depth-averaged flow velocities on the low tidal flat (GSc4) for both the northern and southern transect at the intensive campaign of 2015, together with flow measurement near the navigation channel at Meetpaal Lillo

The statistics of ebb and flood peak velocities recorded throughout the intensive 2016 measurement campaign (Table 4.2, Figure 4.4), show approximately the same values for the northern and southern transect. The maximum flood velocities at the southern transect are slightly higher compared to the northern transect. The mean depth averaged ebb velocities are slightly higher on the northern transect, due to the fact that on the southern transect, the velocities are falling back earlier during the ebb phase, as can be observed in Figure 4.7.

In the past, other velocity measurements were performed on a low tidal flat at Galgeschoor, as is described in Verelst et al. (2011a). These measurements were also performed using an ADV instrument, measuring at one measurement point ca. 0.20 m above the bottom, during 2 days. Maximum velocities of 0.7 m/s were recorded during the flood phase. During the ebb phase, lower velocities were measured (0.4 to 0.5 m/s).

4.2 WIND WAVE REGIME

4.2.1 Long-term wind regime

The long-term (October 2015-February 2017) prevalence of wind direction for five wind speed categories is shown in (Figure 4.5). Overall, wind came primarily from SSE to WSW and to a lesser extent from ENE to E. High wind speeds (>10m/s), however, were exclusively recorded from South-Westerly to Southerly directions. Figure 4.6 shows the seasonal variation in wind direction.

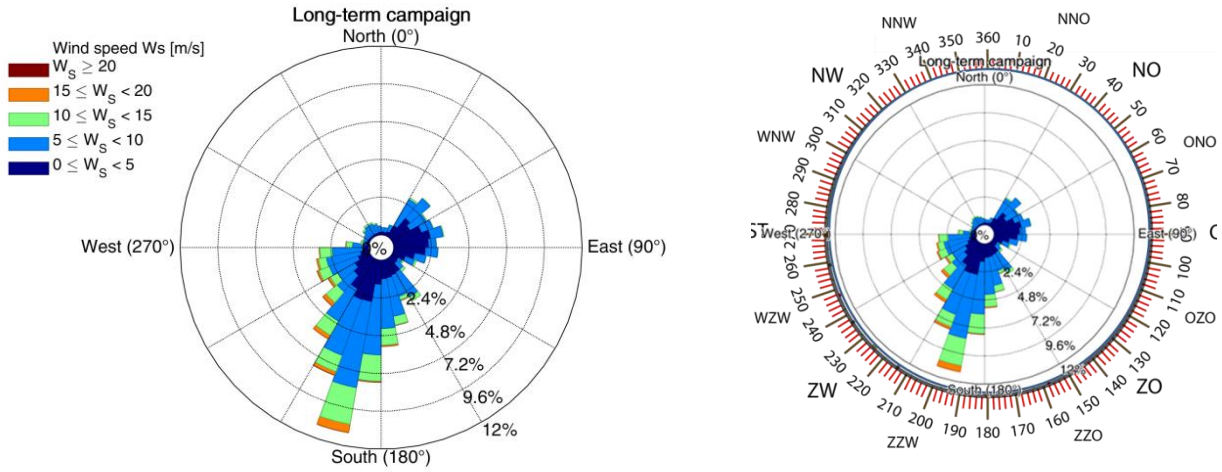

Figure 4.5 Wind rose with directional bins of 5°, along with several wind speed ranges for period of October 2015 to February 2017.

doi.org/10.21436/inbor.17169167

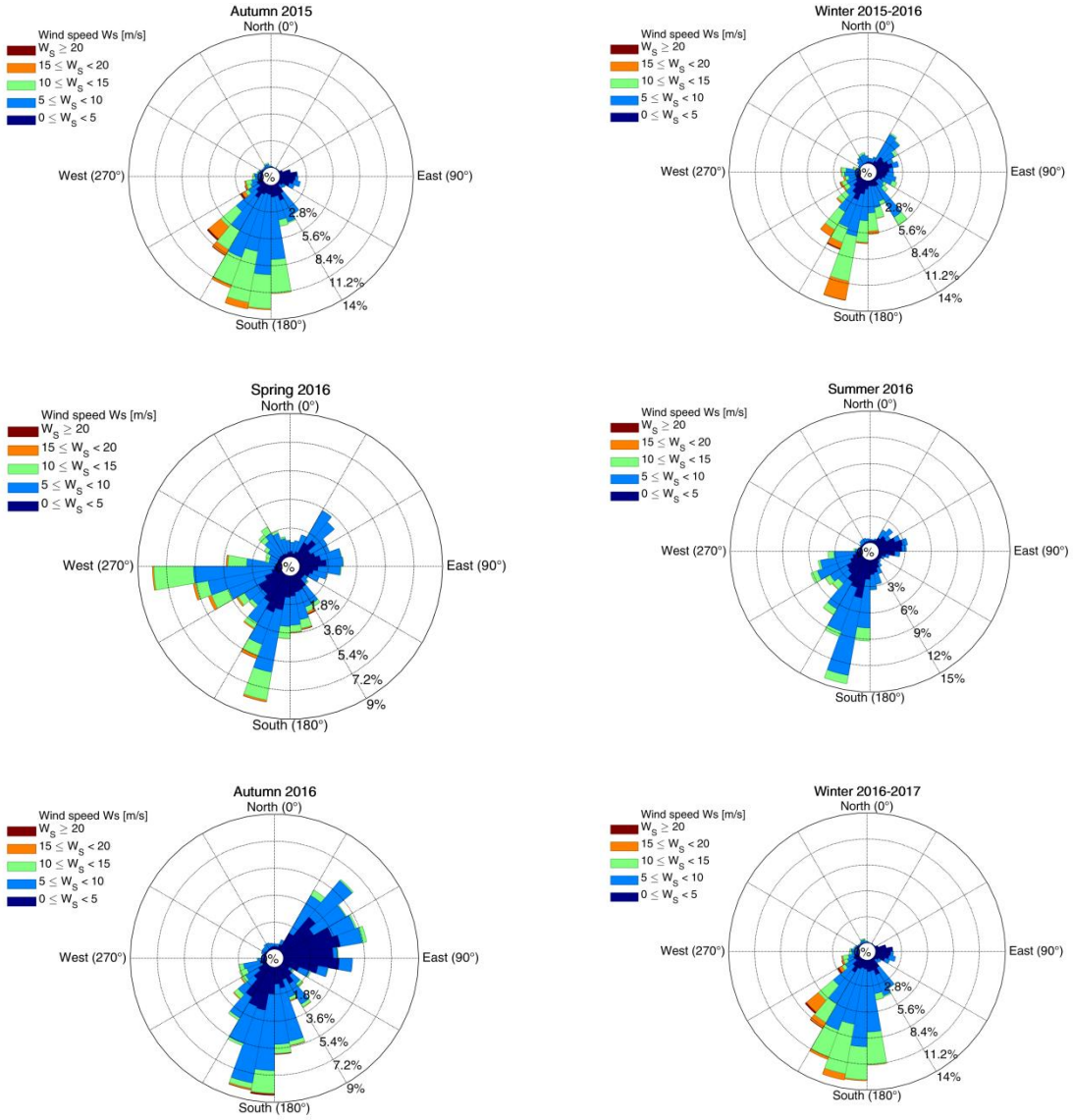

Figure 4.6 Seasonal wind roses with directional bins of 5°, along with several wind speed ranges for every season between October 2015 to February 2017.

4.2.2 Fetch length

The maximum fetch lengths at the two transect at bank full conditions (Figure 4.7) strongly varies with wind direction. This is particularly the case when the wind comes from the direction of the very elongated dock. The northern transect experiences the longest fetch length with a maximum of 4.5 km between 200 and 210°. The longest fetch lengths at the southern transect occurs between S to SW and NW to WNW with a maximum at 220°. It should be noted also that the maximum fetch lengths have a very small directional angle, because of the (relative) small width of the dock. Furthermore, these fetch lengths in the dock have to be considered as an absolute maximum, as due to the high quay walls, the effective stretch length will be smaller.

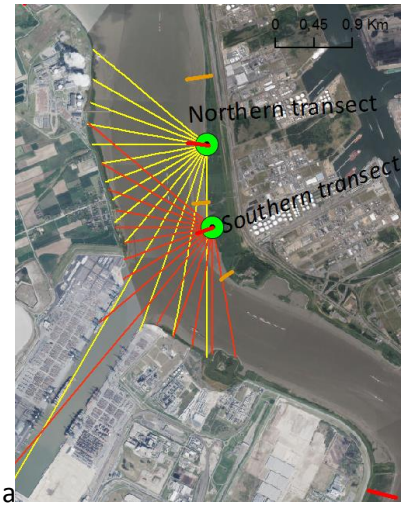

a

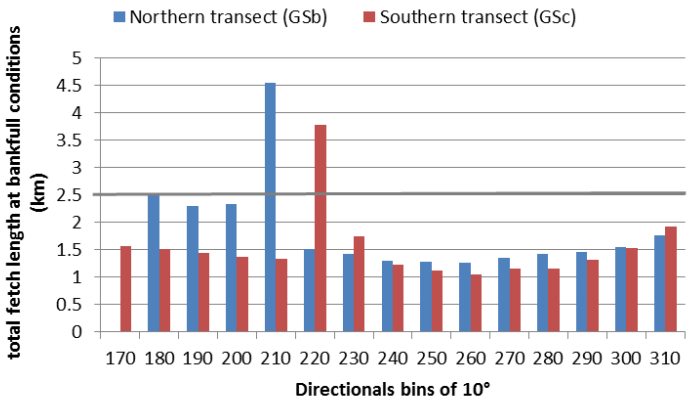

B

Figure 4.7 a) Map with fetch length to the two research stations, b) total fetch length at bank full conditions at the northern (GSb) and southern transect (GSc)

4.2.3 Short-term wind and wind wave regime (October 2015 and 2016)

For the different measurement campaigns, a clearly different wind field was observed (Figure 4.8). In October 2015, the wind was mainly coming from the south south-west and wind velocities higher than 9 m/s were frequently observed. In 2016, two dominant wind directions can be observed, namely from the east and from the southern direction, yet wind was blowing harder and more frequent from the south than from the west. Wind velocities were much smaller during the second measurement campaign (generally below 9 m/s).

doi.org/10.21436/inbor.17169167

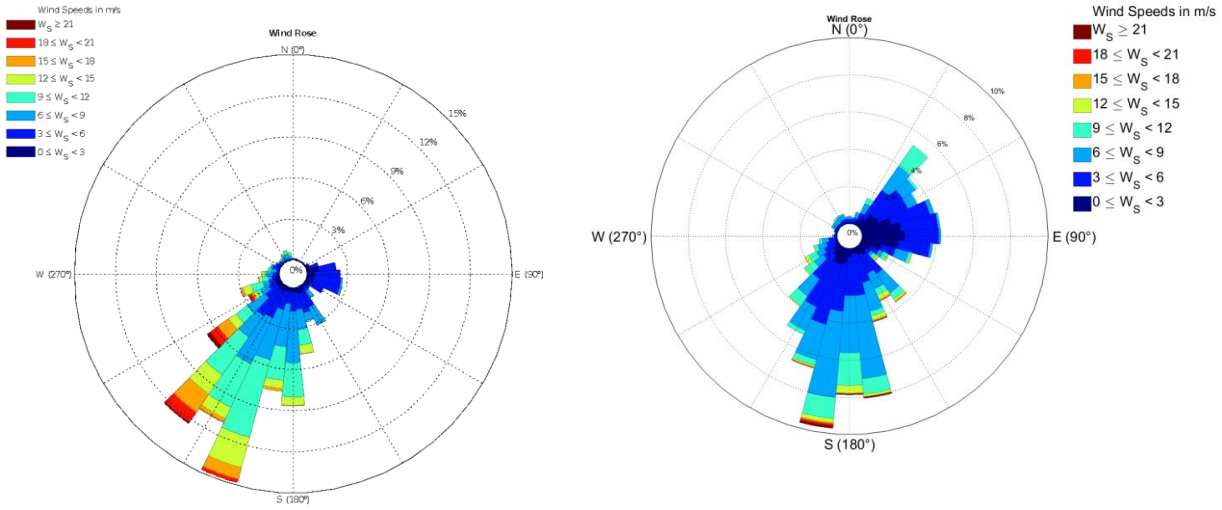

Figure 4.8 Overview of the wind conditions during the intensive measurement campaign of 2015 (left) and 2016 (right)

In general, two options are considered to determine the wave climate on the intertidal area due to the wind action. First of all, the significant wave height ($H_{1/3}$) over a tidal cycle can be related to the average wind condition. It is clear from the data that the maximum wave heights calculated per tide are highly influenced by the ship waves. For the significant wave heights these effect seems smaller, but of course it is not possible to exclude ship wave effects in this parameter. A second option is to consider only wave events for which no ship passages are recorded. Windows of 30 minutes without ship passages were selected, in these periods the wave height (H_{max} or $H_{1/3}$) was determined on a period of 10 minutes. The disadvantage of this method is that, due to the high number of ship passages, the number of wind events is limited. Yet, the relation between the acting force and the resulting wave is more direct.

Because there is no obvious reason (changes of bathymetry, plan form of the estuary, etc.) why another relation between wind velocities and wave heights would exist between the 2 intensive measurement campaigns, the results are combined in the same figure.

1.1.1.1.1 4.2.3.1 (Wind) wave regime per tidal cycle

The significant wave characteristics, which we grouped per tidal cycle and averaged over the measurement period, are listed below in Table 4.3. For all locations, and for both campaigns, a similar significant wave height of 6 to 7 cm was found, yet waves were somewhat higher at the southern transect. In Verelst et al. (2012) wave measurements were performed in the fairway itself, at the end of the discharge point of Evonik Degussa Antwerp NV at -2.7 m TAW. Between 1 June 2010 and 1 June 2011 a calculation of the fortnightly main wave parameters was performed. An average significant wave height of 0.11 ± 0.02 m was found over all periods, with a range between 0.09 m and 0.17 m. This value is slightly higher as the values we find in Table 4.1, however the latter are measured on the intertidal areas itself.

In Figure 4.9 and Figure 4.10, the relation between the wind speed, calculated as an average over the considered tide, and the significant wave height, calculated over the tide, is shown for all measurement locations. It should be noted however, that the significant wave height calculated over the whole tide also includes ship waves. But because of the continuous wind wave action and the episodic ship waves, which occur randomly during the tidal cycle, the significant wave height over the tide is considered as a proxy for wind waves. It is clear from the figures that below a wind speed of 10 m/s, the significant wave heights remain below 0.1

m. Above wind speeds of 10 m/s, a clear increase can be observed in the $H_{1/3}$ values. The data of 2016 confirm this statement, albeit that the number of data points (tides with a high averaged wind speed) is limited. The maximum significant wave heights reach approx. 0.2 m at wind speeds in excess of 15m/s.

Table 4.3 Overview of mean and SD of the significant wave heights for periods without ship traffic, calculated per tide and averaged over all tides, for the different measurement locations.

Transect	**Tidal flat zone**	**Location**	$H_{1/3}$ **2015**	$H_{1/3}$ **2016**
Northern transect	high	GSb2	0.065 ± 0.03	
	low	GSb4	0.070 ± 0.03	0.062 ± 0.02
Southern transect	high	GSc2	0.079 ± 0.03	
	middle	GSc3	0.077 ± 0.03	0.069 ± 0.01
	low	GSc4	0.075 ± 0.03	0.067 ± 0.02

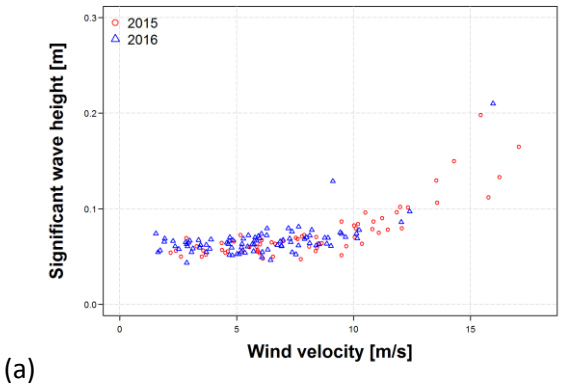

(a)

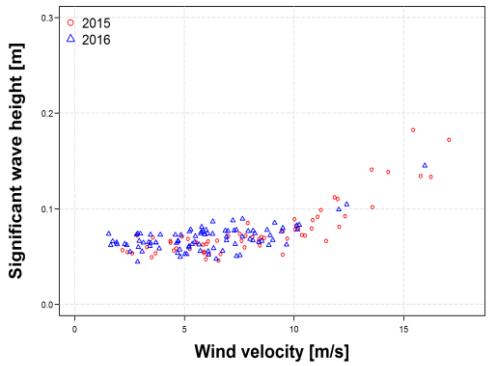

(b)

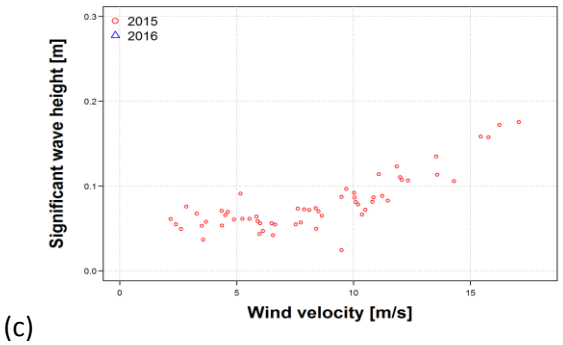

(c)

Figure 4-9: Calculated significant wave height [m] per tidal cycle in relation to averaged wind velocity [m/s] at the Southern transect (a) low flat GSc4, (b) middle flat GSc3 and (c) high flat GSc2.

doi.org/10.21436/inbor.17169167

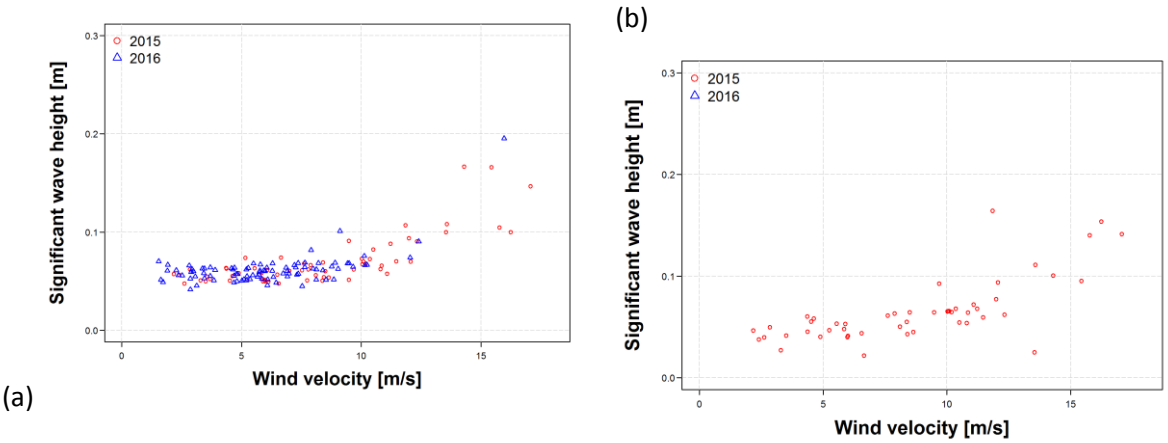

Figure 4.9 Calculated significant wave height [m] per tidal cycle in relation to averaged wind velocity [m/s] at the northern transect (a) the low plot GSb4 and (b) the high plot GSb2.

To investigate the effect of wind direction on wave height parameters, we plotted wind direction against wind speed for the events where wind speed was higher than 10m/s in Figure 4.11, Figure 4.12 and Figure 4.13. It appears that wind was coming from a south west direction for all events in 2015 (Figure 4.11). In 2016 the number of events is smaller, but also the wind direction for the different events is more diverse.

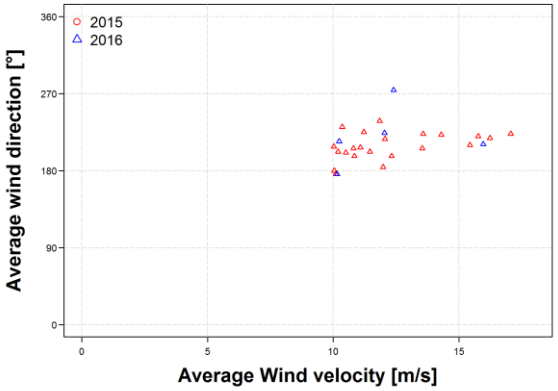

Figure 4.10 Averaged wind direction [°] for wind velocities [m/s] higher than 10 m/s

1.1.1.1.2 4.2.3.2. Wind wave regime per 10 min. periods of no ship passages

The same plots, with significant wave height in relation to wind velocity, are shown in Figure 4.12 and Figure 4.13. In this case the significant wave heights are calculated on 10 minutes time periods, for periods where no ship passages were observed. For the measurement period of 2015 a similar pattern as for the tidally calculated values is observed, with an increase of the values above a wind speed of ca. 10 m/s. For the measurement period of 2016 this pattern cannot be observed. No clear reason for this difference could be found, except maybe that in 2016, because of a more southerly wind direction, the Galgeschoor shore was often more sheltered from wind. The maximum significant wave heights reaches approx. 0.40 m at the low tidal plots and 0.3 m at the high tidal plots at wind speeds in excess of 15m/s.

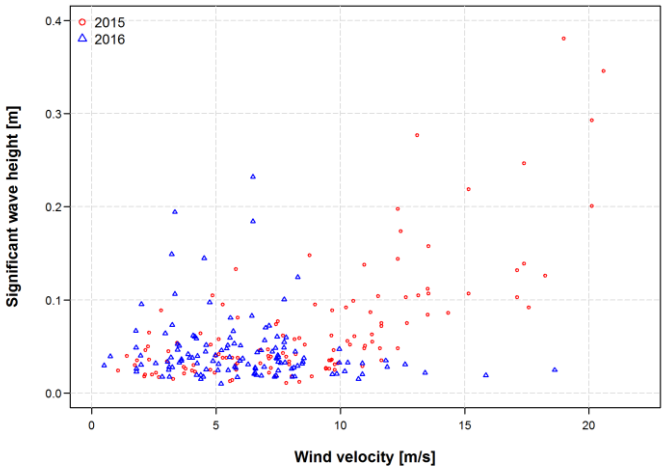

Figure 4.11 Calculated significant wave height [m] in relation to averaged wind velocity [m/s] at GSb4 in periods of no ship passages

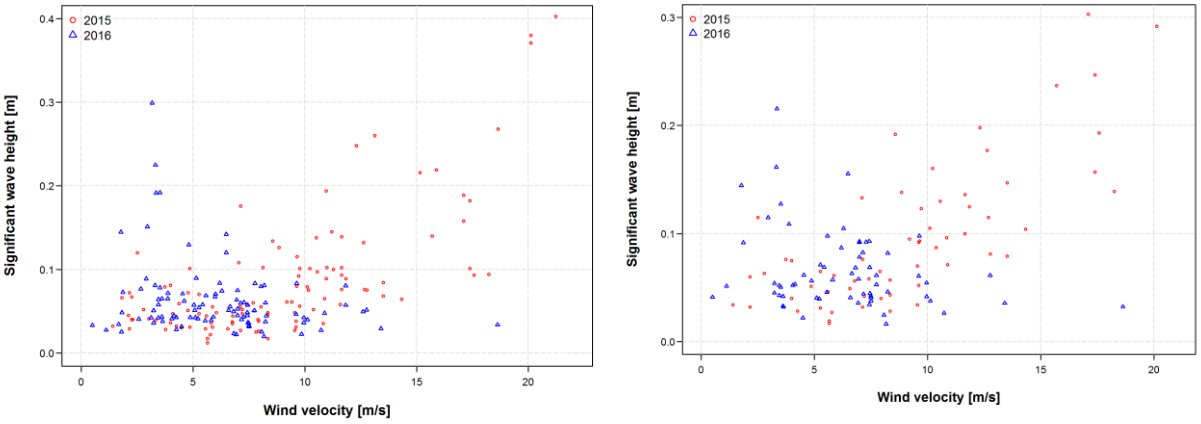

(a) (b)

Figure 4.12: Calculated significant wave height [m] in relation to averaged wind velocity [m/s] at (a) low tidal flat GSc4 and (b) high tidal flat GSc2 in periods of no ship passages

1.1.1.1.3 Wave amplification and attenuation of wind waves

Wind-generated waves recorded at the low tidal flat (GSb4 and GSc4) were compared directly to the waves measured at the high tidal flat (GSb2 and GSc2). Figure 4.13 gives an overview of the wave heights recorded for all detected wind events at all plots in November 2015 and 2016 (with limited data for the high plots in 2016). Wind wave heights were lower in 2016 than in 2015 although the higher outliers for the different November 2016 plots denote higher extreme wind events. Overall slightly higher wind waves occur on the high plots and lower waves on the low tidal flat, except for GSb in 2016, but only 3 values were recorded for the high plot GSb2. A clear explanation for this observation cannot be found.

doi.org/10.21436/inbor.17169167

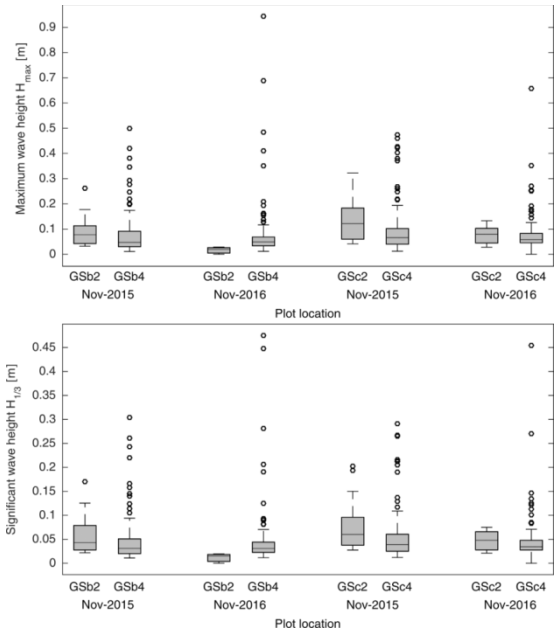

Figure 4.13: Comparison of wind waves (maximum, Hmax, and significant, H1/3, wave heights), recorded at the high (GSb2 and GSc2) and low (GSb4 and GSc4) tidal flat plots for the respective Northern (GSb) and Southern (GSc) transects for the measurement campaigns of November 2015 and November 2016. The boxes represent the interquartile range of the data

4.3 SHIP WAVE REGIME

4.3.1 Ship traffic

Both in 2015 and 2016 the number of ship passages – both seegoing vessels and inland vessels – and the related characteristics of the ships were recorded by the AIS ("Automatic Identification System"). The intensity of ship traffic increased with 15% in the studied period: the average ship passage per day is 215 in November 2015 and 252 in November 2016. For November 2015 and November 2016 the proportion of passages from inland and seagoing vessels is identical, accounting for respectively 78% and 22% of the total.

The number of ship passages during the intensive campaigns, passing the Galgeschoor, in 2015 was 7097 at the southern location (GSc) and 7159 at northern location (GSb). In November 2016 the total number of ship passages was 11926 (GSc) and 11881 (GSb). In November 2015 a total number of respectively 677 seagoing and 934 inland ships were observed.

Figure 4.14 displays the daily time series of ship passages (max. of 347 at 9 Dec. 2016), notice the clear 7-day periodicity with minima at Sundays and holidays.

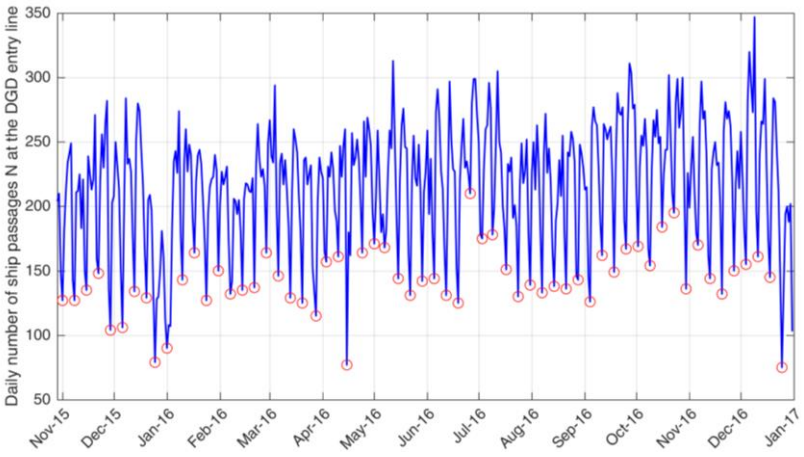

Figure 4.14 Time series of daily ship passages at the Deurganck dock (GSc) entry line from November 2015 to January 2017. The red dots depicts all local minima.

In Figure 4.15 the number of ships is depicted, sailing with a minimum speed of 2,50 knots. In this figure, no distinction is made between seagoing and inland vessels, and the ship type is based on the AIS code (as depicted in Kolokythas, 2019). Cargo ships account for nearly half of the total number of ship passages in the area, followed by tankers and special category ships. The highest ship traffic per month occurred in October 2016 with 236 passages per day.

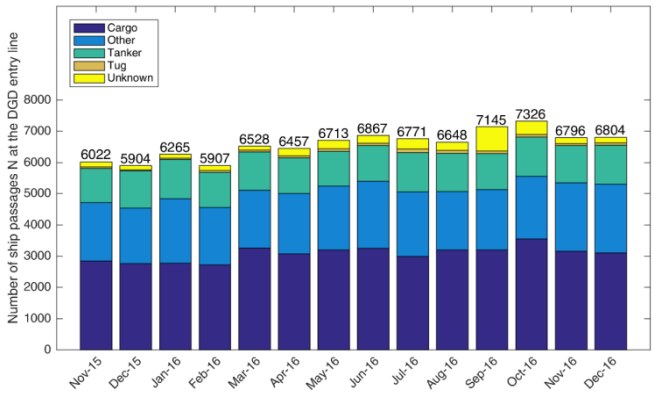

Figure 4.15 Temporal evolution of monthly ship traffic differentiated by ship type that crossed the Deurganck dock (GSc) entry line from the period of November 2015 to January 2017. Each bar is supplemented with the corresponding number of ship passages. Only passing ships with speed > 2.5 knots have been considered similar to Kolokythas et al. (2016) and Levy et al. (2017).

doi.org/10.21436/inbor.17169167

In Table 4.4 the relative passing velocities, i.e. the speed of the same vessel at GSc relative to GSb, of tugs, cargo ships and tankers at the GSb and GSc measurement locations are shown. Tug boats moving upstream are generally slower at the southern measurement location (GSc) compared to the northern location (GSb), respective values of 0.93 and 0.86 are found for 2015 and 2016. This means that tug boats moving upstream have a higher velocity at Gsb compared to Gsc. Cargo ships are travelling approximately 5 % faster at the GSb transect compared to the GSc transect if they are travelling upstream. In the downstream direction, no difference could be observed. For tankers, no distinction can be made between the relative velocities at GSb or GSc.

Table 4.4 Relative velocities [%] of ships passing at southern location (GSc) versus the northern location (GSb) for three types of ships.

Type of ship	2015		2016	
	UP	DOWN	UP	DOWN
Tug	0.93	1.05	0.86	1.05
Cargo	0.96	0.99	0.95	0.99
Tankers	1.00	1.00	0.99	1.01

If we compare the distance from the passing ships to the lowest point of the transects at the low tidal flat (GSb4 for northern GSb transect and GSc4 for the southern GSc transect), we observe no differences. We can observe ships passing from 400 to 750 m from GSc4 and ca. 500 – 800 m from GSb4. No clear difference in the average distance to the measurement points can be observed for seagoing and inland vessels.

4.3.2 Ship waves

In the signal of a single ship wave, two different phases can be observed, a primary wave and a secondary wave, which are superimposed. The primary wave pattern is a water level depression (drawdown) observed along the hull of the ship that propagates in the direction of the movement. Its wave length is about equal to the ship's length (Schiereck, 2001). The secondary wave pattern includes transverse and diverging waves induced by discontinuities in the ship's hull profile, which are found at the bow and the stern. These wave patterns form interference cusps, of which the envelope propagates obliquely towards the river bank with an angle of attack equal to 55° considering that the bank is parallel to the sailing line (De Roo, 2013). A typical ship wave pattern for a heavy trimmed displacement ship is shown in Figure 4.16.

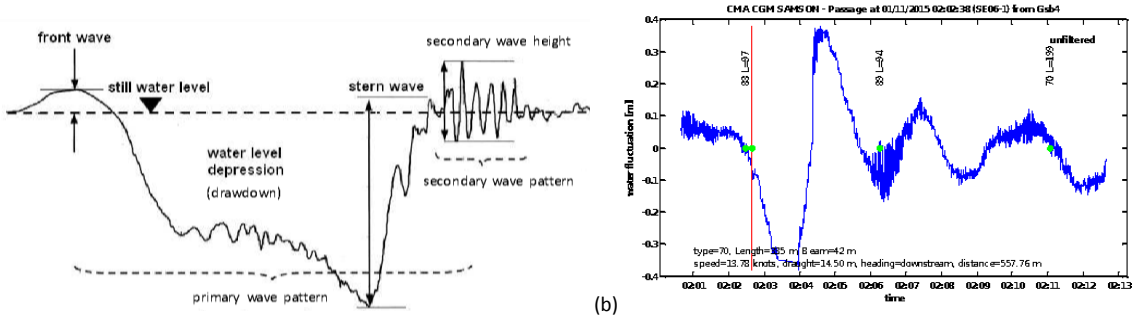

Figure 4.16 (a) Typical ship wave pattern for a heavy trimmed displacement ship consisting of a primary wave and a secondary wave pattern (De Roo, 2013, p. 51); (b) An example of a registered ship wave in the first intensive campaign November 2015.

Primary waves

To find the signals of primary waves in the total wave signal, a specific methodology was used to detect (and isolate) this type of waves (Figure 4.16). For the primary waves, special focus was put on the largest ships, as the water level depression is related to the volume of the displaced water (and as such the volume of the ship). Time windows of 9 minutes before and after the passage of ships, longer than 200 m and faster than 2.5 knots, were selected. Within these time windows no other large ships should be present, to consider the event as a clear wave event originating from one large vessel. The wave height is calculated on the resulting fluctuations, after using a low pass filter (0.05 Hz).

In 2015 maximal primary wave heights of ca. 0.65 m were recorded in the northern transect and 0.35 m in the southern transect (Figure 4.18 and Figure 4.20). These highest waves are created by cargo ships in the northern transect, in the southern transect it are mainly roro ships which are responsible for the higher primary waves. It is very prominent that in the results of 2016, the primary waves recorded are much smaller (ca. 0.30 m and 0.20 m respectively for the northern and southern transect). A positive relation between sailing speed and wave height can be found for the results of 2015, albeit that for the highest velocities the wave height seems to drop again. A clear inverse relation can be observed between the water level and the recorded wave height. This is probably due to the larger relative water displacement of the ship at low water compared to high water.

Depending on the location primary waves at the northern transect NL- GSb4 (GSb) are clearly higher than at the southern transect SL- GSc4 (GSc). The maximum primary wave values at SL-GSc4 of approx. 0.25 m are found in 2016 (Figure 4.19). In 2015 a few primary waves had higher values (approx. 0.5 m, Figure 4.20), which were caused by roro ships instead of general cargo ships. The large cargo ships do not seem to induce high primary waves at the low tidal flat SL-GSc4.

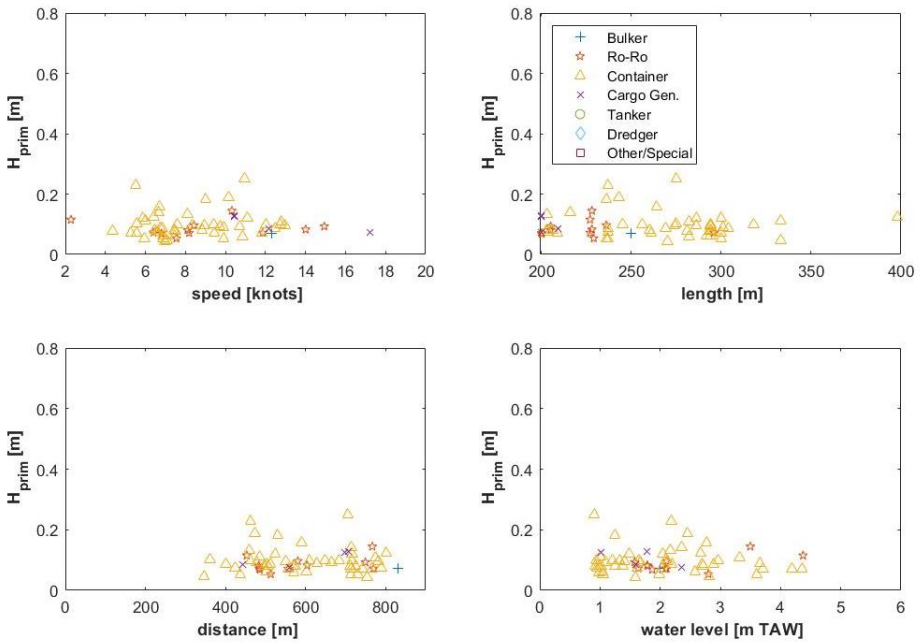

Figure 4.17 Maximum wave height (primary) versus ship speed & length, distance from the measuring gauge, and water level for the selected ship events at **NL-GSb4** (north) location in **2016**.

doi.org/10.21436/inbor.17169167

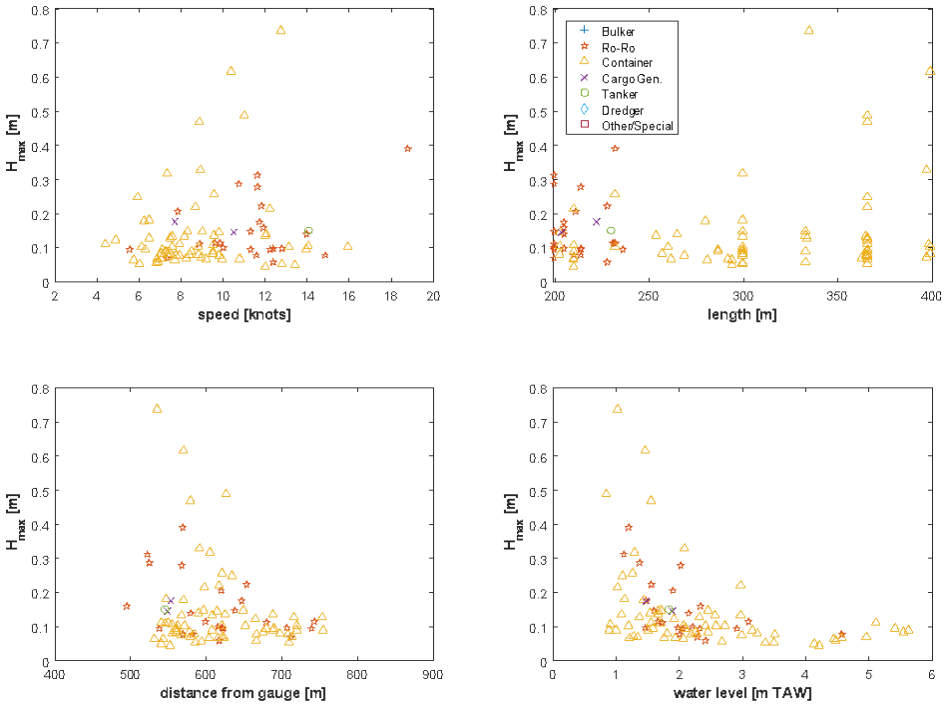

Figure 4.18 Maximum wave height (primary) versus ship speed & length, distance from the measuring gauge, and water level for the selected ship events at **NL-GSb4** (north) location in 2015**.**

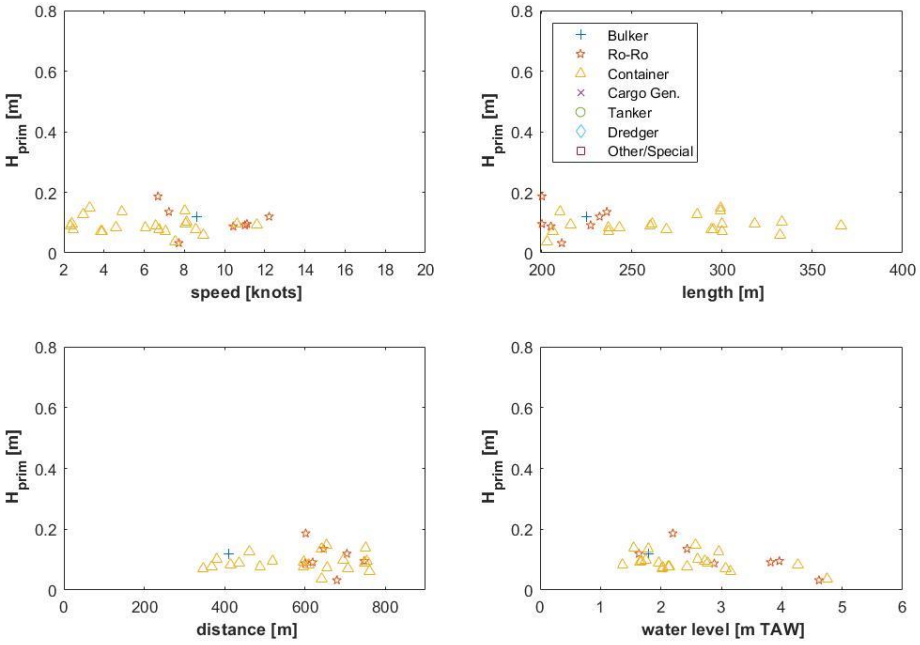

Figure 4.19 Maximum wave height (primary) versus ship speed & length, distance from the measuring gauge, and water level for the selected ship events at **SL- GSc4** (south) location in 2016

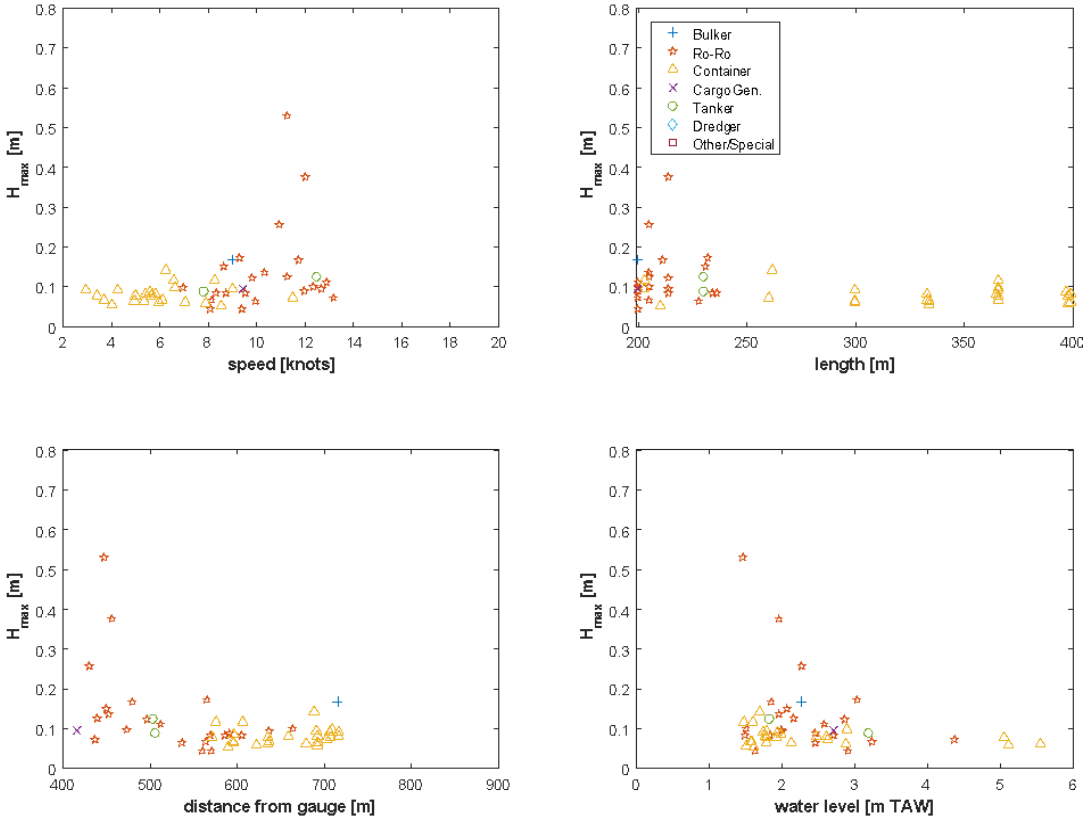

Figure 4.20 Maximum wave height (primary) versus ship speed & length, distance from the measuring gauge, and water level for the selected ship events at **SL- GSc4** (south) location in 2015.

Secondary waves

For the secondary waves, clear windows, meaning time periods where only one ship is passing, are selected, to get a clear link between the ship type and its sailing behaviour and the generated waves. For the description, we only consider here to the two lowest measurement locations. For more in depth information, the reader is referred to the specific reports of the intensive measurement campaigns.

A distinction is made between inland and seagoing vessels. For the inland vessels, the results of the measuring campaign of respectively 2015 and 2016 are plotted in Figure 4.22 and Figure 4.21. The maximum wave heights range to ca. 0.50 m in 2016 and 0.45 m in 2015, as such a consistent value is found. A slight positive correlation exists between wave height and sailing speed, which is less obvious for the 2016 data. In 2016 (northern transect) the highest waves are caused by tug boats, cargo and ships labelled as “other”, in 2015 tug boats create high waves as well, but some cargo ships have similar wave heights. At the southern location, GSc4, the wave heights peak, for a very limited number of events, to higher values compared to the north. It are mainly the tug boats which are accounting for these highest waves. The maximal recorded waves are slightly higher, from 0.6 to 0.55 m for respectively 2016 and 2015.

doi.org/10.21436/inbor.17169167

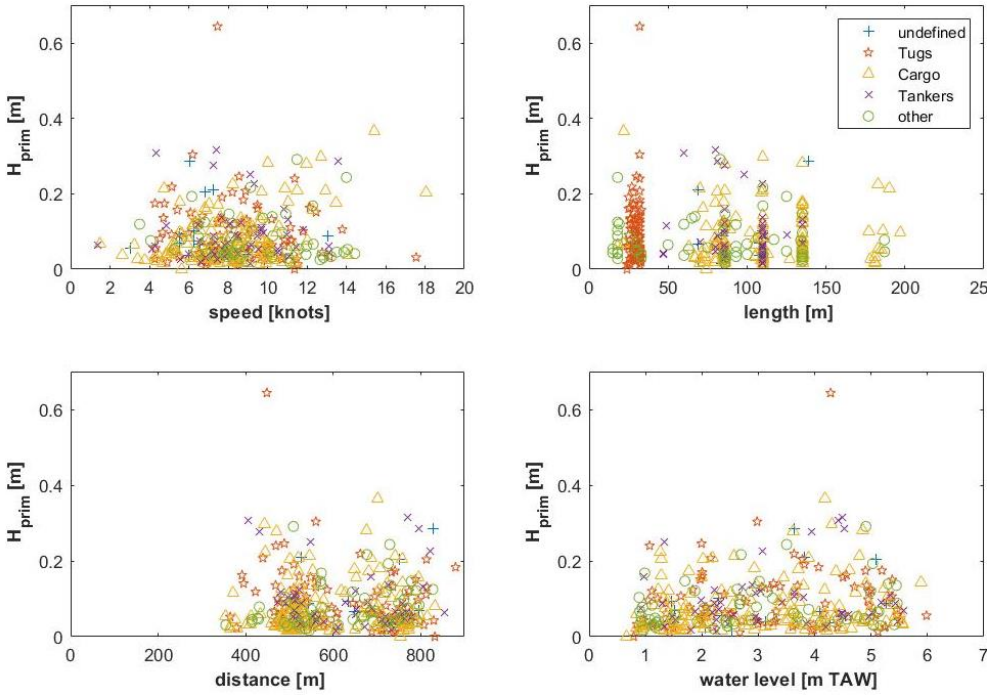

Figure 4.21 **Secondary wave** height versus sailing speed, ship length, distance from the measuring gauge, and water depths for the selected inland ship events at the northern low tidal flat **NL- GSb4** in **2016**.

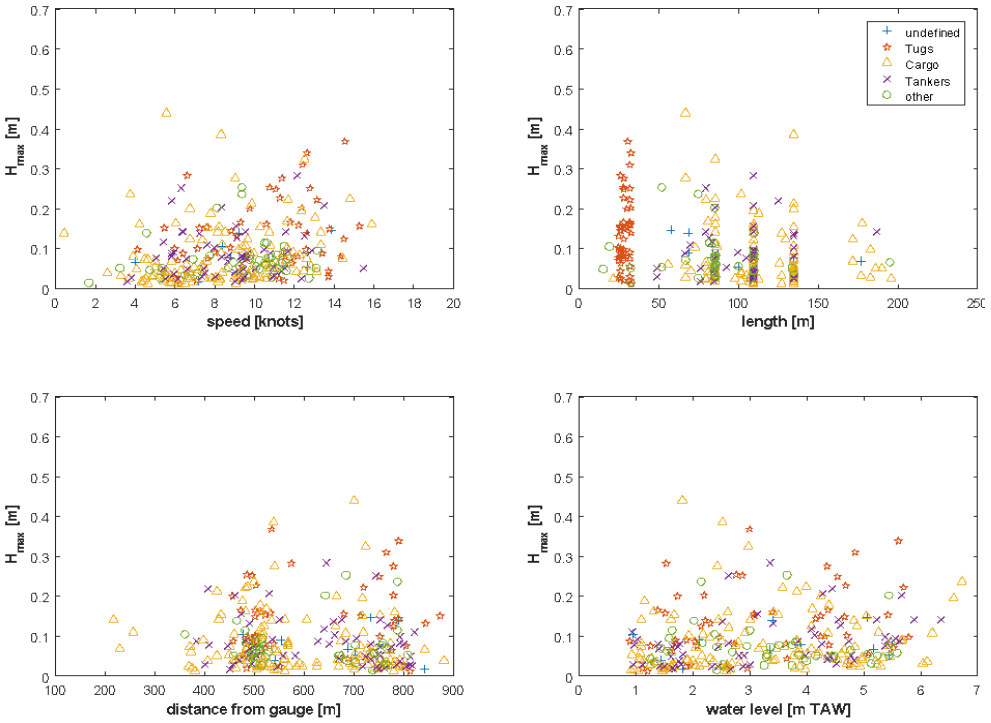

Figure 4.22 **Secondary wave** height versus sailing speed, ship length, distance from the measuring gauge, and water depths for the selected inland ship events at the northern low tidal flat **NL-GSb4** in **2015**.

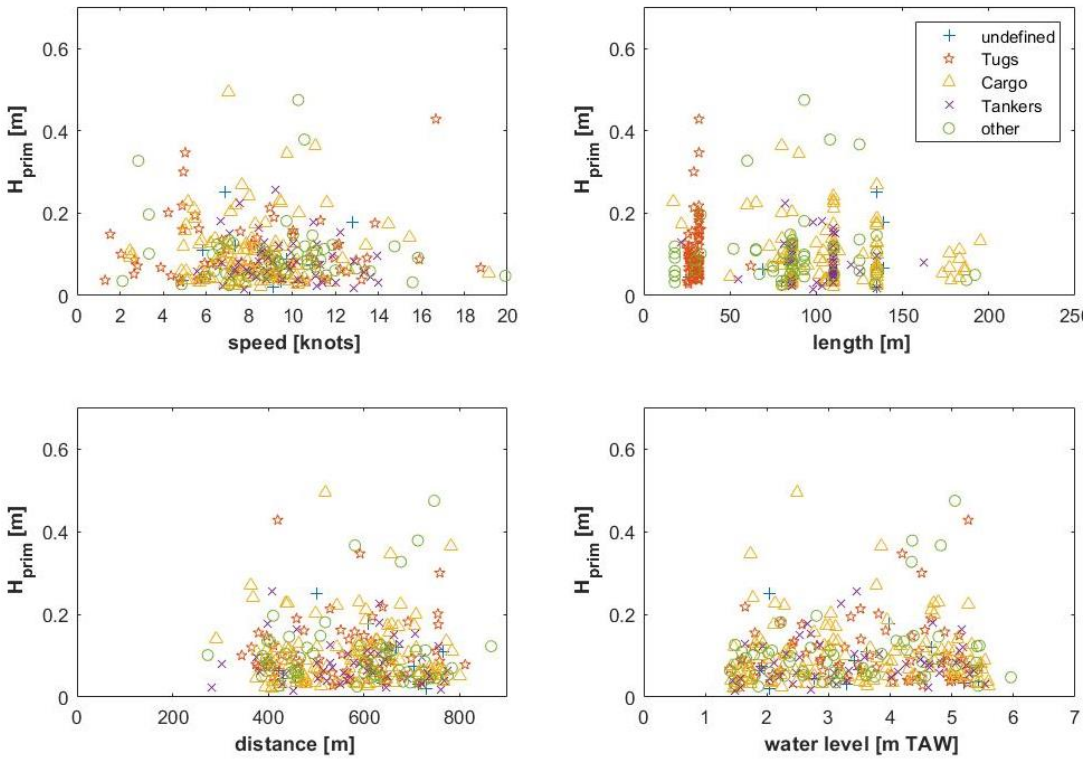

Figure 4-23: **Secondary wave** height versus sailing speed, ship length, distance from the measuring gauge, and water depths for the selected inland ship events at the southern low tidal flat **SL- GSc4** in **2016**.

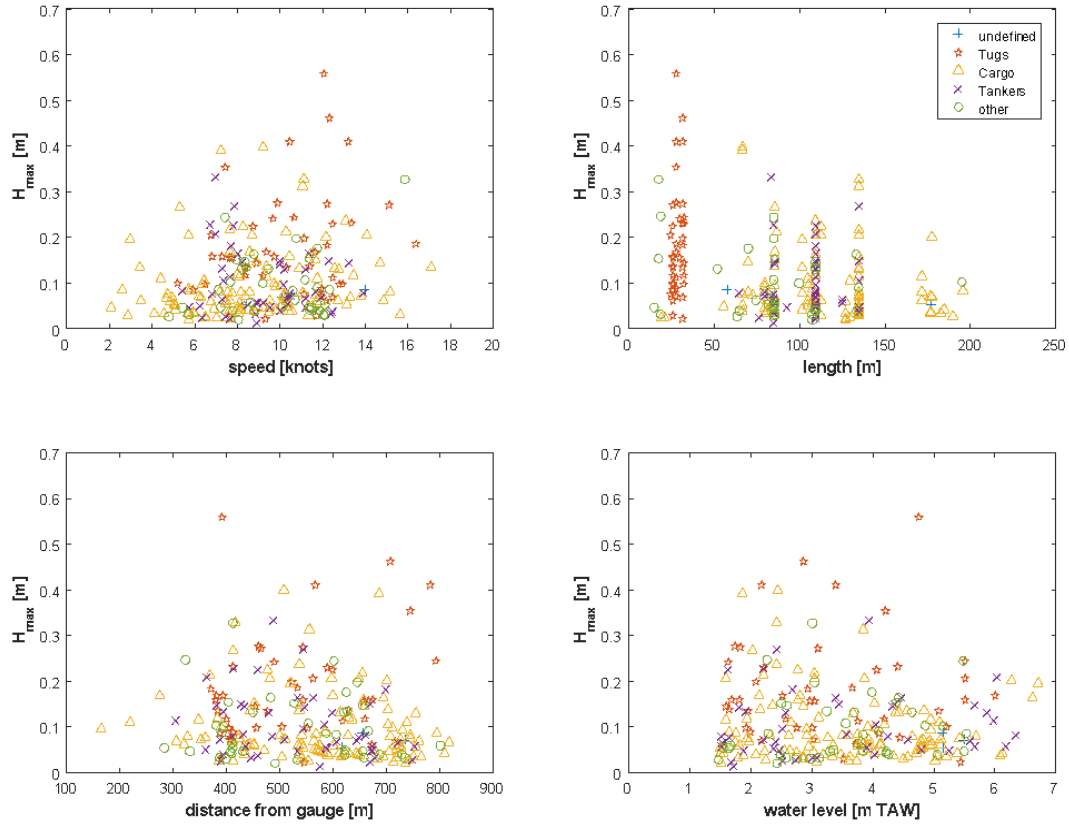

Figure 4.23 Secondary wave height versus sailing speed, ship length, distance from the measuring gauge, and water depths for the selected inland ship events at the southern low tidal flat SL-GSc4 in 2015.

doi.org/10.21436/inbor.17169167

In Figure 4.24 and Figure 4.25 the secondary wave heights from seagoing ships are presented for respectively 2016 and 2015. In the northern transect, the difference between the values of 2016 and 2015 are rather high, with respectively maximum values of ca 0.35 m and 0.65 m. In 2015 a slightly positive relation between the speed and the wave height can be observed. At SL- GSc4, in the GSc transect (Figure 4.25 & Figure 4.26), the secondary waves generated from seagoing vessels seem smaller compared to the waves created by inland vessels, with maximum wave height around 0.35m (except one peak value).

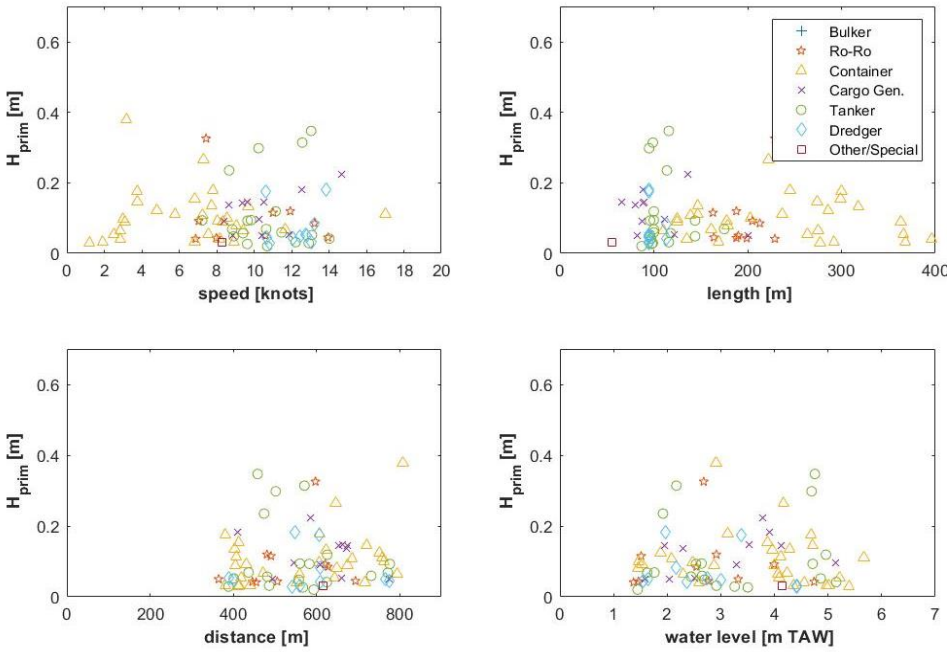

Figure 4.24 Secondary wave height versus ship speed & length, distance from the measuring gauge, and water level for the selected seagoing ship events at **NL- GSb4** (north) location in **2016**

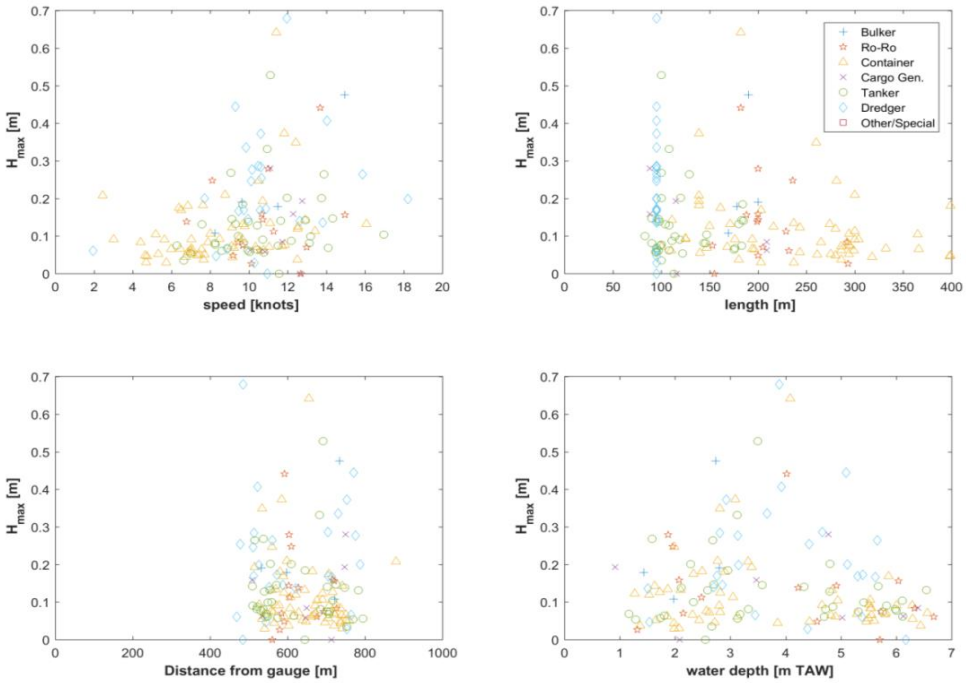

Figure 4.25 Secondary wave height versus ship speed & length, distance from the measuring gauge, and water level for the selected seagoing ship events at **NL-GSb4** (north) location in **2015**

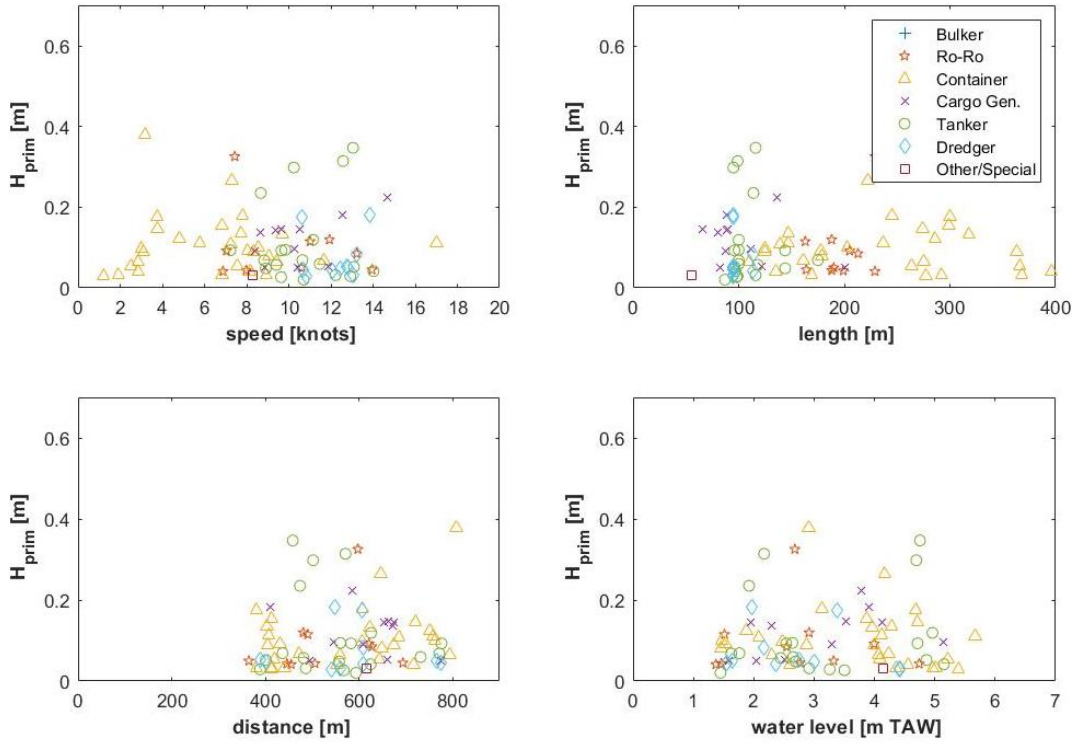

Figure 4.26 Secondary wave height versus ship speed & length, distance from the measuring gauge, and water level for the selected seagoing ship events at **SL-GSc4** (south) location in **2016**

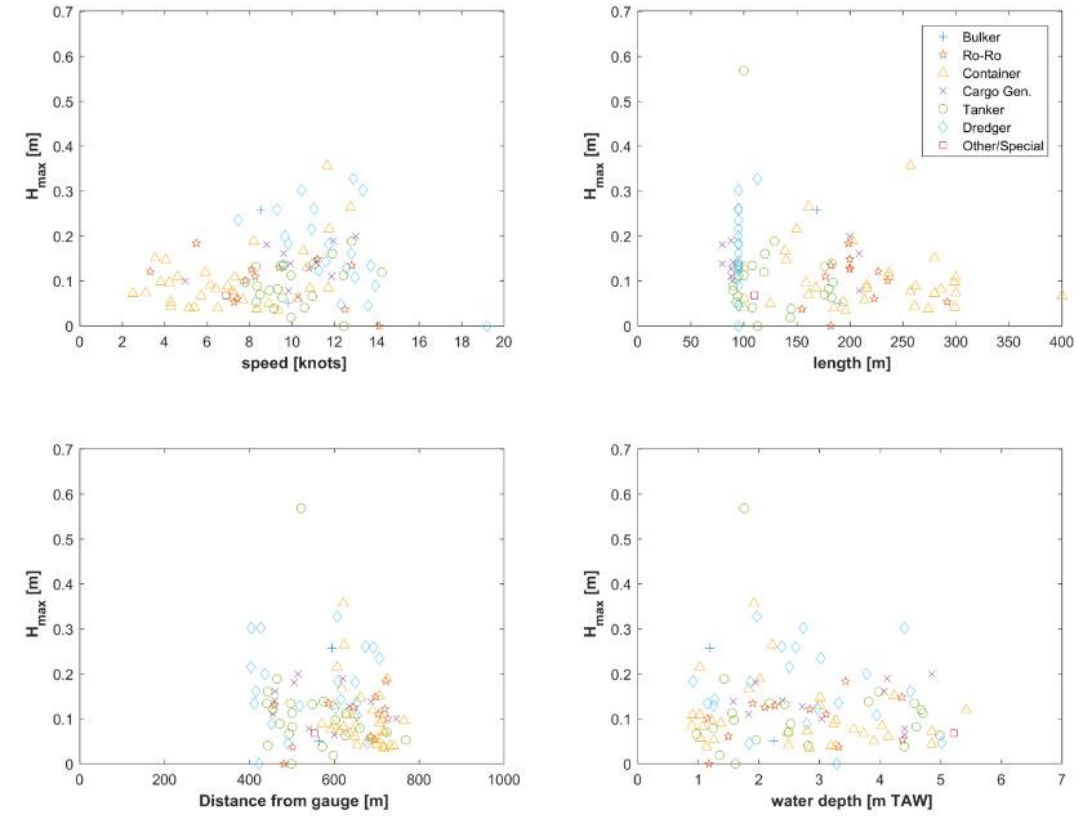

Figure 4-28: Secondary wave height versus ship speed & length, distance from the measuring gauge, and water level for the selected seagoing ship events at **SL-GSc4** (south) location in **2015**

doi.org/10.21436/inbor.17169167

Wave attenuation of secondary ship waves

In the following, ship-induced wave heights using a filter of short period waves (2-10s), recorded at the low tidal flat plots (GSb4 and GSc4; elevation~1m TAW) are compared to those recorded at the high tidal flat plots (GSb2 and GSc2; elevation ~5m TAW) for the Northern (GSb) and Southern (GSc) transects. Figure 4.27 shows the distribution of wave heights for all recorded waves at the four plots (n(GSb2)=33, n(GSb4)=524, n(GSc2)=43, n(GSc4)=431) during the 2015 and 2016 intensive measurement campaign.
Ship waves are attenuated because both maximum and significant ship wave heights are lower in the high tidal flat plots than in the low tidal flat plots (both variables significant at $p < 0.001$ using Mann-Whitney U-test).
Additionally comparing the intensive campaign in 2015 and 2016, a decrease in maximum and significant ship wave height can be observed on the high tidal flat plots (GSb2 & GSc2), despite the higher outliers of the maximum wave height at the low tidal flat (GSb4 & GSc4).
The behaviour of ship waves along the low to high tidal flat gradient is shown in Figure 4.27. For some instances, differences are marginal and insignificant, but the trend is consistent: ship waves are higher at the low tidal flat and decrease towards the high tidal flat.

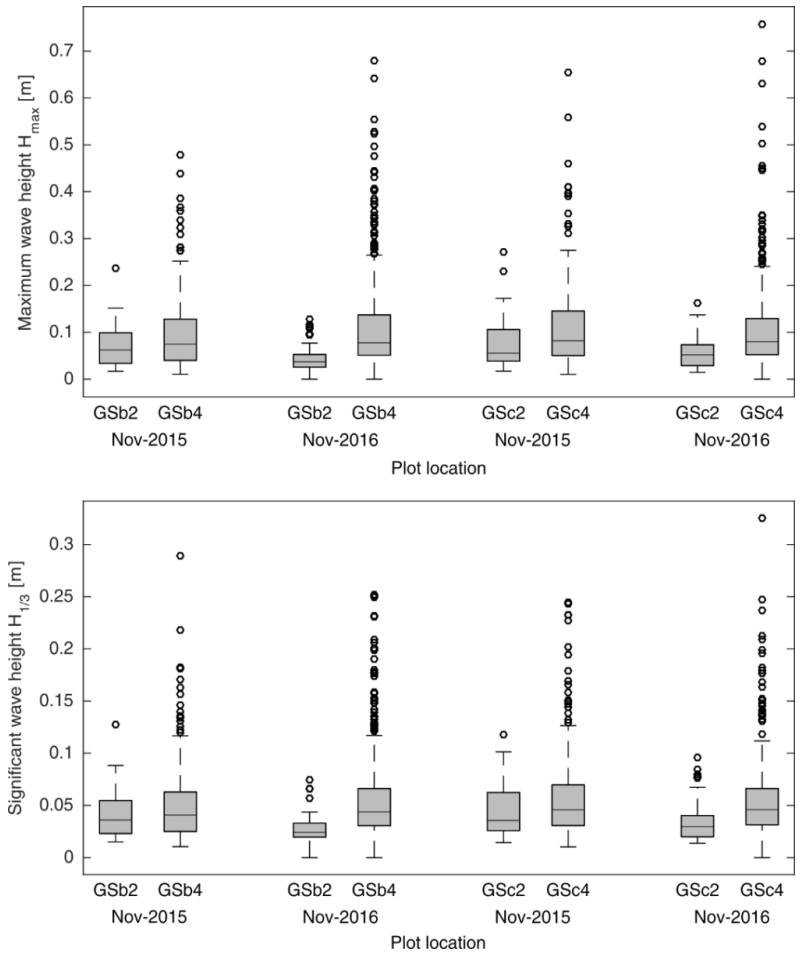

Figure 4.27 Comparison of (top) maximum secondary ship wave heights and (bottom) significant ship wave heights recorded at the high (GSb2 and GSc2) and low (GSb4 and GSc4) tidal flat plots for the Northern (GSb) and Southern (GSc) transects for the measurement campaigns of November 2015 and November 2016. The boxes represent the interquartile range of the data and the whiskers delimit 1.5 times the interquartile range. The horizontal line indicates the median and crosses indicate outliers.

4.4 COMPARING WIND AND SHIP WAVE HEIGHT BETWEEN LOW AND HIGH TIDAL FLAT

Globally, during the 2016 intensive campaign, (secondary) ship-induced waves by single ship events were higher than wind waves, recorded during "no-ship" events, both at the Southern (Figure 4.28) and Northern (Figure 4.29) transects. Such results are not surprising considering the geographical situation of the study site. Indeed, the Galgeschoor is located within the area of the port of Antwerp, characterized by heavy shipping traffic where the shipping channel passes very close to the lower limit of the tidal flat while the wind fetch of the dominant south-westerly winds is rather short to moderate. The heavy shipping traffic in the area also explains the lower recorded number of wind waves compared to ship waves in both transects during the 2016 intensive campaign.

Interestingly, both maximum and significant ship wave heights for common ship events were generally higher at the low tidal flat plots (GSb4 and GSc4) than at the high tidal flat plots (GSb2 and GSb2) when measured simultaneously. This means that for a same single ship event, secondary ship waves typically decrease in height when moving to the high tidal flat. This observed *attenuation*, is attributed to the energy loss by frictional dissipation, particularly experienced by the ship waves, having typically the highest wave heights, while travelling across the tidal flat. On the other hand, despite the lower number of records, both maximum and significant wind waves for common "no-ship" events were generally higher at the high tidal flat plot (GSc2) than at the low tidal flat plot (GSc4) at the Southern transect, meaning that during a same "no-ship" event, wind waves typically increase in height when moving to the high tidal flat, also called *wave amplification*. In particular, the increase in wind wave heights becomes more pronounced at high wind speed (see Figure 4.28) and when the wind blows from the south-west, although we have too few data to clearly establish the latter relationship (see **Fout! Verwijzingsbron niet gevonden.**). The increase in wind wave height towards the higher tidal flat, especially at strong wind force, may reflect the role of the wave shoaling as well as wind fetch which gets longer as the water inundates the tidal flat.

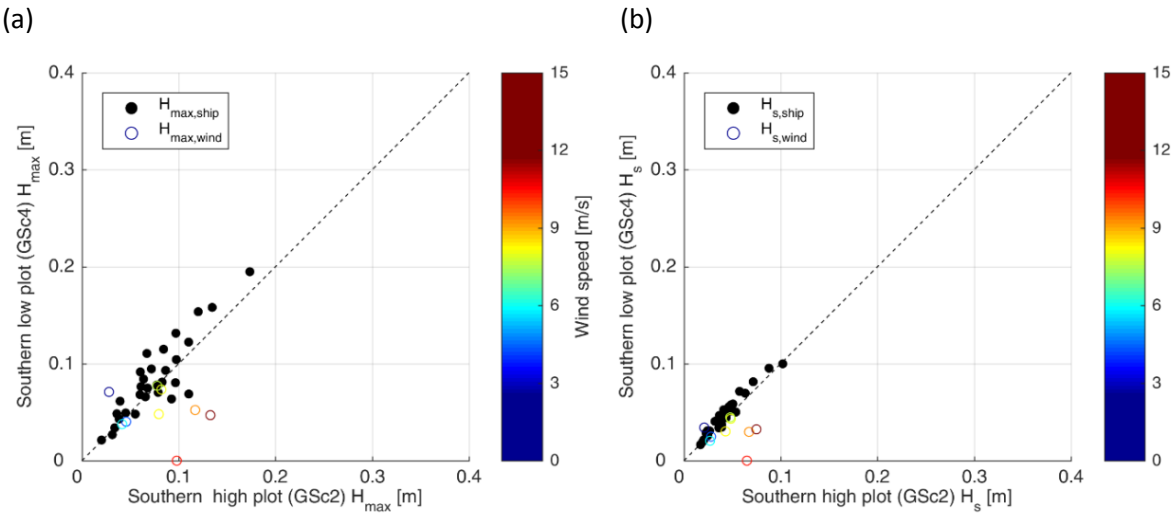

Figure 4.28 (a) Maximum (H_{max}) and (b) significant (H_s) wave heights for single ship and wind waves recorded commonly at the low (GSc4) and high (GSc2) tidal flat plots of the **Southern transect**. Wind waves are differentiated by the corresponding wind speed recorded during the detection of the "no-ship" event. The dashed lines indicate where x=y.

doi.org/10.21436/inbor.17169167

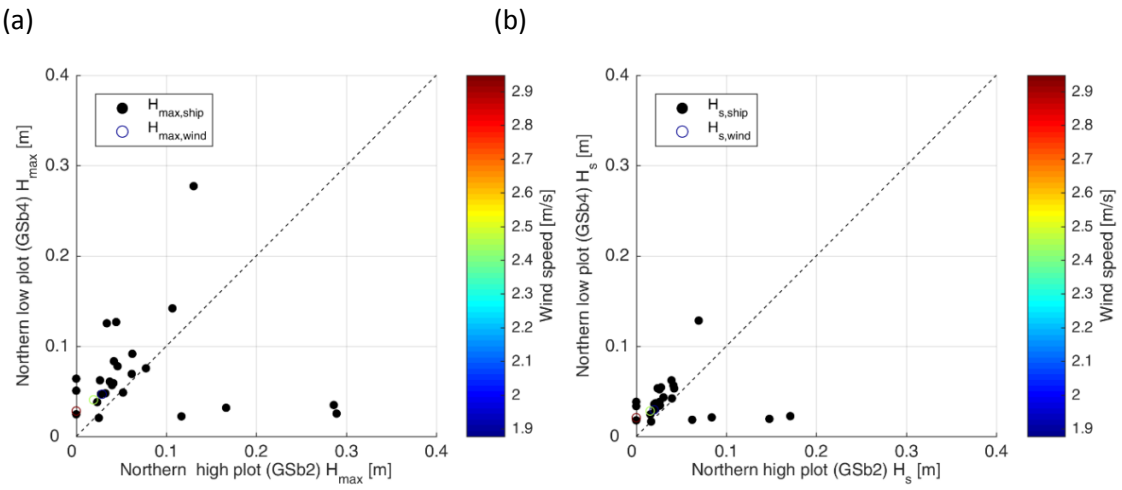

Figure 4.29 (a) Maximum (Hmax) and b) significant (Hs) wave heights for single ship and wind waves recorded commonly at the low (GSb4) and high (GSb2) tidal flat plots of the Northern transect. Wind waves are differentiated by the corresponding wind speed recorded during the detection of the "no-ship" event. The dashed lines indicate where x=y.

4.5 CONCLUSIONS ON HYDRODYNAMICS

The observed changes in morphology described in chapter 3 are the result of physical forces acting on the mudflat and the marsh edge. In current chapter we report the behaviour of three principal physical forces acting at the Galgeschoor: tidal currents, wind waves and ship waves.

Tidal current velocity varies between 0.3 m/s and 1.25 m/s, yet high current velocity is invariably recorded near spring tide and during the flood phase. Tidal current velocity is relatively constant at ebb over the whole neap-spring tide cycle. During the flood phase however, tidal current velocity may both be lower (near neap tide) or much higher (near spring tide). These results emphasize that the flood phase may be predominant in tidally-induced morphodynamics. The above description of tidal current at the Galgeschoor is based on recordings at the low tidal flat domain. Less is known of current velocities at the high tidal domain but the available data suggest current velocities are lower.

Wind speed positively affected **wind wave** height, yet this effect did not act below wind speeds of 10 m/s. At higher wind speed, significant wave height per tidal cycle increased to 0.2m (approx. 0.38m maximum wave height) at the highest wind speeds recorded during the study (between 15-20 m/s). Wind wave height appeared marginally higher at the southern transect compared to the northern transect, but in general no clear differences can be observed.

In general the **ship wave climate** intensified during the study period with an increase of ship passing intensity of 15% between October 2015 and 2016. Tug boats and cargo ships, sailing upstream, are slower in southern then northern transect, for tankers there was no difference. The percentage in seagoing and inland ship passages remains similar for both intensive measurement campaigns.

Looking to the Galgeschoor wave data is very challenging. Similar studies have been performed to a study area close to the Saeftinghe area (the east side), which is only a few kilometres downstream of the Galgeschoor area. Ship waves here are very clearly recognizable, with (for larger ships) a clear primary wave followed by a secondary wave. This clear patterns are not often monitored in the Galgeschoor section. Moreover, a wave pattern with long wave period (few minutes) is clearly present on peculiar times of the tidal period (see Kolokythas et al., in prep), which additionally adds noise to the different selected wave events.

Some trends about the observed ship waves are revealed in this report. For primary waves, a clear difference in maximum wave heights is observed between 2015 and 2016 without a clear reason. It is clear on the data of 2015 that there is an inverse relation between the tide and the primary wave height, maximum waves are observed during the moments of lower water levels. This can be important with relation to the morphodynamics of tidal marshes, as the important wave loadings due to (high) primary waves are not felt on this level. For some vessel types, and for some years, sailing speed correlated positively with wave height. Maximum ship wave height was largely below 0.2m but some peaks were recorded up to 0.7m. As such, overall, ship maximum wave height was higher than wind maximum wave height.

For the secondary waves, it is clear that in the southern transect the waves due to inland navigation seems to be higher compared to seagoing vessels. Ship waves are attenuating from low to the high tidal flat. This means that they tend to decrease in height when they advance towards the shoreline, a pattern opposite from that observed for wind waves (at least at high wind speed).

doi.org/10.21436/inbor.17169167

5 RELATIONSHIP BETWEEN HYDRO- AND MORPHODYNAMICS

5.1 GENERAL OBSERVATIONS

To explore the relations between hydrodynamics and morphodynamic of a low versus a high tidal mudflat plot, we can use long term data at the Southern transect in the Galgeschoor from October 29th 2015 to January 17th 2017 (Figure 5.1). The bed level changes Δz (subplot f) are compared with wind regime U_{wind} including stormy conditions (subplot a) and related wave regime with wave heights H_{max} and H_s (subplot b and c). Bed level changes can also be related to the tidal regime h_{max} (subplot d) and the available suspended matter near the estuarine channel (subplot e).

Some **general patterns** can be observed from the superposed time series of data in Figure 5.1.

Dominant wind directions during the long-term campaign ranged from southerly to southwesterly winds (Figure 5.1, subplot a), with 69% of all recorded W_{dir} belonging to the south-west quadrant.

While no seasonal pattern arose in W_{dir} during the long-term campaign, seasonality in winds speed was observed, with higher wind speeds typically occurring during the winter months (e.g. November 2015 – February 2016), and lower wind speeds during the spring and summer months (e.g. May 2016 – September 2016). During stormy conditions (light blue-shaded areas), defined by the 90th percentile threshold of wind speed and here taken as 11.2 m s^{-1}, the averaged wind speed was 13.5 m/s and mostly occurred in winter, coinciding with the dominant W_{dir}.

Globally, wave climate measured at the southern transect showed a seasonal trend similar to wind climate, where higher H_{max} and H_s occurred during winter, and lower H_{max} and H_s during spring – summer (Figure 5.1 subplot b). Episodically, high peaks in H_s, and especially H_{max}, were noticed outside periods of strong winds, which are likely the result of (primary) ship-induced waves which are particularly frequent in the study area.

Time series of water depths at high tide, $\mathrm{h_{max}}$, measured at the southern transect are shown in (Figure 5.1 subplot d. Mean $\mathrm{h_{max}}$ at SH-GSc2 was 0.65 m, reaching a maximum value of 1.97 m on January 13, 2017, while mean $\mathrm{h_{max}}$ at SL-GSc4 was 4.14 m, and reaching a maximum value of 5.64 m on that same day. Variation in $\mathrm{h_{max}}$ is primarily attributed to the spring–neap tidal constituent although a seasonality is also present. The latter is associated with the inter-annual variability in wind climate, with higher $\mathrm{h_{max}}$ resulting from winter storm tides (e.g. January 13, 2017). Similar inter-annual variability in wind climate as well as in freshwater river discharge resulted in a seasonality of tidally-averaged SSC measured by the upper sensor of the Lillo measurement pole in the nearby estuarine channel (Figure 5.1 subplot e).

Although long-term seasonal bed level changes recorded at SH- GSc2 and SL- GSc4 (Figure 5.1 subplot f) seem to coincide with the seasonality in wind climate and associated hydrodynamics (waves and tides), effects of these various forcing factors on the observed short-term (daily) bed level changes are not so discernible at first glance (see 3.2.2). Daily erosional events during stormy conditions (light blue-shaded areas) can be indeed identified both at SH- GSc2 and SL-GSc4, yet other erosional events sometimes of even higher magnitudes occurred during calmer conditions.

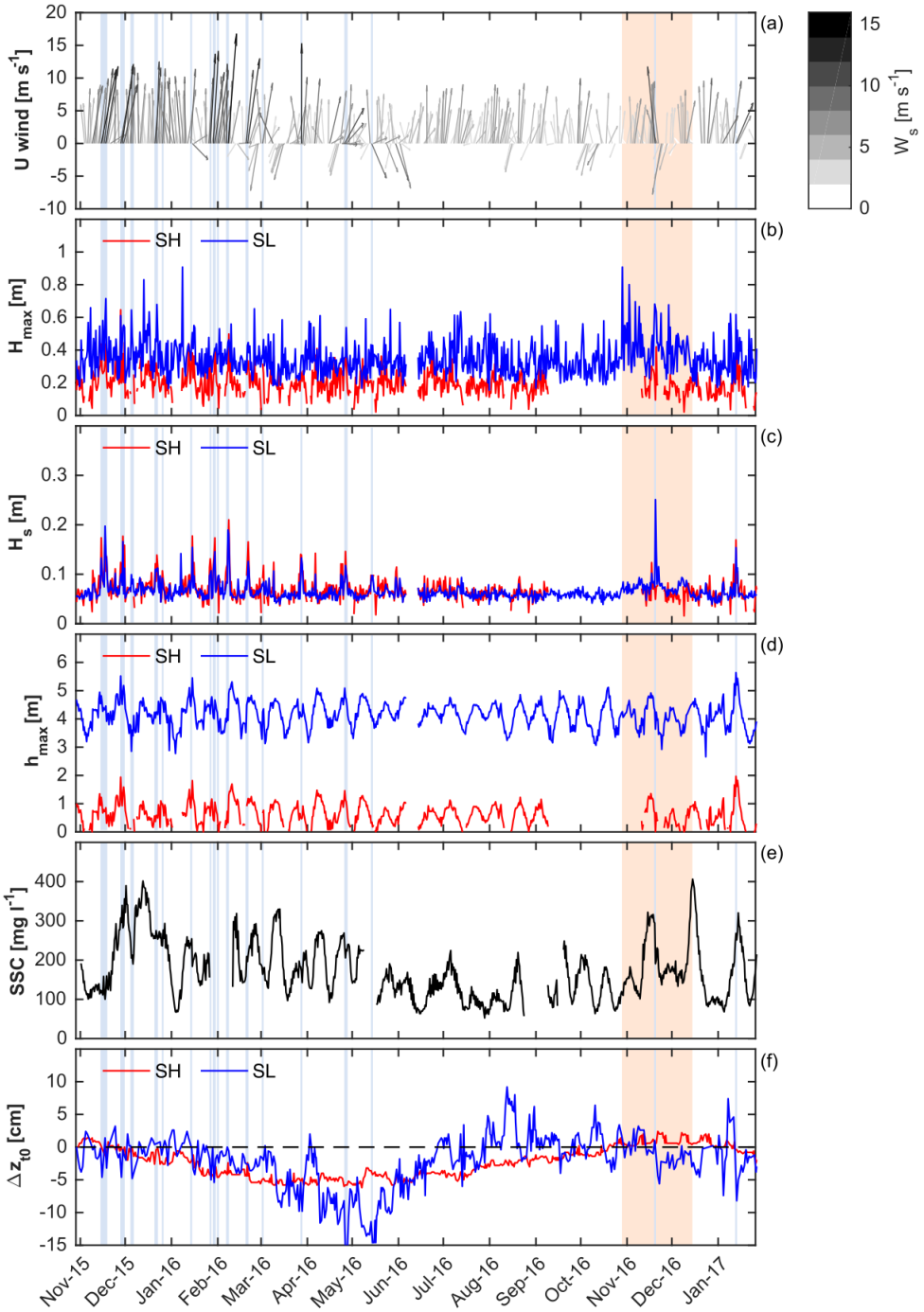

Figure 5.1 Temporal evolution of (a) daily-averaged wind speed W_s and direction W_dir, (b) tidally-maximum wave heights H_max, (c) tidally-significant wave height H_s, (d) water depth at high tide h_max, (e) tidally-averaged SSC and (f) bed level changes 〖Δz〗_t0 from October 29, 2015 to January 17, 2017 (for clarity purpose all time series were displayed until January 17, 2017 corresponding to the end of the wind measurement records). Figure 5.1b, c, d and f are further differentiated by measurements performed at the southern high (SH-GSc2, red lines) and low (SL-GSc4, blue lines) tidal flat stations. Only validated SSC data of the upper Anderaa Seaguard sensor at the Lillo measurement pole is displayed in subplot e. SSC was derived using a SSC – turbidity linear relationship drawn up following calibration campaigns that took place at Lillo. Light blue-shaded areas indicate stormy conditions, as defined by the 90th percentile of wind speed, here taken as 11.2 m s-1. The light beige-shaded area delineates the period where the intensive campaign took place.

doi.org/10.21436/inbor.17169167

5.2 WHERE AND UNDER WHICH CIRCUMSTANCES IS THE WAVE CLIMATE DOMINANT TO TIDAL CURRENTS?

To compare the hydrodynamic forcing between the two transects, we have to rely on the measurements performed during the last intensive campaign, i.e. during November 2016, where the experimental set-up allowed us to measure both wave (wind and ship waves) and tidal characteristics in the high (GSb2, GSc2) and low (GSb4, GSc4) tidal flat plots of the two transects simultaneously.

In particular, the addition of ADVs measuring 10cm above ground level on the high tidal flat plots (GSb2, GSc2) during the 2016 intensive campaign allowed to perform velocity measurements and to calculate proxies of hydrodynamic forcing.

The proxies for current-induced bed shear stress are computed based on the classical quadratic friction law commonly used (Van Rijn, 1993). The proxies for wave shear stress are computed using a quadratic friction law based on the linear wave theory following Fagherazzi and Wiberg (2009). These estimates for current-induced bed shear stress which, together with the wave-induced bed shear stress, constitute relevant parameters to compare the relative potential contribution of tides and waves to sediment mobilization and transport.

Figure 5.2 displays this estimate of a tidally averaged dimensionless wave-induced bed shear stress $\langle\theta_w\rangle$ and the equivalent current-induced bed shear stresses $\langle\theta_c\rangle$ differentiated by transect location, i.e. between the Northern transect high plot (NH-GSb2) and its Southern analogue (SH- GSc2 Figure 5.2 a), and between the Northern transect low plot (NL- GSb4) and its Southern analogue (SL- GSc4; Figure 5.2 b).

A first pattern that emerges is that, regardless of the transect considered, the wave-induced bed shear stress $\langle\theta_w\rangle$ was dominant over the current-induced bed shear stresses $\langle\theta_c\rangle$ at the high tidal flat plots, while at the low tidal flat plots, the current-induced bed shear stress was more dominant then the wave-induced bed-shear stress. That the current-induced bed shear stress $\langle\theta_c\rangle$, which is further modulated by the tidal regime (neap-spring tide cycle), is the dominant force at the low tidal mudflat, was revealed before by the spectral analysis of the SED-derived elevation change data (3.2.2).

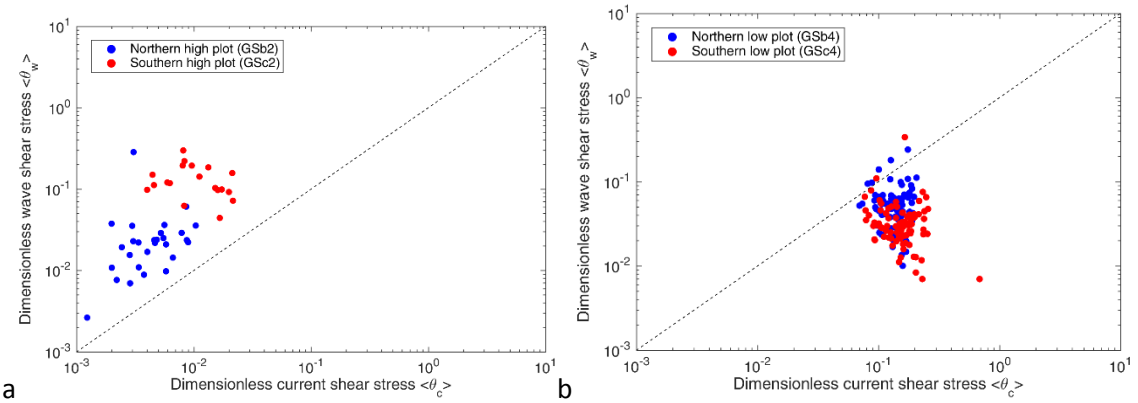

a b

Figure 5.2 (a) Dimensionless tidally-averaged wave-induced bed shear stress $\langle\theta_w\rangle$ vs. dimensionless tidally-averaged current-induced bed shear stress $\langle\theta_c\rangle$ differentiated by the high tidal flat plots of the Northern and Southern transects (GSb2 and GSc2 respectively) during the 2016 intensive campaign; (b) Dimensionless tidally-averaged wave-induced bed shear stress $\langle\theta_w\rangle$ vs. dimensionless tidally-averaged current-induced bed shear stress $\langle\theta_c\rangle$ differentiated

by the low tidal flat plots of the Northern and Southern transects (GSb4 and GSc4 respectively) during the 2016 intensive campaign.

In addition, $\langle\theta_w\rangle$ at SH- GSc2 was dominant over $\langle\theta_w\rangle$ at NH-GSb2 (see Figure 5.1 a), thus indicating a stronger effect of wave regime in the Southern transect high tidal flat compared to its Northern counterpart.

The lower $\langle\theta_w\rangle$ observed at NH-GSb2 may be explained by several reasons. First, the elevation of the high tidal flat plot of the Northern transect (GSb2; 5 m TAW recorded using RTK-GPS in November 2016) is somewhat higher than its southern counterpart (SH-GSc2; 4.66 m TAW), thus experiencing a higher wave energy loss due to wave dissipation by bottom friction, and depth-limited wave breaking (thus smaller waves). Second, the riprap belt in the Northern transect is larger than in the Southern transect, where it can cover an elevation gradient of maximum 2 m locally, therefore acting more substantially in attenuating wave heights as well as wave orbital velocities (Figure 2.4). Third, the more sheltered location of NH-GSb2, being somewhat in a corner very close to the marsh edge, may likely experience a lower wind fetch, hence lower wave heights although wind fetch in the study area is considered short to moderate (< 2.5 km, Figure 4-7), except for the Deurganck dock direction.

5.3 RELATION BETWEEN HYDRODYNAMICS AND POTENTIAL MORPHOLOGICAL CHANGES

- *Can hydrodynamics (currents or waves) observed in November 2016 induce morphological changes at the high tidal flat domain?*

Southern transect

Focusing on the high tidal flat domain, during the 2016 intensive campaign, the estimate of wave-induced bed shear stress $\langle\theta_w\rangle$ exceeded current-induced bed shear stress $\langle\theta_c\rangle$. At some points, tidally averaged wave-induced bed shear stress even exceeded the local critical Shields shear stress for sediment motion θ_{cr}; during several tidal cycles (Figure 5.3b), therefore suggesting a significant wave impact on sediment dynamics during those moments. Indeed, monitoring data for water turbidity indicate parallel increases in wave velocities and turbidity (Figure 5.4). Current shear stress at the high tidal flat plot, barely exceeded the critical threshold for resuspension during the November 2016 campaign, therefore suggesting a lower wave impact on sediment dynamics during the intensive campaign.

doi.org/10.21436/inbor.17169167

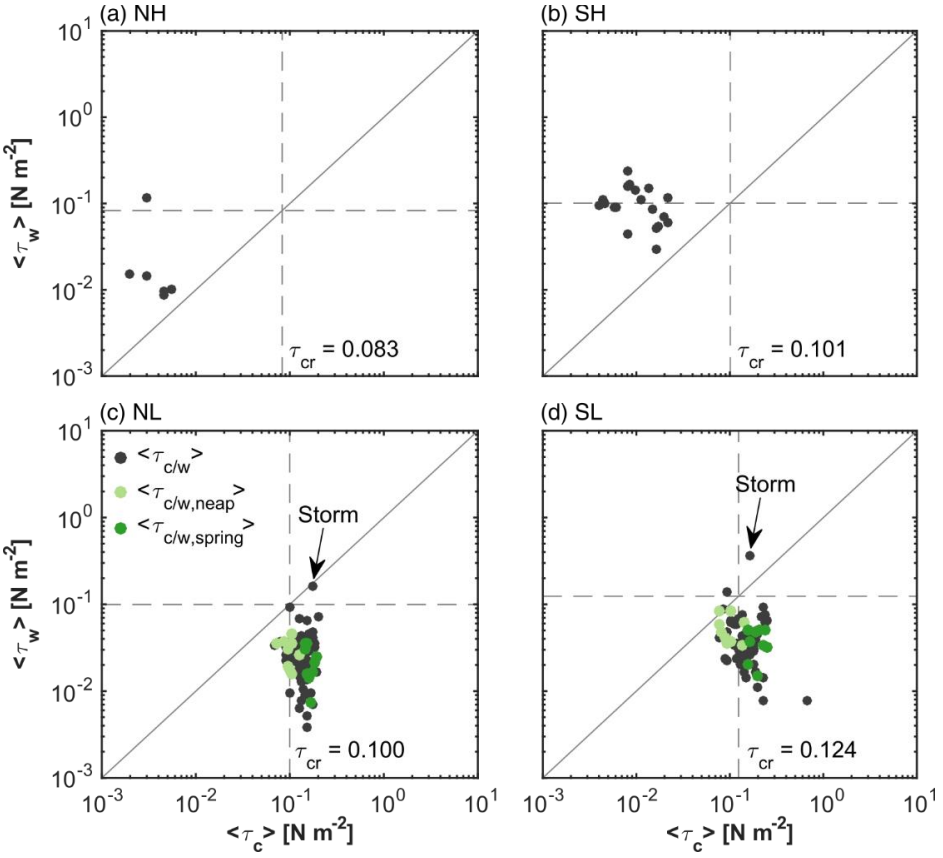

Figure 5.3 Scatter plot of tidally-averaged dimensionless wave-induced bed shear stress ⟨ 〖θτ〗_w ⟩ vs. tidally-averaged dimensionless current-induced bed shear stress ⟨ 〖τθ〗_c ⟩ recorded at the (a) northern high (NH-GSb3), (b) southern high (SH-GSc2), (c) northern low (NL-GSc4) and (d) southern low (SL-GSc4) tidal flat measurement stations during the intensive campaign (i.e. from October 27, 2016 to December 12, 2016, except for SH where the pressure sensor was repaired and reinstalled on November 09, 2016). Dashed lines with corresponding critical Shields bed shear stress 〖τθ〗_cr for sediment motion are displayed for every station considered. ⟨ 〖τθ〗_w ⟩ and ⟨ 〖τθ〗_c ⟩ at NL and SL are further differentiated by periods of neap and spring tides.

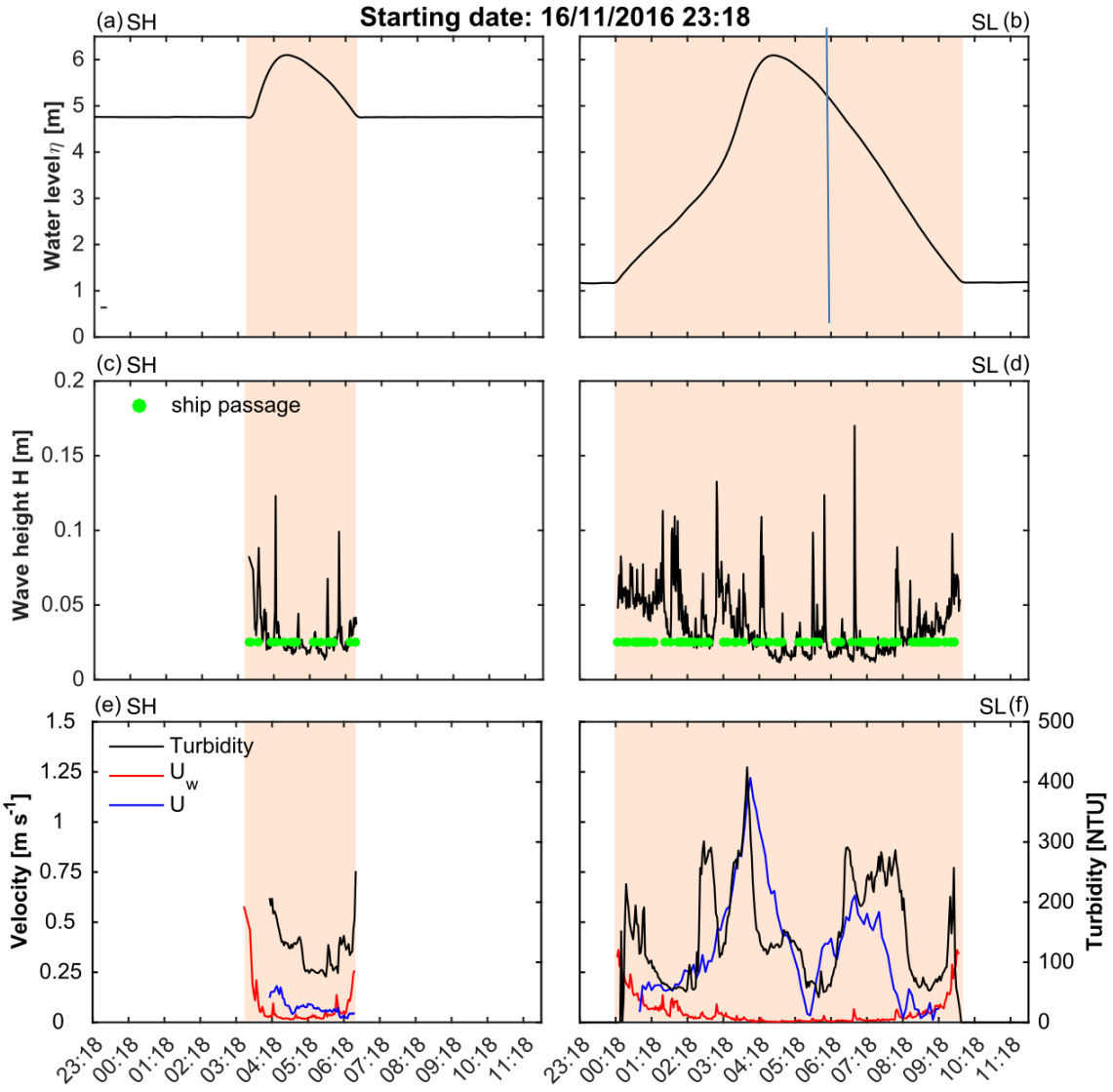

Figure 5.4 Temporal evolution of water level η, wave height H, wave orbital velocity U_w current velocity U and turbidity respectively recorded at the (a, c, e) southern high (SH –GSc2) and (b, d, f) southern low (SL-GSc4) tidal flat measurement stations during a spring tidal cycle starting on November 16, 2016 23:18:00. Tidally-averaged W_s was 7.0 m s-1 and tidally-averaged W_dir corresponded to southwesterly winds. For a matter of visualization, recorded η, H, U_w and turbidity were averaged over 2 min at both locations. U measured at SH –GSc2 corresponds to (ADV-derived) point current velocities measured at 10cm above the bottom, also averaged over 2 min, whereas U at SL-GSc4 represents (ADCP-derived) depth-averaged current velocities, kept at the original measurement frequency (i.e. 5 min; see Table 1). Every green dot represents the time of passage of a ship in the S entry line, retrieved using the AIS data. The light beige shaded areas delineate the actual inundation phases at SH and SL during the recorded tidal cycle

At the low tidal domain of the southern plot (SL-GSc4), dominance of wave shear stress shifts to the benefit of current shear stress (Figure 5.3d). Current shear stress also becomes morphologically more relevant, as it exceeds the critical threshold in the majority of cases. Yet, contrary to the high tidal flat, the low tidal flat is more subject to incoming ship waves due to corresponding longer inundation time and frequency as well as proximity to the estuarine channel. These ship waves that are characterized by high wave heights, which can result in

doi.org/10.21436/inbor.17169167

more pronounced wave orbital velocities near the bottom during the shallow water periods of early flood and late ebb, eventually amplifying θ_w (Verelst et al. 2011a). In this regard, $\langle\theta_c\rangle$ is higher than $\langle\theta_w\rangle$, except during storm conditions, which therefore denotes a higher impact of tides than waves on the short-term morphological changes at this location (Figure 5.3; storm of 20/11/2016).

Northern transect

Patterns of wave-induced bed shear stress and current induced bed shear stress for the tidal flat plots of the Northern transect follows those described at their respective Southern counterparts; in other words wave regime is dominant over tidal regime in the high tidal flat plot (NH- GSb2, Figure 5.3a&b) and the opposite occurs in the low tidal flat plot (NL-GSb4; Figure 5.3c&d). Yet, there are much less instances where $\langle\theta_w\rangle$ at NH and $\langle\theta_c\rangle$ at NL exceeded their corresponding θ_{cr}during the 2016 intensive campaign. This accords with the earlier findings that the temporal evolution of bed level changes at the locations of the Northern transect are characterized by little elevation changes compared to the southern transect. These results therefore suggest an insignificant wave (at NH-GSb2) or tidal (at SH-GSb4) impact on the morphological changes during the 2016 intensive campaign, correspondingly.

Despite $\langle\theta_w\rangle$ sometimes exceeding θ_{cr} during several tidal cycles at SH- GSc2, therefore causing causing sediment resuspension, the opposite still occurs during the majority of the tidal recorded during the 2016 intensive campaign at this location (see Figure 5.2a) allowing for the settlement of resuspended material. In addition, correlation analyses between wave heights (significant, maximum and relative wave heights) and daily bed level changes during the long-term campaign at SH- GSc2 did not yield highly significant results (

Table 5.1). Therefore, in view of the above results, the conclusion is that waves have a higher impact than tides at the high tidal domain (SH-GSc2) and can trigger sediment resuspension episodically, yet the significance of wave impact on the net morphological change at SH- GSc2 or on the possibility for vegetation development appears to be limited or in some periods the sediment is less cohesive then assumed[3]. Further research is needed to answer that question.

Nevertheless the comparison of the hydrodynamic shear stresses with the local critical shear stress for sediment motion gives no quantitative predictions, but reveals the relative differences in spatial patterns of bed sediment motion in between the different locations.

[3] *The local critical shear stress for sediment motion of Soulsby and Whitehouse (1997) is initially made for non-cohesive sediments*

doi.org/10.21436/inbor.17169167

Table 5.1 Correlation analyses between deseasonalized bed level changes 〖Δz〗_t0 and corresponding forcing factors recorded at the Southern high (GSc2) and low (GSc4) tidal flat plots during the long-term campaign. H_s = significant wave height; H_max = maximum wave height; H_rel = relative wave height; D = water depth at high tide; C: suspended sediment concentration recorded at the Lillo measurement pole located in the estuarine channel in the proximity of the tidal flat of Galgeschoor. ρ = Spearman's rank correlation; r = Pearson product moment correlation. Significant correlations (p < 0.05) are underlined.

Variables	Southern transect High plot - GSc2		Southern transect Low plot - GSc4	
	Score	p-value	score	p-value
H_s vs. Δz_{t0}	ρ = 0.001	p = 0.970	ρ = -0.11	p = 0.016
H_{max} vs. Δz_{t0}	ρ = -0.056	p = 0.237	ρ = -0.013	p = 0.797
H_{rel} vs. Δz_{t0}	ρ = 0.093	p = 0.05	ρ = -0.172	p = < 0.001
D vs. Δz_{t0}	ρ = -0.121	p = = 0.01	ρ = -0.427	p < 0.001
C vs. Δz_{t0}	ρ = -0.236	p = < 0.001	ρ = -0.154	p = 0.002

5.4 WHERE IS TIDAL REGIME DOMINANT IN THE MORPHOLOGICAL CHANGES?

Tidal regime is clearly dominant with regard to the short-term morphological changes at the low tidal flat plot of the Southern transect (SL-GSc4). First, $\langle\theta_c\rangle$ was higher than $\langle\theta_w\rangle$ and even exceeded θ_{cr} in the majority of the tidal cycles recorded during the 2016 intensive campaign (see Figure 5.2 c). The dominance of tides over waves at SL-GSc4 is further illustrated when looking at Figure 5.4-right where the temporal variation of the turbidity primarily follows the variation of tidal flow velocities. High values of wave orbital velocities at the shallow leading and trailing edges of advancing and retreating waters also trigger high turbidity, yet in the form of sudden and shorter peaks. Moreover, unlike wave characteristics, water depth at high tide is significantly correlated with daily bed level changes at GSc4 recorded during the long-term campaign (r_s = -0.47 in Figure 5.5a,

Table 5.1), therefore confirming a tidal impact on the net morphological changes over the long-term.

Compared to the global correlation over the long-term campaign the correlations between water depth at high tide and bed level changes recorded in March-May 2016 (r_s = -0.47), August-September 2016 (; r_s = -0.68) and January-February 2017 r_s = -0.77 at SL-GSc4 were even stronger negatively (Figure 5.5).

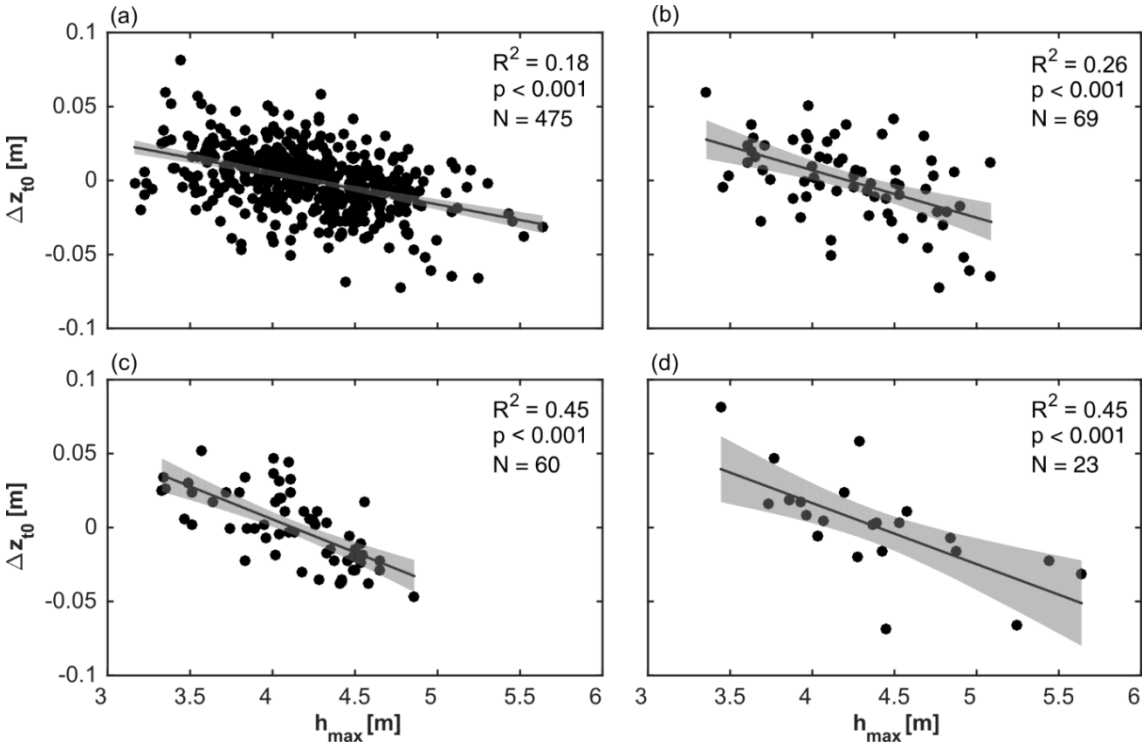

Figure 5.5 Scatter plots of detrended bed level changes 〖Δz〗_t0 against water depth at high tide h_max measured at SL during (a) the entire long-term campaign, (b) March – May 2016, (c) July – September 2016 and (d) January – February 2017. Every scatter plot is supplemented with an Ordinary Least Square (OLS) linear regression model of equation (a) 〖Δz〗_t0=0.09-0.021h_max, (b) 〖Δz〗_t0=0.135-0.032h_max, (c) 〖Δz〗_t0=0.184-0.045h_max and (d) 〖Δz〗_t0=0.182-0.041h_max. Coefficients of determination R2, prediction bounds (95%), p-values and number of observations N are also displayed

Interestingly, this significant correlation points out a negative relationship between water depth and bed level changes at SL-GSc4; in other words, negative bed level changes (i.e. erosion) increase with water depth. This result reveals the role of tidal flow velocities in controlling sediment dynamics since tidal flows typically increase with the tidal range/inundation depth via a well-documented linear relationship and which has also been tested and validated in situ during the 2015 and 2016 intensive campaigns at NL-GSb4 and SL-GSc4 (see Figure 4.1 and Figure 4.2). Therefore, at SL-GSc4, tidal flow velocities increase together with tidal depth, being proportional to tidal range, from the lowest values at neap tides up to values above 1 m/s during spring tides (see Figure 5.4-right). These high tidal flow velocities, at this site with cohesive sediment, lead to $\langle\theta_c\rangle$ exceeding θ_{cr}, thus causing sediment resuspension at SL-GSc4, in particular during spring tides whereas during neap tides $\langle\theta_c\rangle$ rarely exceeds θ_{cr} comparatively (Figure 5.3d).

doi.org/10.21436/inbor.17169167

5.5 LOCATION-DEPENDENT HYDRODYNAMIC FORCING

Southern transect

In the *low tidal flat zone,* tides and related current velocities are clearly the dominant driving forces that control morphological changes. First, water depth at high tide, which depends on the alternating spring-neap tidal cycles, is highly correlated with the net daily bed level changes during the long-term campaign at the low tidal flat plot of the Southern transect (SL-GSc4). Second, tidal current velocities measured within tidal cycles at SL during the 2016 intensive campaign were well above 1 m/s during spring tides, generating high current shear stress that exceeded critical Shields stressθ_{cr} for sediment mobility on this non-cohesive sediment location. Whereas the presented shear stress values are mathematical approximations based on wave and current characteristics, their relevance is clear from field observations showing concomitant peaks of turbidity (a proxy of sediment resuspension) during high tide when current velocities are highest. These observations also fit with the long-term imprint of tidal cycles on sediment morphology. Episodically occurring waves at SL-GSc4 could generate bottom orbital velocities above 0,3 m s^{-1} and sometimes even higher during storm events. Indeed we find a negative correlation between wave height parameters and bed level change indicating high waves induce erosion (Table 5-1). In summary, at the low tidal mudflat, the impact of waves is secondary to tidal currents in shaping morphodynamics, yet they are an important additional factor shaping local morphology.

In the *high tidal flat zone*, both waves and tidal currents are less strong, and the observed bed-level changes are much less pronounced. Current velocities are less than half those of their low counterparts. Waves are relatively more important within tides in controlling morphological changes, especially when focusing on the comparisons of shear stress. This accords to the observation that, within a single tidal cycle, turbidity primarily covariated with bottom wave orbital velocities at the high tidal flat plot of the Southern transect (SH-GSc2), especially at the shallow leading and trailing edges of advancing and retreating waters, causing wave-induced bed shear stress stress $\langle\theta_w\rangle$ sometimes exceeding the local critical shear stress (Shields stress) for sediment motion θ_{cr}. However, contrary to the low tidal flat, wave height parameters did not relate to the net (between tidal cycles) bed level changes over the long-term campaign, thus suggesting that waves have a poor impact on the net morphological changes (Table 5-1). Long-term deseasonalized bed-level changes exhibited a weak yet significant recurrent pattern related to the tidal cycle. Indeed, bed-level changes correlated negatively with local water depth (D), a proxy for current velocity, but the correlation was less strong compared to the low tidal flat.

Northern transect

As mentioned earlier, similar patterns of hydrodynamic forcing took place at the Northern transect: tidal currents dominate morphodynamics in the low tidal flat zone while waves and currents both contribute to morphodynamics at the higher tidal flat zone. Yet, contrary to their Southern counterparts, neither tides nor waves trigger significant morphological changes at the respective low (NL-GSb4) and high (NH-GSb2) tidal flat plots over the long-term. The nearly absence of tidal cycles in bed-level changes (spectral analysis) is congruent with the near-absence of tidally-averaged wave-induced bed shear stress $\langle\theta_w\rangle$ at NH- GSb2 or the dominant tidally-averaged current-induced bed shear stress $\langle\theta_c\rangle$ at NL- GSb4 exceeding the critical shear stresses for sediment motion θ_{cr}.

Location dependency of the impact

Besides the large scale hydrodynamic and morphological setting of the study area, one reason for the observed differences in the impact of hydrodynamic forcing on the morphological changes between the two transects can be attributed to the difference in surficial sediment characteristics. The mud fraction (grain size < 63µm) at the NH-GSb2, NL-GSb4 and SH-GSc2 accounts for more than 50 % of the total sediment composition throughout the long-term campaign. Cohesion between muddy sediment grains is relatively strong. Sediment composition at SL-GSc4 on the other hand is characterized by a dominant sand (non-cohesive) fraction throughout most of the long-term campaign (Figure 3.1). The combination of fine cohesive sediments with a comparatively reduced tidal regime and wave climate at the respective low and high tidal flat plots of the Northern transect as opposed to their Southern counterparts may explain the observed low morphological changes.

5.6 CONCLUSIONS ON THE RELATION BETWEEN HYDRO- AND MORPHODYNAMICS

At the southern transect a long term seasonal trend is found in the bed level changes with a sedimentation trend between spring and autumn and an erosion trend between autumn and spring. Although these long-term seasonal bed level changes at the southern transect seem to coincide with the seasonality in wind climate and associated hydrodynamics (waves and tides), effects of the various forcing factors on the observed short-term (daily) bed level changes play a role. Under maximal tidal conditions (i.e. spring tide) the current shear stress exceeds the local critical shear stress at *the low tidal flat* of both transects, thus suggesting a tidal current impact on morphology. In average conditions only the southern low tidal flat plot exceeds the critical value. The effectiveness of the impact of this hydrodynamic forcing is also dependent on sediment type. In contrast to the other sites the southern low tidal flat has non- cohesive (sandy) sediment and endure the highest impact. Also this site shows a positive correlation of water depth or the strong related maximum flow velocities with the net daily bed level changes on the longer term.

doi.org/10.21436/inbor.17169167

6 DISCUSSION

The tidal mudflat of the Galgeschoor shows an ecotope evolution after the third deepening (2009-2010) similar to other estuarine areas more upstream. The middle tidal flat area has increased mainly at the expense of low tidal flats (Van Braeckel et al. 2012). Also the potential pioneer zone, the mudflat area above mean high water at neap tide, has declined. More recently (2014-2016), morphological monitoring of the Sea Scheldt (Van Braeckel & Elsen in Van Ryckegem et al. 2017) revealed that large tidal mudflats at inner bends in the upper Sea Scheldt display shrinking sedimentation areas and increasing erosion areas. This phenomenon is expanding yearly in upstream direction, and is observed in the Galgeschoor as well. On the Galgeschoor this process changes soft bottom low tidal areas into hard substrate. There is some debate on as to why this is happening, yet one current hypothesis is that hydrodynamic pressure on the intertidal areas has increased during flood, the tide phase with the highest current velocities on the intertidal areas.

The marsh cliff of Galgeschoor is retreating continuously since 1940. Originally, cliff erosion occurred by meters per year. After the installation of a rip rap zone retreat rates became in the order of cm's per year. The nature of the marsh has changed due to the rip rap from an exposed-bare marsh to a sheltered-bare and pioneer marsh, due to the shrinking of adjacent mud flats and decreasing width of the marsh after dike reinforcements (Wang et al. 2017). Recently (2010-2012) erosion rates have been rather high again (31.7 cm/year). This coincided with the third deepening and widening of the navigation channel, yet there is no other evidence to link both phenomena. After 2013, retreat rates have decreased again to the normal background level (Figure 3.5). Overall, the marsh edge at the southern transect showed higher retreat rates (15–32 cm/year) than the marsh edge at the northern transect (2.5 cm/ year).

Research in the Westerscheldt (Wang et al. 2017) by NIOZ revealed a scale-dependence of factors driving tidal marsh edge retreat. (i) At a large scale, wind exposure (fetch length, orientation,…) and presence of vegetation in front of the cliff govern the cliff retreat rates; (ii) at the intermediate scale, foreshore morphology was related to cliff retreat; (iii) at the local scale, the erodibility of the sediment itself at the marsh edge played a large role in determining the cliff retreat rate; and (iv) at the mesocosm scale, cliff erodibility was determined by soil properties and belowground root biomass. Thus, both extrinsic (wind exposure and foreshore morphology) and intrinsic factors (soil and vegetation properties) determine the fate of the salt marsh edge, but at different scales.

Galgeschoor, which is located at an inner bend (from east to north direction; Figure 4.7) at the right bank of the Scheldt, is one of the areas of the inner estuary that (i) experiences a high wind exposure. On the other hand the increasing abundance of the pioneer vegetation *Glaux maritima* in front of the marsh cliff may temper impact on the marsh cliff however this is a minute type of vegetation (GSb2, Figure 3.4, Figure 3.14). Along the southern transect the (rather scarce) increase of *Vaucheria* and some pioneer vegetation G*laux maritima* (southern part in Figure 3.4) may have helped slowing down the cliff rate erosion in GSbc (Figure 3.4). As such, the northern transect can be seen as a sheltered-pioneer and the southern transect as a sheltered-bare marsh type (Wang et al. 2017) (ii) At the intermediate scale the foreshore morphology at Galgeschoor is highly influenced by the width, height and shape of the soft bottom mudflat and the (maximal) height of the rip rap zone (Figure 2.4) and width of the natural hard peat layer at the low tidal mudflat in the north. (iii) At the local scale near the tidal marsh cliff on the high tidal flat, the composition and grain size of the mud substrate (Figure 3.15) is important as well as the depth of the clay subsurface (old marsh soil). The highest median grain size values for GSc2 are found in erosion periods. (iv) at the very local

scale, cliff erodibility is determined by soil properties. In April 2011 we sampled in a previous project the tidal marsh zone at the northern and southern transect (Michels et al. 2012) and found a clear difference in volume percentage of the tidal marsh soil between the two sites (Figure 6-1a) in concordance with sedimentological results of this study.

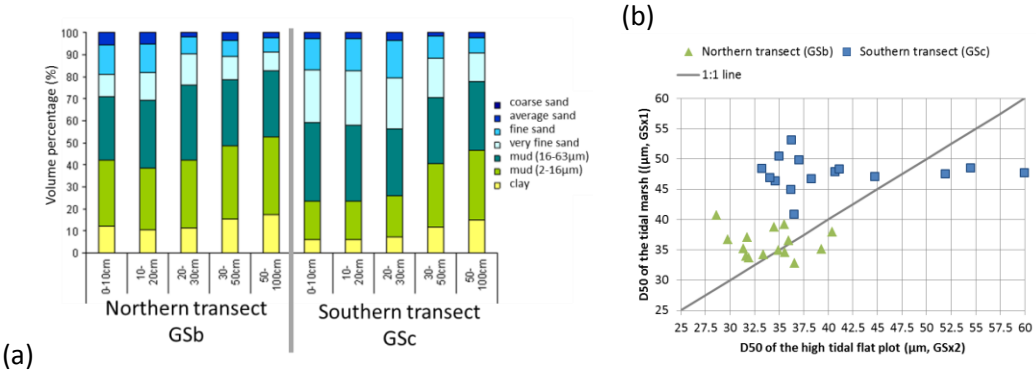

Figure 6.1 a) Composition of the different fraction (% volume) per transect and depth zone (Michels et al. 2012); b) relation between D50 of the upper soil layer in this study on high tidal flat plot and the nearest tidal marsh plot

The southern transect, which is located at an inner bend and endures more differentiation in current velocity patterns, shows a higher variability in soil layers than the northern plot. The marsh soil at the northern transect (raai3) consists for 70-80% of muddy/clay fraction (<63µm), whereas this was less than 60% at the southern transect. The marsh soil profile at the southern transect also showed a clearer stratification then the northern GSb. This may explain partly the higher vulnerability of the southern marsh edge to erosion. Furthermore the median grain size of the tidal marsh surface layer is similar to that of the high tidal flat for the northern transect (Figure 6-1a) but not for the southern transect where it seems coarser on the tidal marsh indicating differences in hydrodynamic forces in the marsh edge.

In the Westerscheldt, four tidal flat–salt marsh ecosystems with contrasting wave exposure (sheltered vs. exposed) and lateral development (shrinking vs. expanding) were studied by Callaghan et al. (2010). They found that hydrodynamic forces and related sediment bed motion are consistently higher at sites with shrinking marshes than sites with expanding marshes, regardless of wind exposure of the sites. The main cause was the bathymetry of the tidal flat in front: tidal flat bathymetry determines hydrodynamic forces and whether waves will reach the cliff or not. Therefore our research focused on sediment bed motion and proxies of hydrodynamic forcing which are relevant to bed sediment motion.

In the Galgeschoor the bed level changes showed a clear seasonality with a tendency (2 years data) for mudflat erosion in (late) winter and spring and deposition during the rest of the year. These seasonal bed level changes are similar to what Kirby et al. (1993) noticed over a 22 month period on a mudflat of the mesotidal Ardmillan Bay (UK). In particular, storm-generated waves were found to cause erosion in winter and spring, and deposition under calmer summer conditions was enhanced by algal binding of the bed sediment. They concluded that episodic wind waves were the main cause of tidal flat instability and noted that this seasonal pattern in accretion and erosion is consistent with previous studies. Uncles and Stephens (2010) concluded similarly for the Tavy estuary that a summer solstice period of weaker spring tides has slower wind speeds, smaller waves, lower freshwater runoff and, potentially, the growth of stabilizing benthic algae over the mudflats to facilitate deposition and consolidation of mud. For Galgeschoor we also ascribe this seasonality in bed level changes at GSc2, GSc4 and to a lesser extent at GSb2 to both seasonality of hydrodynamics (generally more windy

doi.org/10.21436/inbor.17169167

weather/higher waves in the winter compared to summer) and benthic biology (biostabilization by benthic diatoms and bioaggregation of *Vaucheria* and *Glaux maritima* (see photos in Figure 6.3) in winter compared to summer (Uncle & Stephens 2010, Anderson et al. 2006). We do not have actual data on benthic life at the site to confirm this as this was not part of the study.

Superimposed on this seasonal pattern, we also noticed recurring erosion-sedimentation cycles linked to the spring-neap tidal cycle. Erosion typically occurred near the spring phase of the tidal cycle, whereas sedimentation occurred near the neap tide tidal phase. The effect size of this pattern varied greatly and was likely dependent on e.g. interactions with bioturbating and/or coagulating benthic organisms or the quantity of suspended solids or was overruled by e.g. episodic wave forcing. Therefore, such observations confirm that despite the dominance of tides in driving the morphological changes, the latter is fundamentally controlled by the combined action of the dominant periodic tidal forcing and other factors such as episodic wave forcing, biological activity or SPM levels.

In a detailed analysis of the variations of sediment flux and bed level measured for one year in the Spurn Bight, Humber estuary, UK, Christie et al. (1998) found that during the winter, periods of offshore transport typically coincided with the erosion of several centimetres of sediment per tide. Conversely, positive fluxes predominated during the calmer, summer months, and coincided with net accretion rates of a few millimetres per tide. Anderson et al. (2006) found also that spatial differences occurred and the bed level change at the inner and outer part of the mudflat was generally in opposition to each other. We also observe such clear seasonality in bed level dynamics both at GSc2 and GSc4 with same tendencies, yet unlike Anderson t al. (2006), bed level changes between the upper and lower tidal mudflat locations are not opposite.

At Galgeschoor, tidal forcing represents a main driver of bed level dynamics, particularly at the low tidal flat plots (significant relation between inundation depth and short-term (daily) relative elevation changes at GSc4; Figure 5.5). An increasing tidal range/inundation depth and correlated increasing tidal currents (Figure 4.1, Figure 4.2) induce higher erosion. Also bed-level dynamics at most sites except for the northern high tidal flat plot show the presence of a 15-day periodicity in the times series of relative elevation changes, which indicates the importance of the tidal forcing. Deloffre et al. (2005) concluded that tidal forcing was also the dominant driving force responsible for the erosion of a mudflat located in the upper macrotidal Seine estuary, France. This characteristic time-scale is also present in the variation of τc as well as τ_{tot} during storm events, which was significantly correlated to bed-level dynamics at Zuidgors and Baarland (Hu et al. 2017). Yet, contrary to Hu et al. (2017) tidal forcing cannot explain variation in long-term bed level dynamics along the Galgeschoor. Spatial variations in sediment characteristics (mud content, particle size, Figure 3.16) interact with tidal forcing in shaping elevation changes at the high plot of GSc2 over the long-term, and possibly other factors may be at work.

Similarly at Zuidgors and Baarland, tidal flats in the Westerschelde with a contrasting wave exposure, Hu et al. (2017) has found using SED sensors that the magnitude of short-term bed-level variations increased with a higher inundation depth. They also found that only at the wind wave exposed site of Zuidgors short-term (daily) fluctuations in bed level dynamics were significantly related to the local wave forcing variation (τ_w), especially wave forcing during storm events which lead to abrupt erosion. In the sheltered site of Baarland no correlations

were found with wave forcing. Galgeschoor, characterized by mainly short fetch lengths (< 2.5 km, Figure 4.7) except 10 degrees of winds coming from the Deurganck dok (GSb 210°, GSc 220°), can also be considered as a sheltered site compared to Westerscheldt sites. The absence of relations between tidal forcing and bed level dynamics in the high sites and the low site of GSb is in line with the findings at Baarland.

Ship traffic is high at Galgeschoor and manoeuvres related to the docks may amplify wave exposure locally. At the Galgeschoor maximum ship wave height measured at the low water line was largely below 0.2 m but some peaks were recorded up to 0.7 m. As such, overall, ship maximum wave height was higher than wind maximum wave height. However, ship waves were observed to attenuate from the low to the high tidal flat. Similar to the Galgeschoor study, wave measurements were also performed in Dendermonde (Upper Sea Scheldt) and Saeftinghe (Western Scheldt) recently. In Dendermonde, clearly smaller wave characteristics were observed. Maximum wave heights of approx. 0.45 m were observed. The higher waves can be linked to ship traffic, even with the much smaller ships (max. length 100 m) passing here. In the signature of the ship waves, only secondary waves could be discerned. In Saeftinghe, maximum wave heights of 1.1 m were recorded. The significant wave heights, calculated over a full tide, ranged between 0.06 m and 0.10 m, which is similar for the Galgeschoor case. The relation between the secondary wave heights and the ships characteristics showed large variation, similar to the Galgeschoor measurements. Maximum secondary wave heights of approximately 1.1 m were recorded. In contrast with the Galgeschoor measurements, the primary wave signal of ships was in most cases much more pronounced. Maximum primary wave heights of ca. 0.8 m were recorded. These high values are mostly accounted for by the largest ships (>350 m length).

Looking at estimates of both current and wave forcing, wave-induced bed shear stress $\theta_{w,max}$ at GSc2 and GSc4, occurring during the early and late stages of the tidal inundation, were higher than the current-induced bed shear stress $\theta_{c,max}$. This is also found by Zhu et al. (2014) in an intensive study on the intra-tidal sedimentary processes (Yangtze River Delta, China). At the high plot at the southern transect (GSc2) the calculated wave-induced bed shear stress $\langle\theta_w\rangle$ also more often exceeded the local critical shear stress for sediment motion than current-induced bd sgear stress (θ_{cr}, Figure 5.3a) in comparison to the northern transect (Figure 5.3b). Measurements on turbidity at high and low tidal flat plot at the southern transect (GSc2,GSc4; Figure 5.4) also showed high values at the early and late stages of the tidal inundation. At the high tidal plot GSc2 it is even higher than the overall turbidity induced by the currents. Similar results were found by Verelst et al. (2011a; Figure 6-2) for 20 - 22 April 2011 measurements at the low tidal flat at the southern transect (ADV: 1.15m T.A.W.)

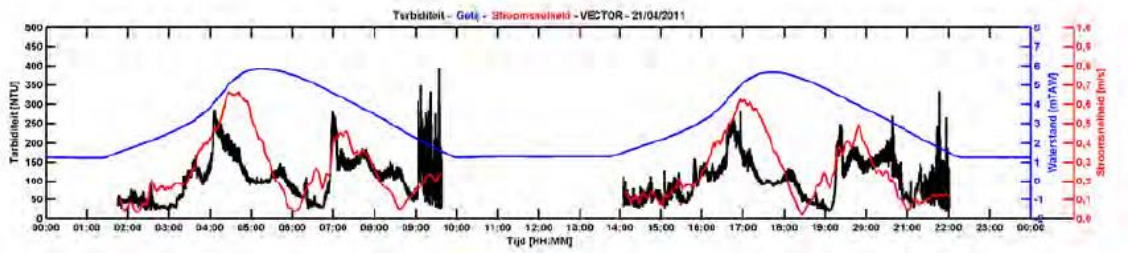

Figure 6.2 Turbidity (black, NTU), current velocities (red, m/s) and water level (blue, m T.A.W.) measured with an ADV at 20 to 22 April 2011 (adapted from Verelst et al. 2011a)

Uncles and Stephens (2010) describe these intratidal variations in turbidity over the mudflats. Generally it exhibits a 'U'-shaped temporal behaviour within each tidal inundation, except in

doi.org/10.21436/inbor.17169167

the presence of wave -induced sediment resuspension. With or without substantial waves, higher turbidity is experienced as the mudflats initially inundates. In the absence of wave resuspension, this is followed by a rapid decrease in SPM for most of the tide, indicating that the mudflats are depositional at these times. SPM concentrations on the mudflats again increase sharply prior to uncovering. This 'U' profile is partly due to the advection of lower and mid-salinity, higher turbidity waters across the mudflats during the early flood and late ebb, with the possibility of local resuspension of sediment into the shallow layer of ebbing waters during peak spring tidal currents, especially with additive wave- driven currents, or following a high runoff event. Based on visual observations they also indicate that even relatively slow winds can lead to small breaking waves and resuspension in the very shallow, leading or trailing edge of advancing and retreating waters on the mudflats.

These early and late stages of tidal inundation have been defined in the study of Verelst et al. (2011a & 2012) at Galgeschoor. During these shallow moments, based on a restricted dataset, they found a significant influence of ship waves on turbidity and flow velocity.

Water depth is a critical control on sedimentation (Hunt et al. 2016), as the short period waves generated within estuaries are attenuated rapidly with increasing water depth and this water depth varies throughout the spring neap cycle. Therefore, morphologically significant wave conditions occur even under weaker winds in the shallower parts of the estuary and this influence increases with increased wind speeds. This result matches with the relative wave dominance observed in the upper tidal flat at Galgeschoor (GSc2) characterized by shallow conditions.

Figure 6.3 Algal mat of *Vaucheria* with pioneer vegetation *Glaux maritima* grew at the transect from May 2016 to late autumnConclusions and recommendations

6.1 MORPHOLOGICAL CHANGES

The Galgeschoor tidal marsh **historically** endured high morphodynamic changes with high historical marsh cliff retreat rates since the 1940s. The driving forces were the shrinking width of the adjacent mud flat from the riverside as well as dike enforcements from the landside. The construction of the rip rap wall on the riverside around 1990 apparently slowed down the long-term erosion of the marsh cliff, likely by exposure reduction on the marsh edge.

Nowadays the total area of tidal marsh ecotope in Galgeschoor near the marsh edge seems relatively stable. On the initial marsh **cliff retreat** areas pioneer marsh vegetation seems to establish, currently compensating the loss of tidal marsh by retreat, albeit a different successional phase. Consequently the proportion of high solid old marsh area decreases. The marsh cliff retreat rate also differs between the northern and southern transects with retreat rates of 2.5 and 15–32cm/year since 2010, respectively. Michels et al (2012) concluded that in view of its long term evolution an average marsh edge retreat of 25 cm/year can be considered as a background value for a normal tidal marsh cycle at the Galgeschoor, allowing for establishment of pioneer marsh. Apparently this coincides with the current observations in most of the area. However these changes are very recent and it is yet impossible to judge whether this is resilient in nature and part of the natural tidal marsh cycle.

At the Galgeschoor (low) tidal mudflat, high morphodynamics were observed during the past decade. This **ecotope** lost quantity as well as quality. It evolved into middle tidal mudflats due to accretion in 2012-2013 or into hard substrate zones by erosion in 2015-2016. These transitions are not only locally observed but also more widely in the estuary. The accretion period of the mudflats is believed to be an initial morphological reaction of the system to the last widening of the navigation channel (2009-2010) along the Scheldt estuary (Van Braeckel et al. 2014). In the more recent years, lower mudflat zones tend to erode more in the Flemisch part of the Scheldt (Van Ryckegem et al. 2017).

On the **long term, bed level** of the high tidal flat at the northern transect tended to increase and traps small volumes of sediment while the tidal mudflat zones beneath the riprap decreased and lost sediment volume. The southern transect has shown an opposite trend with bed levels of lower mudflats increasing, trapping large sediment volumes while the high tidal flat fluctuates around zero accretion. The sediment trapping at the southern transect tended to slow down since 2014 and the net increase stopped since 2016 at the middle and high mudflat. At the northern transect only the middle tidal mudflat level eroding trend changed since 2016 and started to accrete.

During the 2-year intensive monitoring campaign (2015-2016), **bed level changes** were generally much more pronounced at the southern plots (order of magnitude 5 – 10 cm) as compared to the northern plots (<5 cm). This may be attributed to differences in sediment properties (more sandy at the low southern plot). Both seasonal and day-to-day variations were clearly larger at the southern plots of Galgeschoor. This means that the southern transect was more dynamic. Further, low tidal plots were much more dynamic than high tidal plots. The seasonal variation at southern transect exhibits a period of sedimentation between spring and autumn while between autumn and spring mostly erosion takes place. The daily fluctuations in bed level in the low and to a lesser extent in the high tidal flat plots, reveals a spring-neap tidal cycle (i.e. 14.77 days).

doi.org/10.21436/inbor.17169167

6.2 PHYSICAL FORCING FACTORS

The observed morphological changes result from the combined and simultaneous action of several **physical forcing factors** on the mudflats and marsh edge.

Tidal current velocity as measured during two one month autumn campaigns varied between 0.3 m/s and 1.25 m/s. High current velocity is invariably recorded near spring tide during the flood phase. Tidal current velocity at ebb (0.5-0.75 m/s) is relatively constant over the neap-spring tide cycle. During the flood phase however it is lower near neap tide and much higher near spring tide. These high velocities in the flood phase during spring tide emphasize that flood may be predominant in tidally-induced morphodynamic changes. The above description of tidal currents at the Galgeschoor is based on recordings at the low tidal flat. Less is known about current velocities at the high tidal flat but the available data suggest that current velocities are generally lower.

Wind speed positively affected **wind wave** height, yet this effect did not act below 10 m/s. At higher wind speed, significant wave height per tidal cycle increased to 0.2 m (approx. 0.38m maximum wave height) at the highest wind speeds recorded during the study period (between 15-20 m/s, 7-8 Beaufort). Further analysis also suggested that wind waves tend to increase from the low towards the high tidal flats indicating an amplifying behaviour of the incoming wind waves, yet only at high wind speeds. At high wind speed, fetch may become increasingly important and is longest at the high plots, at least for the common wind directions that were observed (dominant SW-wind). Lastly, wind wave height appeared marginally higher at the southern transect compared to the northern transect.

In general the **ship wave climate** intensified during the study period with an increase of ship passing intensity of 15% between October 2015 and 2016. Tug boats and cargo ships, sailing upstream, are slower at the southern than at the northern transect, for tankers and downstream sailing vessels there was no difference.

The **ship wave** study revealed several important trends yet more sophisticated statistical analyses may be needed to deal with collinearities and demonstrate unique relationships. A possibly important trend was that ship wave height may fairly strongly increase when the tide is low. This pattern may be attributed to the proportionally large displacement of water at low tide. For some boat types, and for some years, sailing speed correlated positively with wave height. Maximum ship wave height was mostly below 0.2 m but regularly higher peaks were recorded up to 0.7 m. As such, during periods when wind speed was low to moderate (most of the time), ships frequently generate waves that exceeded the background wind maximum wave height, yet for short durations. A peculiar aspect of ship waves is the attenuation behaviour from low to the high tidal flat. This means that they tend to decrease in height when they advance towards the shoreline, a pattern opposite to that observed from wind waves at high wind speed.

In order to translate driving forces to potential morphodynamic effects, calculated **shear stress parameters** were used during the intensive campaign in 2016. At the high tidal flat, wave-induced bed shear stress was higher than the current shear stress, especially in the southern plot, while on the low tidal flat current bed shear stress was more important. Expected morphological effects were obtained by comparing calculated wave- and current-induced bed shear stresses to the local critical Shields stress for sediment motion, based on sediment characteristics obtained during the study. During the flood phase of tides near spring tide, the current shear stress exceeded the local critical Shields stress causing sediment

resuspension/erosion, thus suggesting a significant tidal current impact on morphology, at *the low tidal flat* of both transects. During average tidal conditions, the critical Shields stress was only exceeded on the southern low tidal flat plot , which is due to its different substrate condition and related lower Shield stress (thus resuspension/erosion occurs already at lower current velocities). For *the high tidal flat*, current shear stress did not exceed critical Shields stress on any occasion while the wave-induced bed shear stress did so at some instances, especially at the southern transect. Turbidity measurements indicated steep increases just after inundation or just prior to local water retreat, suggesting temporary bursts of erosion. It is hypothesized that at very low water levels at the river's edge, waves transfer their energy more efficiently to the underlying sediment. More research is needed to confirm this hypotheses.

For the low tidal flat, water depth at high tide, was highly correlated with net daily bed level changes, especially if the sediment mainly consisted of less-cohesive sands such as was the case at the low plot of the Southern transect. The impact of hydrodynamic forcing may thus be strongly location dependent, according to sediment type.

6.3 RECOMMENDATIONS

The results of the present study are more conclusive, compared to Michels et al (2012) and Verelst et al (2011), with respect to the relative importance of hydrodynamic stressors on the related morphological response of the Galgeschoor lower and higher tidal mudflats and marsh edge facing Deurganck dock and the location of the possible future Saeftinghe dock. With regard to ship types and behaviour, we found tendencies for larger ships and ships sailing at high speeds to generate higher waves, especially near low tide, but more detailed analyses could possibly refine and confirm the observed trends. From studies elsewhere in the estuary, we know that the shape of the tidal flat in front of the marsh cliff is deterministic in how waves will affect cliff erosion. This suggests that waves that do not have an impact at this point, may become harmful when tidal flat shape changes and deteriorates, as is observed in recent years. Both studies on how and why tidal flat bathymetry changes and more detailed studies on ship wave data are recommended.

In view of the long term evolution Michels et al (2012) concluded that an average marsh edge retreat of 25 cm/year can be considered as a background value for a normal tidal marsh cycle at the Galgeschoor, allowing for establishment of pioneer marsh. This might be what is happening at the Galgeschoor, however the establishment of the pioneer marsh is very recent and it is yet impossible to judge whether this will consolidate and is really the onset of regeneration as is part of the natural tidal marsh cycle. It is recommended to monitor this pioneer marsh more closely in relation to the physical driving forces

doi.org/10.21436/inbor.17169167

References

Andersen, T. J., Pejrup, M., & Nielsen, A. A. (2006). Long-term and high-resolution measurements of bed level changes in a temperate, microtidal coastal lagoon. Marine Geology, 226(1–2), 115–125. https://doi.org/10.1016/j.margeo.2005.09.016

Belliard, J.-P.; Temmerman, S. (2017). Part II: Analysis of elevation changes and potential controls during the long-term measurement campaign from November 2015 to May 2017. University of Antwerp, Belgium

Callaghan, D. P., Bouma, T. J., Klaassen, P., van der Wal, D., Stive, M. J. F., & Herman, P. M. J. (2010). Hydrodynamic forcing on salt-marsh development: Distinguishing the relative importance of waves and tidal flows. Estuarine, Coastal and Shelf Science, 89(1), 73–88. https://doi.org/10.1016/j.ecss.2010.05.013

Christiansen, C., Vølund, G., Lund-Hansen, L. C., & Bartholdy, J. (2006). Wind influence on tidal flat sediment dynamics: Field investigations in the Ho Bugt, Danish Wadden Sea. Marine Geology, 235(1–4 SPEC. ISS.), 75–86. https://doi.org/10.1016/j.margeo.2006.10.006

Christie, M. C., Dyer, K. R., & Turner, P. (1999). Sediment Flux and Bed Level Measurements from a Macro Tidal Mudflat. Estuarine, Coastal and Shelf Science, 49(5), 667–688. https://doi.org/10.1006/ecss.1999.0525

De Roo, S. (2013). Experimental Study of the Hydrodynamic Performance of a Nature-Friendly Bank Protection Subject to Ship Waves in a Confined, Non-Tidal Waterway. PhD Thesis, University of Ghent, Belgium.

Deloffre, J. et al., (2005). Sedimentary processes on an intertidal mudflat in the upper macrotidal Seine estuary, France. Estuarine, Coastal and Shelf Science, 64(4), pp.710–720.

Fagherazzi, S., and P. L. Wiberg (2009), Importance of wind conditions, fetch, and water levels on wave-generated shear stresses in shallow intertidal basins, J. Geophys. Res., 114, F03022, doi:10.1029/2008JF001139.

Hu, Z. & Lenting, W. & van der Wal, D. & Bouma, T. (2015). Continuous monitoring bed-level dynamics on an intertidal flat: Introducing novel, stand-alone high-resolution SED-sensors. Geomorphology. 245. 10.1016/j.geomorph.2015.05.027

Hu, Z., Yao, P., van der Wal, D., & Bouma, T. J. (2017). Patterns and drivers of daily bed-level dynamics on two tidal flats with contrasting wave exposure. Scientific Reports, 7(1), 7088. https://doi.org/10.1038/s41598-017-07515-y

Hunt, S., Bryan, K. R., Mullarney, J. C., & Pritchard, M. (2016). Observations of asymmetry in contrasting wave- and tidally-dominated environments within a mesotidal basin: implications for estuarine morphological evolution. Earth Surface Processes and Landforms, 41(15), 2207–2222. https://doi.org/10.1002/esp.3985

Kirby, R., Bleakley, R.J., Weatherup, S.T.C., Raven, P.J., Donaldson, N.D., 1993. Effect of episodic events on tidal mud flat stability, Ardmillan Bay, Strangford Loch, Northern Ireland. In: Mehta, A.J. (Ed.), Coastal and Estuarine Studies 42. Nearshore and Estuarine Marine Cohesive Sediment Transport. American Geophysical

Kolokythas, G.; Meire, D.; De Roo, S.; Plancke, Y.; Verwaest, T.; Mostaert, F. (2017). Wave measurements at Galgeschoor: Sub report 1 – Analysis of velocities and waves during an intensive measuring campaign. Version 2.0. FHR Reports, 15_054_1. Flanders Hydraulics Research: Antwerp.

Levy, Y. and Meire, D. (2018). Wave measurements at Galgeschoor: Part 1:Analysis of velocities and waves during an intensive measuring campaign. Version 0.18. FHR Reports, 15_054_1. Flanders Hydraulics Research: Antwerp.

Meire, D.; Kolokythas, G.; Smolders, S.; Plancke, Y.; Verwaest, T.; Mostaert, F. (2016). Agenda voor de Toekomst – Waves in the estuary: Analysis of wave measurements at

Saeftinghe. Version 4.0. FHR Reports, 16_000_1. Flanders Hydraulics Research: Antwerp.

Meire, D.; Levy, Y.; Plancke, Y. ;Mostaert, F. (2016). Agenda voor de Toekomst – Waves in the Scheldt estuary: Analysis of wave measurements at Dendermonde. Version 4.0. FHR Reports, 14_082_2. Flanders Hydraulics Research: Antwerp.

Michels, H.; Van Braeckel, A.; Speybroeck, J.; Milotic, T.; Van den Bergh, E.; Verelst, K.; De Mulder, T.;Taverniers, E.; Mostaert, F. (2012). Onderzoek naar de invloedsfactoren van golfbelasting en de morfologische effecten op slikken en schorren in de Beneden Zeeschelde, meer specifiek op het Galgeschoor: Deelrapport 9 - Analyserapport met betrekking tot de morfologische ontwikkelingen op het Galgeschoor. Versie 1_4. WL Rapporten, 837_03. Waterbouwkundig Laboratorium: Antwerpen, België

Silinski, A., and Temmerman, S. (2016). Wave measurements at Galgeschoor Part II : Analysis of velocities and waves during an intensive measuring campaign. Draft report. University of Antwerp, Belgium.

Uncles, R. J., & Stephens, J. A. (2010). Turbidity and sediment transport in a muddy sub-estuary. Estuarine, Coastal and Shelf Science, 87(2), 213–224. https://doi.org/10.1016/j.ecss.2009.03.041

Van Braeckel, A., Elsen, R. & Van den Bergh, E. 2014. MONEOS – Geomorfologie: Hoogteraaien van slik en schor in de Zeeschelde - evolutie van toestand tot 2012. Rapporten van het Instituut voor Natuur- en Bosonderzoek; no. INBO.R.2014.1860252.

Van Ryckegem, G, Van Braeckel, A, Elsen, R, Speybroeck, J, Vandevoorde, B, Mertens, W, Breine, J, Spanoghe, G, Buerms, D, De Beukelaer, J, De Regge, N, Hessel, K, Soors, J, Terrie, T, Van Lierop, F & Van den Bergh, E 2017, MONEOS – Geïntegreerd datarapport INBO: Toestand Zeeschelde 2016: Monitoringsoverzicht en 1ste lijnsrapportage Geomorfologie, diversiteit Habitats en diversiteit Soorten. Rapporten van het Instituut voor Natuur en Bosonderzoek, nr. 37, Instituut voor Natuur- en Bosonderzoek. https://doi.org/10.21436/inbor.13479033

Van Ryckegem, G, Van Braeckel, A, Elsen, R, Speybroeck, J, Vandevoorde, B, Mertens, W, Breine, J, Spanoghe, G, Bezdenjesnji, O, Buerms, D, De Beukelaer, J, De Regge, N, Hessel, K, Lefranc, C, Soors, J, Terrie, T, Van Lierop, F & Van den Bergh, E 2018, MONEOS – Geïntegreerd datarapport INBO: Toestand Zeeschelde 2017: Monitoringsoverzicht en 1ste lijnsrapportage Geomorfologie, diversiteit Habitats en diversiteit Soorten. Rapporten van het Instituut voor Natuur en Bosonderzoek, nr. 74, Instituut voor Natuur- en Bosonderzoek. https://doi.org/10.21436/inbor.15000892

Van Rijn, L. C. (1993). Principles of sediment transport in rivers, estuaries and coastal seas (Vol. 1006). Amsterdam: Aqua publications.

Verelst, K.; De Mulder, T.; Vereecken, H.; Taverniers; E.; Mostaert, F. (2012). Onderzoek naar de invloedsfactoren van golfbelasting en de morfologische effecten op slikken en schorren in de Beneden Zeeschelde, meer specifiek op het Galgeschoor: Deelrapport 8 - Analyserapport golfbelasting op het Galgeschoor. Versie 2_0. WL Rapporten, 837_03. Waterbouwkundig Laboratorium: Antwerpen, België

Verelst, K.; De Mulder, T; Vereecken, H.; Michels, H.; Speybroeck J.; Van Braeckel, A.; Van Den Bergh, E.; Taverniers; E.; Mostaert, F. (2011a). Onderzoek naar de invloedsfactoren van golfbelasting en de morfologische effecten op slikken en schorren in de Beneden Zeeschelde, meer specifiek op het Galgeschoor: Deelrapport 5: Verslag ad hoc-meetcampagne van 20 tot 22 april 2011. Versie 2_0. WL Rapporten, 837_03. Waterbouwkundig Laboratorium & INBO: Antwerpen, België

Verelst, K.; De Mulder, T; Vereecken, H.; Michels, H.; Speybroeck J.; Van Braeckel, A.; Van Den Bergh, E.; Taverniers; E.; Mostaert, F. (2011b). Onderzoek naar de invloedsfactoren van golfbelasting en de morfologische effecten op slikken en schorren in de Beneden Zeeschelde, meer specifiek op het Galgeschoor: Deelrapport 6: Verslag ad hoc-

meetcampagne van 04 tot 06 mei 2011. Versie 2_0. WL Rapporten, 837_03. Waterbouwkundig Laboratorium & INBO: Antwerpen, België

Wang, H., D. van der Wal, X. Li, J. van Belzen, P. M. J. Herman, Z. Hu, Z. Ge, L. Zhang, and T. J. Bouma (2017), Zooming in and out: Scale dependence of extrinsic and intrinsic factors affecting salt marsh erosion, J. Geophys. Res. Earth Surf., 122, 1455–1470, doi:10.1002/ 2016JF004193.

Zhu, Q., Yang, S., & Ma, Y. (2014). Intra-tidal sedimentary processes associated with combined wave-current action on an exposed, erosional mudflat, southeastern Yangtze River Delta, China. Marine Geology, 347, 95–106. https://doi.org/10.1016/j.margeo.2013.11.005